Institut für Erd- und Umweltwissenschaften
Mathematisch-Naturwissenschaftliche Fakultät
Universität Potsdam

THE TECTONIC EVOLUTION OF THE WESTERN TIEN SHAN

Dissertation
von

ALEJANDRO E. BANDE

zur Erlangung des akademischen Grades

DOCTOR RERUM NATURALIUM
»DR. RER. NAT.«

in der Wissenschaftsdisziplin

Geologie

eingereicht an der
Mathematisch-Naturwissenschaftlichen Fakultät
der Universität Potsdam

Potsdam, August 2016

Published online at the
Institutional Repository of the University of Potsdam:
URN urn:nbn:de:kobv:517-opus4- 398933
http://nbn-resolving.de/urn:nbn:de:kobv:517-opus4- 398933

‘‘...la cordillera que en la distancia te cura la visión con su elegancia.’’

W. Rodríguez

ABSTRACT

Intracontinental deformation usually is a result of tectonic forces associated with distant plate collisions. In general, the evolution of mountain ranges and basins in this environment is strongly controlled by the distribution and geometries of preexisting structures. Thus, predictive models usually fail in forecasting the deformation evolution in these kinds of settings. Detailed information on each range and basin-fill is vital to comprehend the evolution of intracontinental mountain belts and basins. In this dissertation, I have investigated the complex Cenozoic tectonic evolution of the western Tien Shan in Central Asia, which is one of the most active intracontinental ranges in the world. The work presented here combines a broad array of datasets, including thermo- and geochronology, paleoenvironmental interpretations, sediment provenance and subsurface interpretations in order to track changes in tectonic deformation. Most of the identified changes are connected and can be related to regional-scale processes that governed the evolution of the western Tien Shan.

The NW-SE trending Talas-Fergana fault (TFF) separates the western from the central Tien Shan and constitutes a world-class example of the influence of preexisting anisotropies on the subsequent structural development of a contractile orogen. While to the east most of ranges and basins have a sub-parallel E-W trend, the triangular-shaped Fergana basin forms a substantial feature in the western Tien Shan morphology with ranges on all three sides. In this thesis, I present 55 new thermochronologic ages (apatite fission track and zircon (U-Th)/He)) used to constrain exhumation histories of several mountain ranges in the western Tien Shan. At the same time, I analyzed the Fergana basin-fill looking for progressive changes in sedimentary paleoenvironments, source areas and stratal geometrical configurations in the subsurface and outcrops.

The data presented in this thesis suggests that low cooling rates (<1°C Myr^{-1}), calm depositional environments, and low depositional rates (<10 m Myr^{-1}) were widely distributed across the western Tien Shan, describing a quiescent tectonic period throughout the Paleogene. Increased cooling rates in the late Cenozoic occurred diachronously and with variable magnitudes in different ranges. This rapid cooling stage is interpreted to represent increased erosion caused by active deformation and constrains the onset of Cenozoic deformation in the western Tien Shan. Time-temperature histories derived from the northwestern Tien Shan samples show an increase in cooling rates by ~25 Ma. This event is correlated with a synchronous pulse

in the South Tien Shan. I suggest that strike-slip motion along the TFF commenced at the Oligo-Miocene boundary, facilitating CCW rotation of the Fergana basin and enabling exhumation of the linked horsetail splays. Higher depositional rates (~150 m Myr^{-1}) in the Oligo-Miocene section (Massaget Fm.) of the Fergana basin suggest synchronous deformation in the surrounding ranges. The central Alai Range also experienced rapid cooling around this time, suggesting that the onset of intramontane basin fragmentation and isolation is coeval. These results point to deformation starting simultaneously in the late Oligocene – early Miocene in geographically distant mountain ranges. I suggest that these early uplifts are controlled by reactivated structures (like the TFF), which are probably the frictionally weakest and most-suitably oriented for accommodating and transferring N-S horizontal shortening along the western Tien Shan.

Afterwards, in the late Miocene (~10 Ma), a period of renewed rapid cooling affected the Tien Shan and most mountain ranges and inherited structures started to actively deform. This episode is widely distributed and an increase in exhumation is interpreted in most of the sampled ranges. Moreover, the Pliocene section in the basin subsurface shows the higher depositional rates (>180 m Myr^{-1}) and higher energy facies. The deformation and exhumation increase further contributed to intramontane basin partitioning. Overall, the interpretation is that the Tien Shan and much of Central Asia suffered a global increase in the rate of horizontal crustal shortening. Previously, stress transfer along the rigid Tarim block or Pamir indentation has been proposed to account for Himalayan hinterland deformation. However, the extent of the episode requires a different and broader geodynamic driver.

ZUSAMMENFASSUNG

Intra-kontinentale Deformation der Erdkruste ist in der Regel das Ergebnis weitreichender tektonischer Kräfte, die durch Interaktion der Erdplatten an entfernten Kontinentalrändern entstehen. Eine entscheidende Rolle bei der Entwicklungsgeschichte der so entstehenden Gebirge, spielt das Vorhandensein und die Orientierung präexistierender Strukturen in der Kruste. Diese Komplexität lässt bekannte Vorhersagemodelle zur Bestimmung der Deformationsgeschichte häufig scheitern. Um die Deformationsprozesse intra-kontinentaler Gebiete dennoch besser zu verstehen, sind detaillierte Informationen über die Entstehungsgeschichte einzelner Bergketten und benachbarter Becken von essentieller Bedeutung.

Die vorliegende Arbeit beschäftigt sich mit der känozoischen Entwicklung tektonischer Prozesse in einer der aktivsten intra-kontinentalen Gebirgsketten der Welt, dem westlichen Tian Shan Gebirge in Zentralasien. Um räumliche und zeitliche Veränderungen der tektonischen Deformation besser nachvollziehen zu können, wird in dieser Arbeit ein breites Spektrum an Datensätzen, aus Thermo- und Geochronologie, Paläoumwelt-Interpretation, Sediment-Provenienz und der Interpretationen seismischer Profile, kombiniert. Die somit identifizierten Prozesse deuten auf einen engen Bezug und können mit regional übergreifenden Prozessen in Beziehung gesetzt werden, die für die Entwicklung des westlichen Tian Shan Gebirges verantwortlich sind.

Ein Paradebeispiel des Einflusses präexistierender Krustenanomalien auf die strukturelle Entstehung eines intra-kontinentalen Gebirges wie dem Tian Shan ist die NW-SE streichende Talas-Fergana-Störung, die den westlichen vom zentralen Tian Shan trennt. Während der östlich gelegene Zentralbereich des Orogens durch subparallele, E-W streichende Gebirgszüge und Becken charakterisiert ist, ist das markant dreieckförmige Fergana-Becken im westlichen Tian Shan von allen Seiten durch hohe Gebirgsrücken flankiert.

Kern dieser Arbeit sind 55 neue thermochronologische Altersdatierungen (aus Apatit-Spaltspuren-Analyse und U-Th/He an Zirkonen), mit deren Hilfe die Exhumationsgeschichte mehrerer Gebirgszüge im westlichen Tian Shan untersucht wurde. Des Weiteren wurde die sedimentäre Beckenfüllung des benachbarten Fergana-Beckens auf sukzessive Veränderungen der Paläoumweltbedingungen, der Sediment-

Provenienz und der geometrischen Konfiguration der Sedimente, am Aufschluss und im Untergrund untersucht.

Ergebnisse dieser Arbeit zeigen niedrige Abkühlungs- (<1°C Myr^{-1}) und Sedimentationsraten (<10 m Myr^{-1}) im Gebiet des westlichen Tian Shan im Paläogen und deuten auf eine tektonisch ruhige und relativ stabile Region. Demgegenüber stehen erhöhte Abkühlungsraten im späten Känozoikum, die in den verschiedenen Gebirgsketten diachron und mit unterschiedlicher Intensität einsetzen. Diese zweite Phase deutet auf erhöhte Erosionsprozesse, hervorgerufen durch aktive Deformation, und markiert den Beginn der känozoischen Deformation im westlichen Tian Shan Gebirge. Temperaturgeschichten im Gebiet des NW Tian Shan zeigen erhöhte Abkühlungsraten vor ~25 Ma und korrelieren zeitlich mit ähnlichen Ereignissen im südlichen Tian Shan. Ich vermute, dass Horizontalverschiebungen entlang der Talas-Fergana-Störung an der Oligozän-Miozän-Grenze zur Rotation des Fergana-Beckens gegen den Uhrzeigersinn, und darüber hinaus zur Exhumation entlang diverser Nebenstörungen führten. Erhöhte Sedimentationsraten (~150 m Myr^{-1}) der Oligo-Miozänen Einheiten im Fergana Becken (Massaget Fm.) deuten ebenfalls auf eine synchrone Deformationsphase umliegender Gebieten zu dieser Zeit. Dies ist durch erhöhte Abkühlungsraten im zentralen Alai (südlich des Fergana Beckens) gut dokumentiert und impliziert, dass die intra-montane Fragmentierung und Isolierung, der ehemals zusammenhängenden Sedimentbecken, zur gleichen Zeit erfolgte. Diese Beobachtungen deuten auf eine Deformationsgeschichte hin, die zeitgleich ihren Ursprung in zwei voneinander entfernten Regionen hat. Diese frühen Hebungen scheinen durch reaktivierte Strukturen (wie der Talas-Fergana-Störung) gesteuert worden zu sein, deren Orientierung optimal für eine N-S Einengung im Bereich des westlichen Tian Shan geeignet ist.

Eine erneute Phase schneller Abkühlung im späten Miozän (~10 Ma) führte zur Aktivierung der meisten heutigen Gebirgszüge und der Reaktivierung prä-existierender Strukturen. Diese Deformationsphase zeigt eine weite Verbreitung und einen Anstieg der Exhumationsraten in den meisten beprobten Bereichen. Darüberhinaus steigen die pliozänen Sedimentationsraten (>180 m Myr^{-1}) im Fergana-Becken und die Faziesanalyse der Sedimente zeigt hoch-energetische Ablagerungsbedingungen.

Fazit dieser Arbeit ist, dass der Tian Shan und ein Großteil Zentralasiens durch erhöhte Verkürzungsraten der Kruste stark beeinflusst wurden. Früher ging man davon

aus, dass Stresstransfer entlang des stabilen Tarim-Blocks oder die Indentation des Pamir-Gebirges zur Deformation im Hinterland des Himalaya führten. Die beobachteten Deformationsmuster deuten jedoch auf einen anderen, viel weitreichenderen geodynamischen Prozess hin.

ACKNOWLEDGEMENTS

Before starting my PhD, Kyrgyzstan was for me a former Soviet Union country with fuzzy borders, located somewhere deep in Asia. Once I visited it, I discovered a strong and rooted culture and a variegated society, where modernity, post-communism and tradition constitute a delicate equilibrium. Being there stimulated my mind, opened my eyes to alternative views of life and gave me a new perspective to understand geopolitical differences. At the same time I was impressed by the generosity and kindness of people, specially the ones living in small villages or directly in the field. Almost immediately, I realized I have experienced the same feelings from people living in rural areas of South America.

This experience was possible because my advisor, Ed Sobel, introduced me for the first time to the Central Asia geology, supported and encouraged me to work there and allow me to follow my interests. During my time in Germany and then in Argentina, Ed has helped me in immesurable ways, ranging from correcting my English writing, rigorously teaching how to count fission tracks, to state key scientific questions of my ideas and manuscripts. As a good teacher and mentor he pushed me by asking questions to think critically of my own work always trying to gain a better geological understanding.

Many people in the institute have helped me along the way and deserve to be acknowledged. Special thanks go to Euan Macaulay, Verónica Torres Acosta, Heiko Pingel, Alexander Rohrmann and Daniel Melnick who have provided important assistance and many suggestions for improving my papers. My work in Potsdam has greatly benefited from fruitful and diverse discussions held in the SMURF weekly seminar. Manfred Strecker is responsible for fostering the broad interests and geoscience disciplines involved in the group making discussion always interesting. Alexander Schmidt kindly helped me acquiring all the zircon U-Pb data. I would like to thank Christine Fischer who has guided me during many hours I have spent in the sample prep lab. Maria Langer and Phil Balling positively helped me during my second field season in Kyrgyzstan.

Outside the institute, Danny Stockli provided the ZHe ages used in one of the manuscripts. An unsuccessful attempt for stablishing a chronology of sedimentation and block rotation with magnetostratigraphy was possible thanks to the friendly help of

Michael Wack and Stuart Gilder from LMU München. Shukrat Radjabov kindly handed-over invaluable subsurface data from the Fergana basin and helped on its interpretation. Marie- Françoise Brunet, Eric Barrier and Hermann Munsch are acknowledged for providing key suggestions and discussions about Central Asian geology.

Alexander Mikolaichuk is specially thanked for being a permanent consultant of Tien Shan geology, as well as organizing the most important things for the three field visits. In particular, the selection of Vasyl Hyshchyn and Roman Teslyuk as field assistants and Ivan Andreev and Yuri Sergeev as drivers. Without these people, much if the work presented here could not have been accomplished.

This study was financially supported by TOTAL S.A., the DARIUS Programme, DFG-Graduate School 1364 and a doctoral fellowship from the German Academic Exchange Service (DAAD) to A. Bande.

I would like to thank my friends and family in Argentina, for making easier my life while away with their continuous support. Finally, my love and thanks go to my wife Lucía, with whom I shared the stimulating experience of living in Germany and pursue a doctoral degree. Thanks to her, my son Feliciano and the baby girl who is coming, I am writing these final lines of my dissertation.

CONTENTS

LIST OF FIGURES

LIST OF TABLES

Chapter 1
Introduction

1.1 Thesis organization

This study constitutes a cumulative thesis that combines two peer-reviewed, published articles and a manuscript that has been submitted for review to a scientific journal. The overall goal of the research conducted in this thesis is to better understand the chronology and mechanisms of mountain building and adjacent intramontane basin formation processes in the western Tien Shan.

In Chapter 1, the manuscripts included in the thesis are listed, together with a short overview of each of them. In addition, the motivation of the thesis and main research goals are laid out following an overview of Central Asian geological history.

Chapter 2 discusses the deformation history of the Talas-Fergana strike-slip fault (TFF). I have used thermochronologic data to constrain exhumation of the northwestern Tien Shan ranges. Regional contextualization of the results suggests that TFF terminations acted as restraining bends and are kinematically-connected. If this is true, slip movement along the TFF is synchronous to the uplift of the fault´s horsetails. According to these results, the Paleozoic-formed TFF was reactivated in the Cenozoic and transferred Pamir shortening to the northern Tien Shan. This chapter has been published by *Alejandro Bande, Edward R. Sobel, Alexander Mikolaichuk and Verónica Torres Acosta* (2015) in *Brunet, M.-F., T. McCann and E.R. Sobel* (eds): Geological Evolution of Central Asian Basins and the Western Tien Shan Range. Geological Society, London, Special Publications, 427, doi:10.1144/SP427.1.

In Chapter 3, new thermochronological data from the southwestern Tien Shan is presented and used to infer the onset of deformation. According to these results, late Oligocene – early Miocene uplift affected the Tien Shan and initiated basin fragmentation in the Central Asian hinterland. Additionally, the western Tien Shan suffered a strong late Miocene exhumational event. Coeval timing of uplift (~10 Ma) accross the entire Tien Shan range suggest that neither Tarim nor Pamir acted as a unique driver for exhumation and deformation. This chapter was submitted for review to the journal Tectonics by *Alejandro Bande, Edward R. Sobel, Alexander Mikolaichuk, Alexander Schmidt and Daniel F. Stockli* (2016).

Chapter 4 explores the evolution of the Fergana basin. Based on paleoenvironmental interpretations, paleocurrents, conglomerate clast-count data, regional seismic lines and a well-log, the main stages of the basin evolution are outlined. For the first time in the Fergana basin, modern seismic surveys are available and interpreted. The new data supplies valuable insights on the extent of the late Miocene deformational event. Additionally, a previously published hypothesis on the subsidence mechanism is backed-up by independent data to account for the impressive ~8 km of Cenozoic deposits. This chapter has been published by *Alejandro Bande, Shukhrat Radjabov, Edward R. Sobel and Tatyana Sim* (2015) in *Brunet, M.-F., T. McCann and E.R. Sobel* (eds): Geological Evolution of Central Asian Basins and the Western Tien Shan Range. Geological Society, London, Special Publications, 427, doi:10.1144/SP427.12.

In chapter 5, I combined the principal results of the individual studies and reviews the data in a regional context. Finally, additional research questions stimulated by this study and possible future efforts to solve them are discussed.

1.2 Thesis motivation and Central Asian geological overview

Argand (1924) compiled the first tectonic map of Eurasia. He documented Cenozoic compression, reactivation of preexisting structures, crustal thickening and anomalous relief throughout much of Central Asia. In the following years many researchers endorsed most of his first findings, providing detailed constraints and quantifying *Argand*'s interpretation. However, not all of Eurasian territory received the same attention and even though almost 100 years passed since his work some areas of the Central Asian interior still require modern techniques to give a complete shape to *Argand*'s exceptional, pioneering work. Until the 1990s, geological surveying of the Tien Shan focused on Paleozoic geology and related economic resources exploration. At the same time, the neighboring Himalayas and Tibet were studied and used as a testbed for modern theories of orogenesis. This information gap was partially covered in the last 15 years, but focused in the central and eastern Tien Shan (e.g. *Dumitru et al*., 2001; *Thompson et al.*, 2002; *Yang & Liu*, 2002; *Sobel et al*., 2006 a and b; *Heermance et al*., 2007, 2008; *Jolivet et al*., 2010; *Fu et al*., 2010; *Glorie et al*., 2011; *Macaulay et al*., 2013, 2014; *Jolivet*, 2015). The lack of modern data in the western Tien Shan was a first motivation to the study presented here, trying to close the data gap

providing state-of-the-art techniques and analysis on the evolution of an important zone in the geodynamic evolution of the India-Asia collision.

The Tien Shan extends for approximately 2500 km from southern Uzbekistan in the west to the China-Mongolia border in the east (Fig. 1.1). Peaks in the range exceed heights of 7000m, making the Tien Shan the second tallest mountain range outside of the Himalayan-Karakorum-Pamir orogen. The extent and position of the orogen makes it the world's largest active intracontinental mountain belt in the world. Thus, is an ideal place to acquire information and present new interpretations on the evolution of intracontinental deformation; a second motivation to conduct the research presented in this dissertation.

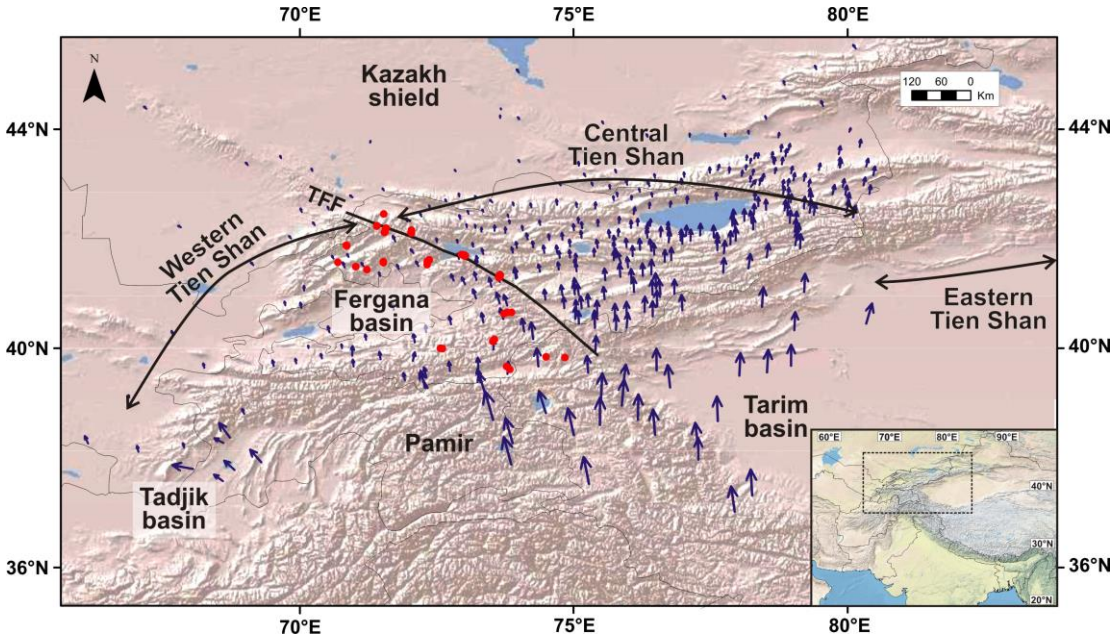

Figure 1.1 Shaded relief image of the Tien Shan and surrounding areas. Blue arrows denote the velocity of GPS stations with respect to stable Eurasia (*Zubovich et al*., 2010). Red dots are sample locations presented in this thesis. Political borders shown in grey lines. TFF is Talas-Fergana fault. Inset map shows location of Figure 1.1 in the Himalayan-Central Asian region.

The collision between India and Asia at ~55 Ma (*Searle, et al*., 1987; *Robinson et al*., 2003) caused not only the formation and exhumation of the Himalayan range, but also tectonic uplift of the Kunlun Shan, Pamir and Tien Shan between the late Eocene and early Miocene (e.g. *Sobel & Dumitru*, 1997; *Burtman*, 2000; *Jolivet et al*., 2001; *Yin et al*., 2002; *Amidon & Hynek*, 2010). The uplift produced by the far-field effects of the collision caused a major change in the Central Asian hinterland. In this area, during Paleogene times, a continuous shallow sea extended across the Eurasian continent as far east as the western portion of the Tarim Basin in western China. Contemporaneous to the onset of uplift, the epicontinental sea retreated and an arid monsoon was installed

in the Asian interior (e.g. *Graham et al*., 2005; *Sun & Wang*, 2005; *Kraatz & Geislet*, 2010; *Bosboom et al.,* 2014). To the west, the anoxic organic rich Paratethys Sea covered most of eastern Europe and western Asia, of which nowadays only the Black Sea, Caspian Sea and Aral Sea remain (e.g. *Popov et al*., 2004; *Allen & Armstrong*, 2008). In this context, the Pamir, Tien Shan and its associated basins should preserve important and still not sufficiently investigated records of the mechanisms of intracontinental deformation and basin fragmentation.

Interestingly, much of the Tien Shan has been a topographic high since the Paleozoic (e.g. *Dumitru et al*., 2001) and as a whole is an ancient plate boundary (*Molnar & Tapponnier*, 1975), providing an important belt of weakness in which deformation could selectively propagate. In orogens where tectonic forces act on a mosaic of inherited structures and other pre-existing crustal weaknesses, it is hard to predict the spatiotemporal distribution of deformation (*Hilley et al*., 2005). Typically, within these settings, deformation will focus on pre-existing weaknesses, reactivating structures that are frictionally weak and suitably orientated with respect to the maximum horizontal stress (e.g. *Holdsworth et al*., 1997). In this kind of setting, where preexisting anisotropies are widely distributed, like an ancient plate boundary, the reactivated structures will control rock-uplift and the related creation of a series of mountain ranges and isolated intramontane basins (e.g. *Jordan & Allmendinger,* 1986). In other words, the morphology and spatiotemporal evolution of intracontinental interiors depends on the preexisting distribution and geometry of reactivated structures (*Neely & Erslev*, 2009). Thus, constrain the timing and effects of tectonic deformation in intracontinental settings is vital to fully understand the mechanism of mountain belt development and intramontane basin formation and isolation.

The right-lateral Talas-Fergana fault separates the central and the western Tien Shan. The central section consists of a regular structural pattern that includes the alternation of ranges and basins separated by steeply dipping reverse faults (e.g. *Macaulay et al*., 2013 and 2014). The roughly uniform east-west oriented topographic trend of ranges and basin terminates abruptly at the fault. To the west, the pattern is different. The triangular-shaped Fergana basin dominates the sector, surrounded by mountain ranges on all three boundaries. Offset of the Talas-Fergana fault is supposed to be ~180 km since Paleozoic time (*Burtman*, 1975). However, a fraction of this offset (60-100 km) occurred in the Cenozoic (*Thomas et al*., 1993; *Burtman et al.*, 1996).

Paleomagnetic declinations in Cenozoic sedimentary rocks *(Thomas et al*., 1993) demonstrate approximately 20° of counter-clockwise rotation of the Fergana block with respect to the stable Eurasia. Modern GPS data surrounding the basin corroborates that the basin now rotates at a rate of $-0.73° \pm 0.08°$ Myr^{-1} with respect to Eurasia (*Zubovich et al*., 2010). This rotation seems to have occurred about an axis at the southwest end of the Chatkal ranges. Thus, shortening should increase from southwest to northeast. Based on the geometry of rotation and current GPS velocity vectors (*Zubovich, et al*., 2010), neither the amount nor the current rate of slip rate on the fault can be constant along it. Some authors (e.g. *Burov & Molnar*, 1998) proposed that different styles of deformation occur at both sides of the fault. However, limited data is available to the test the hypothesis.

The structure of the Chatkal Ranges requires north-northwest directed crustal shortening by reverse faulting and basement folding (*Cobbold et al*., 1996). As in the central Tien Shan, most of the Chatkal ranges (e.g. Chatkal itself, Shandalash, Ugam, etc.) are bounded on at least one side by high angle reverse structures preferentially located to the south. Recent GPS data show that active shortening across the Chatkal Ranges occurs at ~5 mm/yr (*Zubovich, et al*., 2010). The east-west trending Alai range is composed of Paleozoic highly deformed sedimentary beds and volcanics rocks including a well-defined ophiolite belt (*Burtman*, 2010). In active intracontinental orogens, deformation is distributed along and across strike and several faults are usually currently active (e.g. *Hilley et al*., 2005). Soviet and Kyrgyz geologic maps (e.g. *Vlasov et al*., 1991; *Bakirov et al*., 2001) show a complex distribution of structures in the Alai orogen. However, is still not clear wich faults are active. Interestingly, in the eastern sector of the Alai Range, where the mountain belt approaches the Talas-Fergana fault, the strike of the faults clearly diverges and acquires a north-east – south-west direction with a right lateral sense of movement. South of the range, the Alai valley accommodates deformation between the Pamir indentor and the western Tien Shan. Recent geodetic analysis revealed that almost half of the convergence rate between India and Eurasia at this latitude is accommodated along the Main Pamir Thrust, on the south side of the Alai basin (*Argus et al*., 2010; *Zubovich et al*., 2016).

In the study presented here, I have constrained the spatiotemporal evolution of a substantial portion of the western Tien Shan. Using a multi-method approach, I contribute to shorten the data gap on the timing and magnitude of deformation of the

western Tien Shan ranges. Simultaneously, I analyzed and provided new information on the related intramontane basin evolution. The main source of information is obtained by using low-temperature thermochronologic systems like apatite fission track (AFT) and zircon (U-Th)/He (ZHe). Results from this techniques and related thermal modeling are used to constrain the exhumation history of several mountain ranges. The thermochronology-based constraints on the timing of deformation are cross-checked with the stratigraphic record of the Fergana basin. The depositional and provenance record of the adjacent tectonically-related basins has been long recognized as an important factor in extracting timing information on evolving orogens (e.g. *Jordan et al*., 1993; *DeCelles et al*., 1998; *Horton et al*., 2010). Analysis of the Fergana basin sedimentary basin-fill provided constraint on paleogeography, changes in source areas, rate of deposition and ultimately basin evolution. Additionally, for the first time, seismically constrained basin regional cross-sections of the Fergana basin are presented.

The outcome of the thesis provide new insight into far-field deformational processes, mountain building and sedimentary basin evolution in areas characterized by reactivation of inherited basement anisotropies and the resulting formation of intramontane basins.

Chapter 2
Talas-Fergana Fault Cenozoic timing of deformation and its relation to Pamir indentation

Published by Alejandro Bande, Edward R. Sobel, Alexander Mikolaichuk and Verónica Torres Acosta (2015) in Brunet, M.-F., T. McCann and E.R. Sobel (eds): Geological Evolution of Central Asian Basins and the Western Tien Shan Range. Geological Society, London, Special Publications, 427, doi:10.1144/SP427.1

Abstract

Regional strike-slip faults are widely distributed in intracontinental interiors and play a major role in the distribution of far-field effects due to continental collisions. Constraining the deformation history of the Talas-Fergana Fault (TFF), one of the largest of such faults in Central Asia, is vital to comprehend the hinterland kinematics of the India-Asia collision. New apatite fission track results from the northwest Tien Shan define a rapid exhumation event at ~25 Ma. This event is correlated with a synchronous pulse in the South Tien Shan, implying that both ranges experienced a simultaneous onset of rapid exhumation. We suggest that strike-slip motion along the TFF occurred at ca. 25 Ma, facilitating counter-clockwise rotation of the Fergana basin and enabling transpressional exhumation of the restraining bends. Pamir indentation, located south of the western Tien Shan, is postulated to be underway by ~20 Ma. Recently published results show synchronous strike-slip deformation in the western Tarim basin and eastern flank of the Pamir. Based on our results and published data we are able to connect Tarim and Pamir deformation to the onset of TFF slip. We suggest that this preexisting regional structure was responsible for transfering Pamir-induced shortening to the northwestern Tien Shan.

2.1 Introduction

The Tien Shan is a ca. 2500 km long range with peaks up to 7400 m extending from Uzbekistan and Kyrgyzstan far into western China (Fig. 2.1). It is one of the best examples of an intracontinental orogen and has been intensively studied to understand the far-field effects of continental collision (e.g. *Molnar & Tapponnier* 1975, *Allen et al*. 1991, *Hendrix et al.* 1994) and the role of pre-existing discontinuities in a deforming orogen (e.g. *Jolivet et al.* 2010; *Selander et al.* 2012; *Macaulay et al.* 2013). However, most of the scientific efforts have been focused on the Eastern (Chinese) Tien Shan (e.g. *Allen & Vincent* 1997; *Yin, et al.* 1998; *Dumitru et al.* 2001; *Chen et al*. 2007; *Sun et al*. 2009) and the Central (Kyrgyz) Tien Shan (e.g. *Abdrakhmatov et al*. 1996; *Cobbold et al.* 1996; *Sobel et al. 2006*a and b; *De Grave et al*. 2011; *Macaulay et al*. 2014); far less research has been published on the Cenozoic tectonic evolution of the Western (Kyrgyz)

Tien Shan. Note that the Chinese literature typically subdivides the Tien Shan differently (e.g., *Wang et al*. 2011).

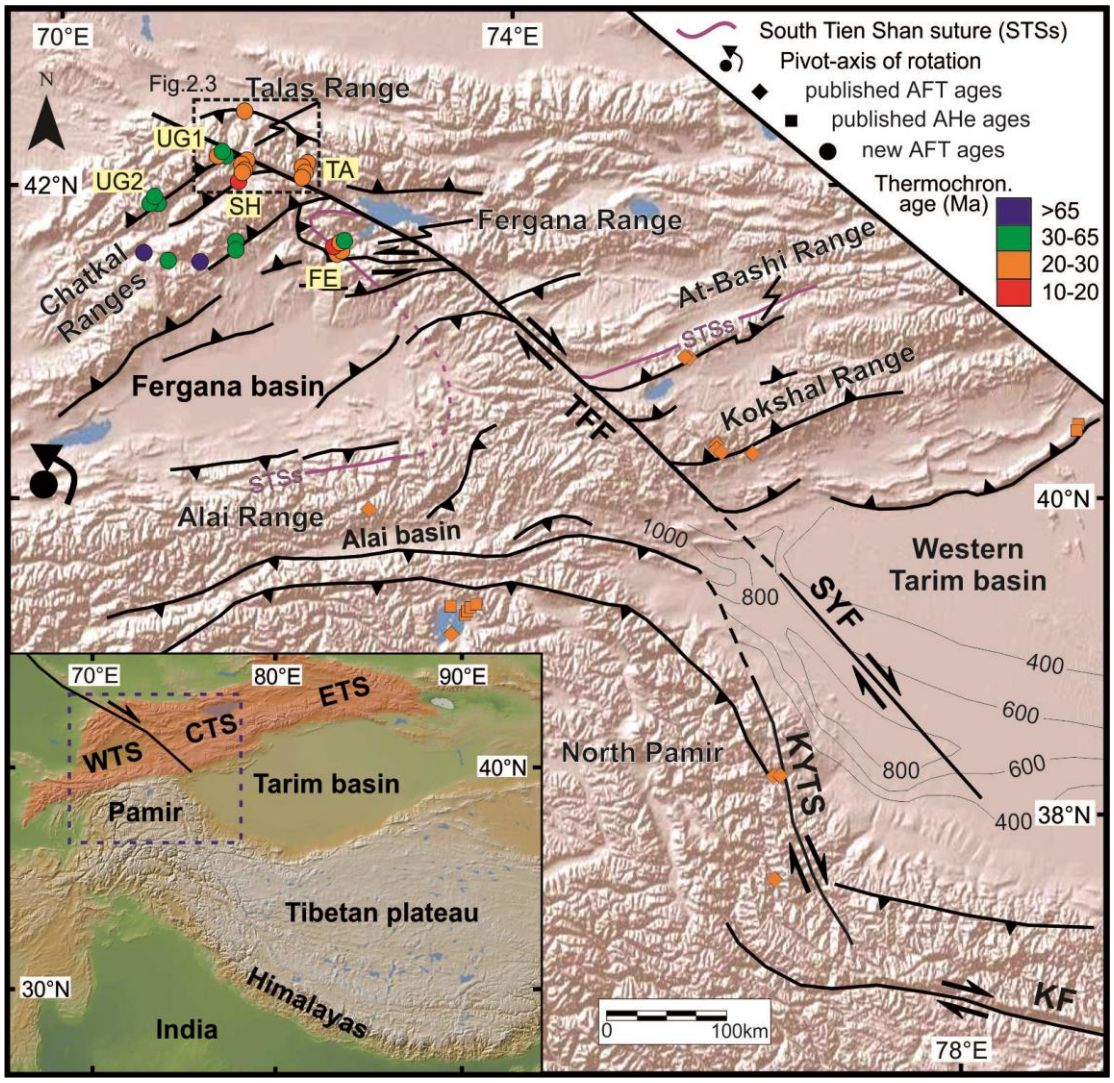

Figure 2.1 Shaded relief image of the Tien Shan and Pamir with superimposed major structures, isopach contours for the late Oligocene–early Miocene Kezilouyi Formation and thermochonological data. Solid circles reflect new AFT ages, diamonds available published AFT data and squares available published apatite (U–Th)/He ages; colours denote ages based on the shown scale. Only published ages between 20 and 30 Ma are displayed to highlight the locations where an Oligo-Miocene exhumational event was recorded. Labels in light yellow are vertical profile locations. Thermochronology ages are from *Sobel & Dumitru* (1997), *Schmalholz* (2004), *Sobel* **et al.** (2006*a*), *Amidon & Hynek* (2010), *Glorie et al. (*2011), *De Grave et al.* (2012), *Chang* **et al.** (2012) and this study. Structures modified from *Vlasov et al.* (1991), *XBGMR* (1993), *Bakirov* **et al.** (2001) and *Cowgill* (2010). Isopachs contours from *Hao et al.* (2002). Black point with large arrow shows Fergana Basin pivot-axis of rotation (*Thomas et al.* 1993). South Tien Shan suture (STSs) drawn in purple. Dashed box shows location of Figure 2.3. Inset map shows location of Figure 2.1 in the Himalayan–Central Asian region. Transparent burnt polygon orange in inset shows the location of the Tien Shan Range. WTS, Western Tien Shan; CTS, Central (Kyrgyz) Tien Shan; ETS, Eastern (Chinese) Tien Shan; TFF, Talas–Fergana Fault; SYF, Shache–Yangdaman Fault; KYTS, Kashgar Yecheng Transfer System; and KF, Karakax Fault.

The ~2000 km long Talas-Fergana Fault (TFF) is one of the best examples of a reactivated intracontinental strike slip fault; it forms the most prominent morphologic feature within the Western Tien Shan. Within continental interiors, strike-slip faults often move in response to distal plate collisions and have long histories punctuated by episodic reactivation (e.g., *Burtman et al.* 1996; *Gilder et al.* 1999; *Yin et al.* 2002). Constraining the spatio-temporal distribution of activity along such faults is crucial for understanding how oblique deformation is accomodated in transpressional settings. In the last decade, bedrock exhumation has been used as a powerful tool to quantify transpressive deformation (e.g., *Spotila et al.* 2007; *Niemi et al*. 2013). In strike-slip settings, restraining bends and horsetail splays accommodate local contraction and focus transpressional deformation (e.g., *Cunningham & Mann* 2007); hence, these present an optimal target for constraining the timing of transpressive deformation.

The past few years has seen a spate of new studies focused on the geologic and geodynamic understanding of the Pamir (e.g. *Cowgill* 2010; *Schmidt et al.* 2011; *Sippl et al.* 2013; *Sobel et al.* 2013). However, the area just to the north, the Pamir-Alai basin-Tien Shan junction, has received much less attention than other parts of the India-Asia collision zone. On the other hand, these novel contributions have focused on the development of the Pamir and rarely explore the distal effects of this deformation on the Tien Shan. Although significant shortening was accommodated north of the intracontinental subduction zone (e.g., *Avouac et al.* 1993; *Cobbold et al.* 1996), the timing of these processes in the Western Tien Shan remains obscure. The scale of late Cenozoic geodynamic changes that are proposed for the Pamir area (e.g. initiation of subduction) should have had a direct effect on the development of the Tien Shan.

In this contribution we focus on constraining the timing of Cenozoic deformation in the Western Tien Shan. To do this, we present new low-temperature thermochronology data for the Chatkal, Ugam, Shandalash, Talas and Fergana Ranges (Fig. 2.1). Based on our results and integrating the database with published ages, we evaluate and constrain the onset of Cenozoic exhumation in the Western Tien Shan. The pre-existing TFF had an important role in how shortening was accommodated there, developing horsetail splays at both ends of the TFF. Finally, we integrate recent models of Pamir geodynamics, published data, and our new results to derive a reinterpretation of the kinematic style of deformation in this part of the India-Asia collision zone.

2.2 Geologic setting

2.2.1 Western Tien Shan

In terms of topography, morphology and location the Tien Shan can be separated into three sectors: the Western, Central and Eastern Tien Shan (Fig. 2.1). At the same time, in terms of geologic history, the Western and Central Tien Shan can be divided into the North, Middle and South Tien Shan, mostly based on the Paleozoic evolution. The description and analysis of the Tien Shan Paleozoic history is out of the scope of the present contribution. Comprehensive review papers are available (e.g. *Şengör et al.* 1993; *Wang et al.* 2006a; *Windley et al.* 2007; *Xiao et al.* 2008; *Burtman* 2010). The geologic Tien Shan units trends roughly east - west and are represented across the different topographic Tien Shan units described previously (Fig. 2.1).

The Western Tien Shan and the Central (Kyrgyz) Tien Shan are separated by the NW-SE trending Talas-Fergana Fault (TFF, Fig. 2.1). The present day morphology of the Tien Shan is strongly influenced by Paleozoic and Mesozoic structures. According to many proposed models (e.g., *Şengör et al.* 1993; *Wang et al.* 2006a; *Windley et al.* 2007; *Xiao et al.* 2008; *Burtman* 2010), the Paleozoic Tien Shan represents the amalgamation of a number of terranes that formed distinctive tectonic zones. In the Western Tien Shan, three main tectonic zones can be distinguished by lithology and geologic history. The western termination of the North Tien Shan (NTS) is formed by the Talas mountains. This range predominantly consists of Precambrian and early Paleozoic metamorphosed sedimentary rocks (*Voytenko & Khudoley* 2012). The Middle Tien Shan (MTS) is represented by the Chatkal Ranges and lies in the northern and northwestern part of our study area. In the term Chatkal Ranges we include the Chatkal Range itself, the Shandalash Range and the Ugam Range, all located in the northwestern sector of the Tien Shan mountains. The MTS is composed of Early Paleozoic passive continental margin sedimentary sequences and Devonian-Carboniferous magmatic rocks (*Seliverstov & Ghes* 2001; *Seltmann et al.* 2011). The South Tien Shan (STS) is a late Paleozoic highly deformed accretionary belt (e.g., *Biske & Seltmann* 2010; *Loury et al*., 2015). Ophiolites and related metamorphic rocks delineate a major late Carboniferous suture zone (e.g., *Hegner et al*., 2010) (South Tien Shan suture) along the southern margin of the Paleozoic Kazakh continent (*Burtman* 1975). The STS has been displaced by the right lateral TFF, forming a regional sigmoid (*Lesik & Mikolaichuk* 2001) and constitutes the southern (Alai Range) and eastern

(Fergana Range) sectors of the Western Tien Shan (*Burtman* 1975). Late Paleozoic strike-slip displacement primarily occurred during the Permian, when the whole Tien Shan experienced significant transpressional deformation (*Bazhenov & Mikolaichuk* 2004; *Alexeiev et al.* 2009; *Konopelko et al.* 2013; *Rolland et al.* 2013).

During the Mesozoic and early Cenozoic, parts of the Tien Shan were periodically reactivated in response to distal collisions (e.g. *Hendrix et al*. 1992; *Sobel & Dumitru* 1997; *Dumitru et al.* 2001). In the Western Tien Shan, transtensional basins formed along the TFF during the Jurassic, and accommodated thick sedimentary successions associated with significant accumulation of organic-rich clastic deposits (e.g. *Burtman et al.* 1996; *Sobel* 1999; *Allen et al.* 2001). Unfortunately, the extent and magnitude of Cretaceous deformation remains poorly understood in the Western Tien Shan. However, the adjacent Central (Kyrgyz) Tien Shan experienced >100 Myr period of tectonic quiescence during the late Mesozoic and early Cenozoic (*Afonichev & Vlasov* 1984; *Bullen et al.* 2003; *Sobel et al.* 2006b; *De Grave et al.* 2011; *Glorie et al.* 2011; *Macaulay et al.* 2013). This event is registered by low relief unconformities exposed at high elevations and used as structural markers of the subsequent Cenozoic deformation (e.g., *Cobbold et al.* 1996, *Macaulay et al.* 2013). In our study area, a clear example of this surface is present on the northern slope of the Chatkal Range.

During the early Cenozoic, regionally well-correlated marine transgressions occurred in the Paleocene – Eocene (*Bosboom* 2013; *Bosboom et al*. 2015 and refs therein). These transgressions are linked to the Paratethys sea that was open to the west, including the Amu Darya, Tajik, Fergana and Tarim basins in Central Asia (*Popov et al*. 2004). The Cenozoic fill of the Fergana basin is up to 8 km thick in the central part of the basin (*Clarke* 1984). Outcrops of Cenozoic sediments are much thinner along the basin borders. In the northern part of the basin, the outcropping section is around 1.2 km thick, mostly comprised of the Massaget Formation (~ 800 m). This unit is characterized by upward coarsening and thickening nonmarine red beds (Fig. 2.2). Massaget strata are strongly tilted to the south (~75°) and are cut by an impressive subhorizontal angular unconformity. The age of the Massaget Formation was traditionally considered to be Oligo-Miocene (Pg^3 -N^1_{ms}) (*Artyomova et al*. 1971). This determination is based on unconformable relations on both the top and bottom of the unit and regional correlations. Recent biostratigraphic work (*Bosboom* 2013; *Bosboom et al*. 2015 and refs therein) confirms a late Eocene age for the uppermost part of the

immediately underlying Fergana Group (Fig. 2.2), supporting the previous age estimates. The Pliocene? Baktriy Formation unconformably overlies the Massaget Formation. Similar time-transgressive syn-tectonic sequences have been described in the NW Tarim basin (e.g., *Heermance et al*. 2008) and in the Issyk Kul basin (*Macaulay et al*. 2014, *Wack et al*. 2014).

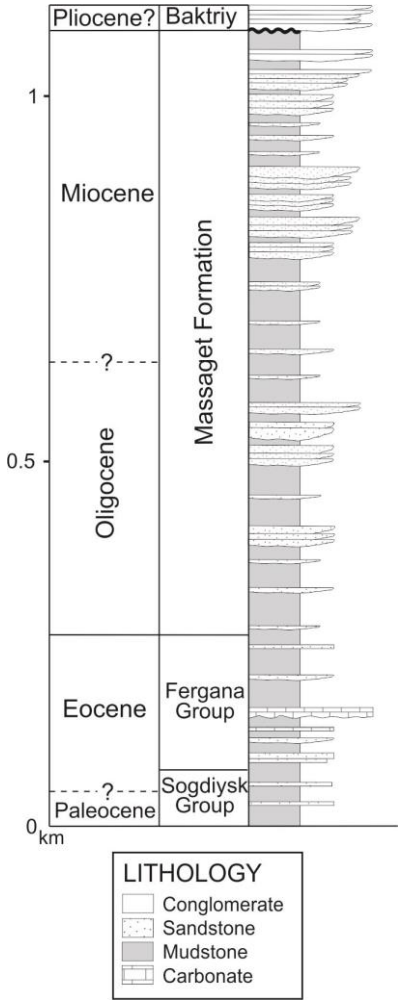

Figure 2.2. Generalized Cenozoic stratigraphic section of the northern Fergana Basin. Section simplified from log measured at the NE corner of the basin.

2.2.2 The Talas-Fergana strike-slip Fault (TFF)

The TFF extends from the western Tarim basin in the southeast to the Turgay basin in the northwest. At ~2000 km long, it is one of the largest intracontinental strike-slip faults on Earth. Traditionally, it is subdivided into two segments, the Karatau segment to the north and the proper Talas-Fergana segment to the south (e.g., *Burtman* 1980; *Rolland et al.* 2013). The TFF formed in the late Paleozoic – Early Mesozoic (*Burtman* 1980; *Alexeiev et al.* 2009; *Konopelko et al.* 2013; *Rolland et al.* 2013) and was reactivated in the Jurassic and Cenozoic (*Bazhenov* 1993; *Burtman et al.* 1996;

Sobel 1999; *Allen et al.* 2001; *Konopelko et al.* 2013; *Rolland et al.* 2013). The maximum net displacement along the TFF reaches ~200 km, based on the offset of the Carboniferous South Tien Shan suture (STSs) (Fig. 2.1) and related units (*Burtman* 1980).

During the Cenozoic, displacement only occurred along the southern segment of the fault (*Thomas et al*. 1993). The overall magnitude of Cenozoic displacement is poorly constrained. The apparent offset of Cretaceous conglomerates with similar compositions suggests ~60 km of displacement (*Verzilin* 1968; *Burtman et al*. 1996). *Thomas et al*. (1993) suggested a Cenozoic displacement of 100 ± 60 km along the TFF based on vertical-axis rotation measured on Tertiary red beds in the Fergana basin. Given the triangular shape, the counter-clockwise sense of rotation of the Fergana basin and the Cenozoic displacement measured on the TFF, many authors proposed that much of slip on the TFF was absorbed by crustal thickening in the Chatkal Range (*Cobbold & Davy* 1988; *Thomas et al*. 1993; *Burtman et al*. 1996; *Zubovich et al*. 2010). According to *Burtman* (1980) and *Trifonov et al*. (1992), around 10 km of displacement occurred since the Pleistocene based on the offset of geomorphic markers. However, geodetic GPS shows very slow (< 2 mm/yr) active slip (*Zubovich et al*. 2010).

The southern termination of the Cenozoic TFF has long been considered to lie in the Kokshal range, which comprises a portion of the South Tien Shan (STS). AFT data from the Kokshal and At-Bashi ranges show that exhumation and hence deformation was underway by ~25 Ma (*Sobel et al*. 2006a; *Glorie et al*. 2011). A sequence of magnetostratigraphically-dated growth strata show that shortening in this area propagated rapidly southward into the Tarim basin between 16.3 and 13.5 Ma (*Heermance et al*. 2008).

Recently, a southern prolongation of the TFF has been described from the subsurface of the Tarim basin (*Wei et al*. 2013). Seismic reflection data show flower structures aligned across this lineament, which is named the Shache-Yangdaman right-slip Fault (SYF). This structure was active syn-depositionally with the Wuqia group (late Oligocene – late Miocene), which is subdivided into three formations: Kezilouyi, Anjuan and Pakabulake. Facies analysis and isopach patterns suggest that a 6-km-thick transtensional basin (Yecheng subbasin) formed in between the SYF and the dextral slip Kashgar Yecheng Transfer System (KYTS). Subsidence possibly commenced during deposition of the poorly dated late Oligocene – early Miocene Kezilouyi

Formation (*Hao et al*. 2002); and was certainly rapid from 21-17 Ma during deposition of the Anjuan Formation (*Wang et al*. 2006b). Accumulation in the basin continued during middle to late Miocene with deposition of the over 3 km-thick Pakabulake Formation (*Wei et al*. 2013). The Anjuan and lower Pakabulake Formations include deep water turbiditic lacustrine strata in the subsurface (*Zhou et al*. 1984), suggestive of a deep, localized, rapidly subsiding pull-apart basin (*Wei et al*. 2013). The seismic data suggests that the structure became inactive and then was briefly reactivated during deposition of the Pliocene (?) Xiyu Formation. The structure is now inactive and buried beneath thick Quaternary deposits, explaining why its significance had not previously been appreciated.

2.3 Methodology and samples

2.3.1 Apatite fission track (AFT) rationale

This method relies on the fact that fission-tracks form at a constant rate from the spontaneous fission of ^{238}U and are subsequently shortened and may eventually disappear at temperatures above ca. 110°C (e.g., *Gallagher et al.* 1998). As a result, the track length distribution is a sensitive monitor of a crystal's thermal history. Significant annealing occurs between ca. 60-110°C, the partial annealing zone (PAZ). Where rocks were buried to sufficient depth that the temperature exceeds the total annealing temperature (*Ketcham et al.* 1999), the fission track clock was reset to zero and fission track data record information on the time-temperature cooling path of the sample as it cooled below this temperature during subsequent exhumation (e.g. *Green et al.* 1989). Track-length data are useful because they allow comparisons with forward modeling of the thermal histories (e.g., *Ketcham* 2005).

2.3.2 AFT methodology

AFT analysis was carried out on 26 samples; horizontal confined fission track lengths were measured in 25 of these. Kinetic properties were assessed for every crystal counted or containing confined tracks by measuring at least 4 D_{par} (*Donelick et al.* 2005) that were averaged and corrected following *Sobel & Seward* (2010). AFT ages were calculated following the procedures of *Galbraith* (1981) using the MacTrackX software. Most AFT ages are based on ca. 20 grains. However, 3 samples contained less than 16 countable grains, resulting in AFT ages with larger errors. Ages are reported as pooled ages (±1σ) because they all pass the Chi-squared test (=>5%). As many

horizontal confined fission tracks (tracks-in-tracks) as possible were measured. To increase the number of measured horizontal confined tracks, additional mounts of 16 samples were irradiated with heavy ions (*Jonckheere et al.* 2007). The complete dataset and the detailed methodology description is included in the supplementary material (Table A1.1); the data is summarized in Table 2.1.

Sample	Latitude (N°)	Longitude (E°)	Elev. (m)	n[a]	**Age (Ma)**	**±1σ**	# lengths[b]	Length (μm)	SD[c] (μm)
				Talas Range					
10TR02	42,163	72,040	2571	20	**22**	**3**	104*	13,6	1,5
10TR03	42,138	72,041	2678	20	**23**	**2**	2	15,4	0,4
10TR04	42,109	72,043	3120	20	**25**	**3**	5*	10,6	2,1
10TR05	42,122	72,037	2921	20	**25**	**3**	71*	11,7	2,1
10TR17	42,459	71,534	1269	19	**25**	**2,8**	13*	13,6	1,7
				Ugam Range					
10UM12	42,233	71,407	3456	18	**52**	**3**	101	12,8	1,5
10UM14	42,240	71,410	2082	7	**28**	**3**	15	12,9	1,4
10UM15	42,242	71,413	2945	17	**38**	**4**	9	12,2	1,5
10CA26	41,887	70,852	3161	8	**41**	**4**	7	12,0	1,9
10CA27	41,881	70,854	2953	21	**44**	**3**	101*	11,8	1,9
10CA29	41,875	70,863	2535	19	**30**	**2**	106	11,5	1,8
				Shandalash Range					
10TR19	42,199	71,586	2978	19	**30**	**2**	19	11,6	2,3
10TR20	42,186	71,574	2815	20	**27**	**4**	13*	11,8	2,0
10TR21	42,184	71,570	2778	20	**25**	**3**	49	12,2	2,4
10TR22	42,129	71,558	2458	19	**26**	**3**	28*	11,6	2,6
10TR23	42,120	71,547	2,71	17	**11**	**2**	4	13,0	2,4
				Chatkal Range					
10CK34	41,574	70,699	1763	20	**124**	**7**	101*	12,8	1,5
10CK37	41,497	71,024	1762	20	**54**	**4**	56	12,1	1,9
10CK41	41,438	71,227	1369	20	**120**	**7**	105*	11,7	1,9
10CK43	41,584	71,527	1874	16	**51**	**6**	14*	12,5	1,7
10CK44	41,566	71,529	1695	20	**65**	**5**	37*	12,2	2,1
				Fergana Range					
10SU67	41,531	72,332	922	7	**19**	**6**	ND	ND	ND
10SU65	41,613	72,364	2578	20	**21**	**2**	101*	13,2	1,4
10SU61	41,590	72,329	1985	20	**16**	**2**	100*	11,6	1,9
10SU62	41,609	72,356	2386	20	**24**	**2**	101*	13,2	1,7
10SU64	41,623	72,368	2767	19	**43**	**3**	105*	12,4	1,9

Note: All samples counted by AB (zeta=369.5 ± 7.9, unpub. 2012)
[a] number of individual crystals dated.
[b] Asterisk (*) indicates track lengths measured from heavy ions irradiation slide.
[c] Standard deviation of measured lengths.

Table 2.1Summary of apatite fission track data

2.3.3 Age-elevation relationships (AERs)

AERs of samples collected at regular intervals along steep topographic profiles are commonly used to date increases in exhumation and quantify exhumation rates (e.g. *Gallagher et al.* 2005). Typically, an increase in exhumation rate will result in a break-in-slope on an age-elevation plot (e.g. *Fitzgerald et al.* 1995), providing the chance of constraining the onset of that event. When possible we sampled following vertical profiles. We also collected spot samples to extend the areal coverage and spatial distribution of our dataset. Vertical profiles and spot samples will be addressed below in the geographic context of the respective ranges.

2.3.4 Thermal modeling

Thermal modeling was performed on 15 samples using the HeFTy (v.1.7.5) program (*Ketcham* 2005). This software models individual sample's time-temperature history by generating synthetic data, which is then compared to the observed data and evaluated using Kuiper's statistics (*Ketcham* 2005). The main aim of the modeling was to identify and date cooling rate variations. Input for the models includes AFT ages, D_{par} values, track lengths, and the angle between each track and the crystallographic c-axis. Models were first run with minimal constraints. In cases where apparent inflection points were depicted, constraint boxes were set and shifted to test the model's goodness and reliability. Selected model results are presented below.

2.4 Results

Significant variations in thermochronological age distribution are found between ranges (Figs. 2.1 and 2.3). In the following sections we will discuss these variations systematically, starting from the north and moving towards the south.

2.4.1 Talas Range

In this range we collected a 4 sample vertical profile (TA, Fig. 2.1) near the headwaters of the Besh-Kol river, located just east of the TFF (Fig. 2.3). We sampled Proterozoic metasedimentary rocks over a vertical range of 550 m. AFT ages are tightly clustered between 25.4 ± 2.9 and 22 ± 3.1 Ma. The highest elevation sample (10TR04) presents the shortest mean track length (10.6 μm) and all samples pass the Chi-squared test.

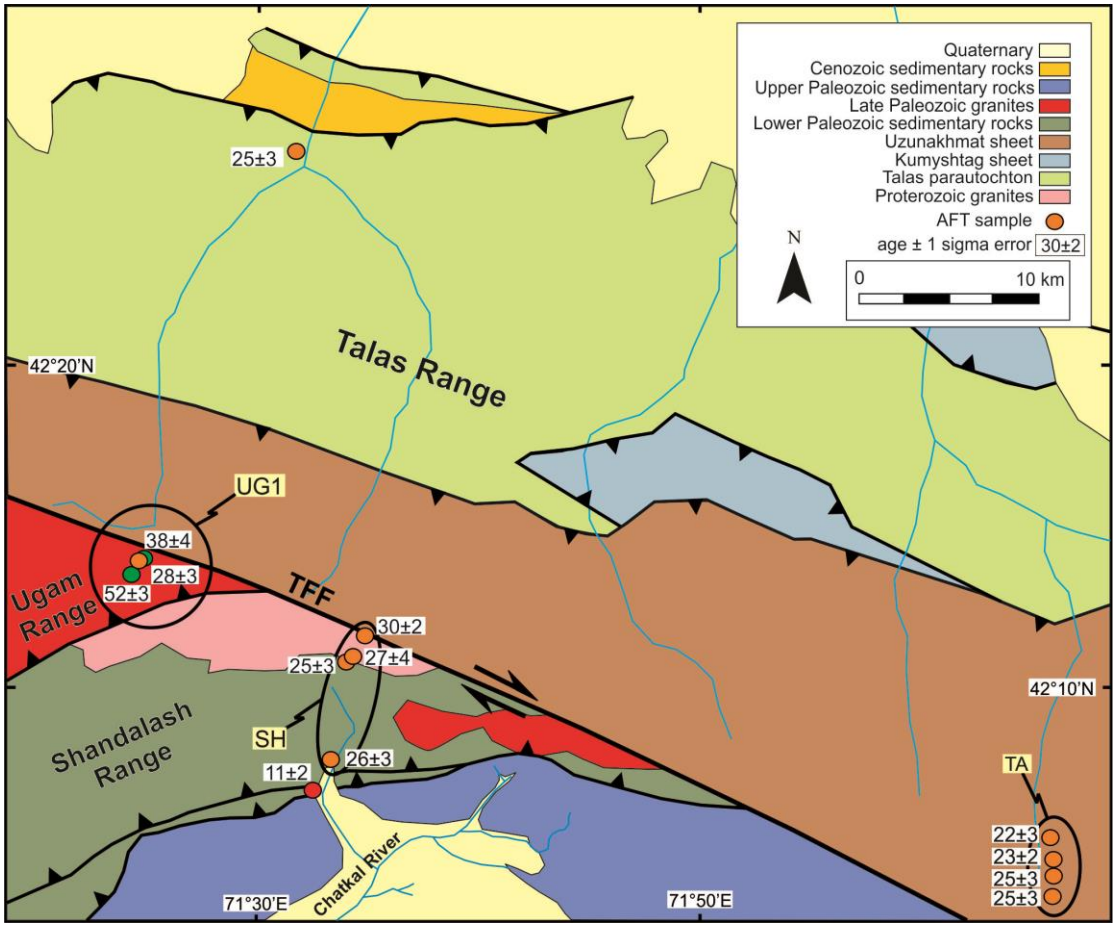

Figure 2.3Geological and tectonic map of the northwestern Tien Shan (modified from *Bakirov et al.* 2001 and *Voytenko & Khudoley* 2012) showing locations of new AFT samples; colours denote ages based on same scale as Figure 1; ages with 1s errors (in Ma) are in white boxes. Labels in light yellow are vertical profile locations

The AER (Fig. 2.4A) of these does not reveal a break-in-slope to define the onset of rapid cooling. This is probably related to the limited relief found in this zone. However, the clustering of ages across 550 m of elevation (Table 1) and the moderately steep slope of 0.14 mm yr-1 of the AER point to a relatively rapid exhumation event around the Oligo-Miocene for the Talas range. Moreover, time-temperature histories derived from thermal modeling (Fig. 2.4) of ages, track-length distributions, and Dpar (Table 1) of two samples from the Talas Range profile help to constrain the onset of rapid cooling. Thermal modelling of the bottom sample (10TR02, Fig. 2.4C) shows a rapid cooling event starting by 22 Ma; together with long confined lengths (13.6 µm), this implies that it is a fully reset sample. In comparison, sample 10TR05, from 350 m higher, has shortened lengths (11.7 µm) and the time-temperature paths better defines a younger rapid cooling episode (Fig. 2.4B).

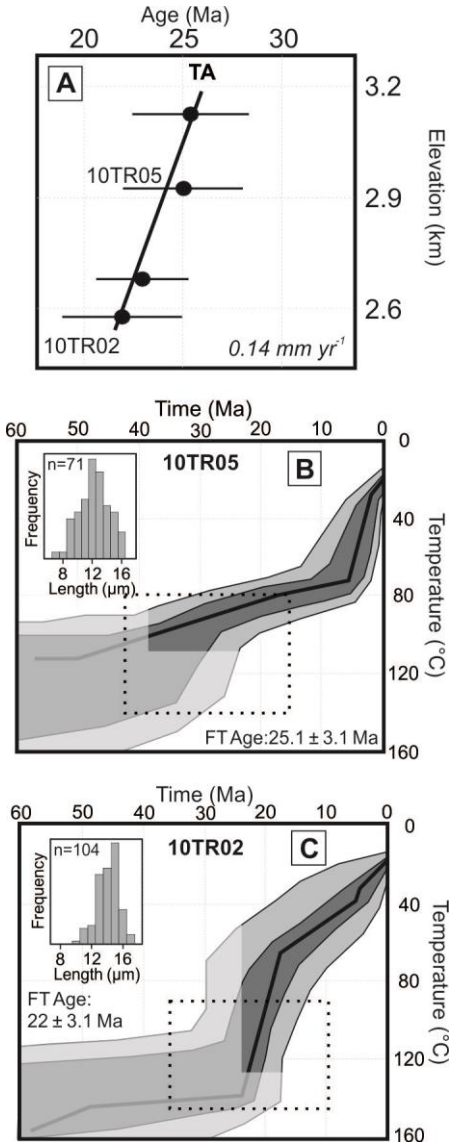

Figure 2.4(A) AERs from the Talas Range vertical profile. Age errors are 1sigma. Apparent exhumation rate based on the gradient of the AER trendline and shown in italics. (B and C) Time–temperature histories obtained by thermal modelling using HeFTy software (*Ketcham* 2005) of samples 10TR02 and 10TR05, respectively. Unconstrained part of the models represented by transparent polygons. Dashed boxes are model input constraints. Inset shows histogram of track-length distribution.

We interpret the latter as a partially reset sample located at the very bottom part of the PAZ. Therefore, between these two samples we can place the lower section of the PAZ, providing a robust constrain of the initiation of rapid exhumation in the Talas Range at 23 ± 3 Ma. Modeling of sample 10TR05 also shows a younger (~ 5 Ma) event, but that modeled episode is not robust because is based in a just a few long track lengths. The lack of an obvious kink in the age-elevation plot is likely due to the exhumation rate and the size of the profile. To complete the picture, a fifth sample comes from the northernmost sector of the Talas Range, in the hanging-wall of the S-SW dipping frontal thrust. This sample yielded an AFT age of 25.2 ± 2.8 Ma with relative long track lengths

(13.6 μm), suggesting a fully-reset sample that was cooling rapidly during the latest Oligocene-early Miocene.

2.4.2 Chatkal Ranges

In this section we will present 16 new AFT ages from the Ugam, Shandalash and Chatkal Ranges, all located west of the TFF in the Western Tien Shan. We sampled the Ugam Range in two sectors: one close to the TFF (UG1, Fig. 2.3) and a second one (UG2, Fig. 2.1) ~65 km along strike to the SW. Both profiles are in the hanging-wall of the same structure. In the first group, we collected 3 samples from Upper Paleozoic granites (Fig. 2.3). This location contains the northernmost samples in this study, distributed between 3456 m and 2082 m in elevation. The AFT ages range between 51.5 ± 2.8 and 27.5 ± 3.2 Ma, without a clear break-in-slope. However, the bottom sample (10UM14) has the youngest age and the longest mean track length value (12.9 μm) as expected for a sample located at a relatively lower section of an exhumed PAZ. The age (27.5 ± 3.2 Ma) is comparable to the higher-elevation samples from the neighboring Talas Range (23 ± 3 Ma), suggesting that sample 10UM14 also represents the very bottom part of the PAZ. Therefore, we conclude that the Ugam Range samples represent an uplifted PAZ with no analyzed totally reset ages. In turn, this suggests that this range has experienced less exhumation than the Talas Range.

At vertical transect UG2, we collected samples from a Carboniferous granitic pluton thrust on top of Cenozoic sedimentary rocks. Three samples distributed over a vertical separation of 626 m yielded apatite grains. The AFT ages range between 43.6 ± 3 and 30.1 ± 2.3 Ma. The mean track-length values are spread between 11.5 and 12 μm. The AFT ages together with the shortened track length values suggest that the samples spent significant time in the PAZ and were not fully-reset during the Cenozoic. Compared to the UG1, the UG2 samples represent a shallower portion of the PAZ and therefore the exhumation in this area is less significant.

The vertical profile (SH, Fig. 2.1) in the Chatkal zone lies on the south side of the Shandalash range, between its crest and the Chatkal River (Figs. 2.3 and 2.5A). In this section, Proterozoic and Lower Paleozoic rocks are thrust on top of Upper Paleozoic units. We collected 4 samples from Proterozoic granites and Cambrian tillites in this structural block (Fig. 2.4A). The AFT ages group between 24.5 ± 2.6 and 29.8 ± 2.4 Ma. The clustering of four ages across ca. 550 m of elevation together with the moderately steep slope (0.14mm yr-1) of the AER (Fig. 2.5A) point to a rapid

exhumation event occurring around the Oligo-Miocene boundary. Although this vertical profile lies to the west of the TFF, the data are remarkably similar to that derived from profile TA in the Talas Range, east of the TFF. The similar apparent exhumation rates of these two profiles is likely caused by similar tectonic rates and erosional processes. We collected a fifth sample in Devonian sedimentary rocks north of the Chatkal River, south of the other four samples (Fig. 2.3). However, this sample lies in a different structural block and shows a significantly younger AFT age (11 ± 2 Ma) and longer mean track-length value (13 μm). Therefore, we interpret it as a fully-reset age reflecting a Late Miocene exhumational event, propagating deformation locally to the south. Although we have little data reflecting this relatively young event in our study area, it is broadly represented in the Central Kyrgyz Tien Shan (*Bullen et al*. 2003; *Sobel et al*. 2006b; *Macaulay et al*. 2013).

Finally, we collected 5 spot samples along the Chatkal Range distributed roughly along a transect perpendicular to the tectonic strike (Fig. 2.1). A north-dipping erosional surface can be traced on the northern side of the Chatkal Range. Samples collected in this area from Carboniferous granites and Lower Paleozoic gneisses yield Mesozoic (124±7 and 120±7 Ma) AFT ages with relatively large mean track-length values (12.8 μm). Thermal modeling of sample 10CK34 (Fig. 2.5B) suggests that these ages represent the tail end of a Late Mesozoic cooling event followed by a limited younger cooling episode. Those samples might reflect the same Late Mesozoic cooling event that is present in other parts of the Tien Shan (e.g. *Dumitru et al*. 2001; *Jolivet et al*. 2010; *Glorie et al*. 2011, *De Grave et al*. 2011). After this event, samples spent around 100 Ma at 60 – 70°C in the PAZ until an increase in the exhumation rate roughly around 25 Ma cooled them to surface temperature. Finally, we collected samples on the southern slope of the Chatkal Range from Devonian sandstones in the hanging-wall of the main south vergent thrust. These samples yield early Paleogene (65±5 and 51±6 Ma) AFT ages and pass the Chi-squared test. These are partially reset ages representing the exhumed PAZ located in southern slope.

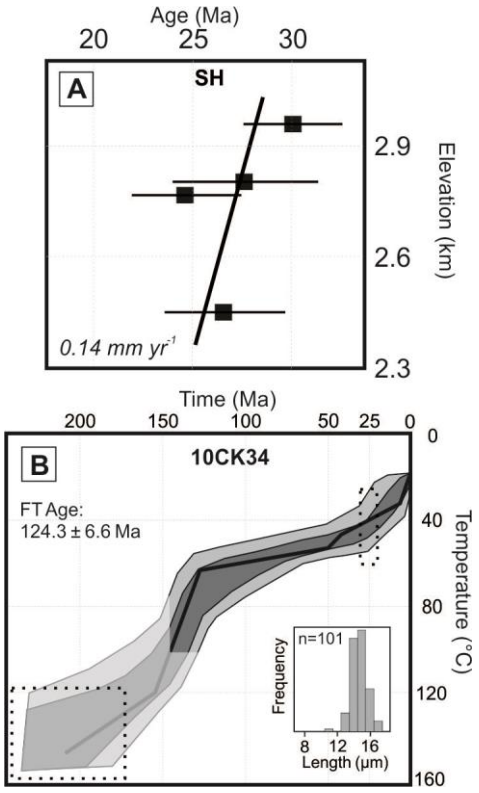

Figure 2.5(A) AERs from the Shandalash Range vertical profile. Age errors are 1 sigma. Apparent exhumation rate based on the gradient of the AER trendline and shown in italics. (B) Time–temperature histories obtained by thermal modelling using HeFTy software (*Ketcham* 2005) of samples 10CK34, collected in the axial zone of the Chatkal Range; this sample is not included in SH vertical profile. Unconstrained part of the model represented by transparent polygons. Dashed boxes are model input constraints. Inset shows histogram of track-length distribution.

2.4.3 Fergana Range

We sampled the range in its north-western sector (Fig. 2.1). The northern Fergana Range is crossed by a left-lateral strike-slip fault that merges with a thrust fault dipping to the east (*Kalmetieva et al.* 2009). The latter thrust places Paleozoic sedimentary rocks on top of Cenozoic sediments. We collected 5 samples from an 1845 m vertical profile (FE, Fig. 2.1 and 2.6A) from Late Paleozoic units. AFT Ages range between 16 ± 2 and 43 ± 3 Ma. All samples pass the Chi-squared test, representing single populations. The AER (Fig. 2.6A) presents a classic kinked profile. The bottom 4 samples are relatively young and form a steep area reflecting a high exhumation rate (0.19 mm yr^{-1}). The uppermost sample does not follow this trend; it is significantly older and probably represents the base of the PAZ. At first sight, one of the lower samples (10SU61) is too young for this trend (Figure 2.6A). However, this sample has a smaller D_{par} value than the other samples. The D_{par} value is a measure of the annealing kinetics of the apatite grain (*Donelick et al.* 2005); lower D_{par} values indicate low annealing resistance (*Carlson et al.* 1999) and hence yield younger ages. Because sample 10SU61

is less resistant to annealing, it has a younger age than the adjacent, more annealing-resistant samples.

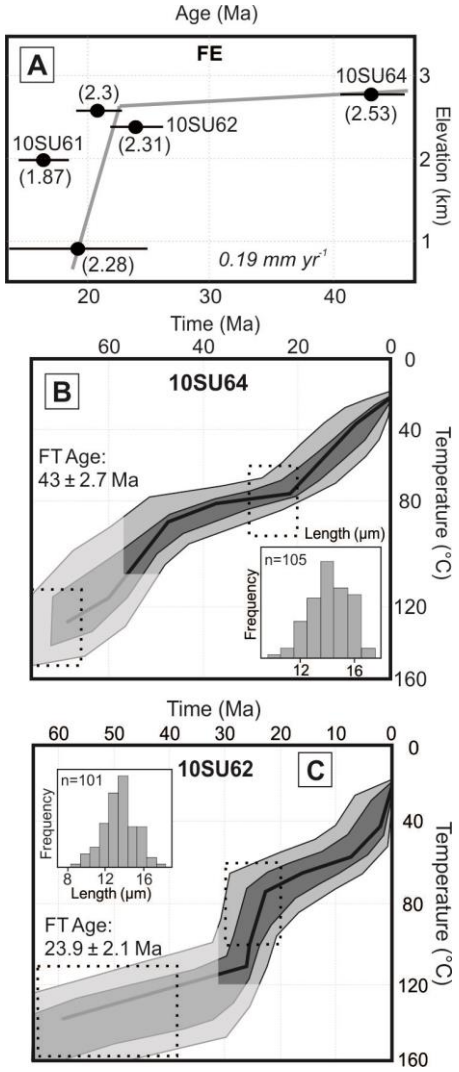

Figure 2.6(A) AERs from the Fergana Range vertical profile. Age errors are 1s; numbers between brackets are D_{par} values. Apparent exhumation rate based on the gradient of the AER trendline and shown in italics. (B and C) Time–temperature histories obtained by thermal modelling using HeFTy software (*Ketcham* 2005) of samples 10SU64 and 10SU62, respectively. Unconstrained part of the models represented by transparent polygons. Dashed boxes are model input constraints. Inset shows histogram of track-length distribution.

The relation of the 5 samples in the AER draws a well-defined break-in-slope dating the exhumational increase at ca. 23±3 Ma (Fig. 2.6A). Thermal modeling from the highest sample (Fig. 2.6B) shows a slightly linear path with a subtle break in the slope at around 20 Ma. Thermal modeling yields time-temperature paths from sample 10SU62 (Fig. 2.6C) showing slow cooling in the Paleogene with a major increase in cooling rate at ca. 25 Ma This event is relatively short and slow cooling is reestablished after 20 Ma. These models confirm the interpretation based on the AER, placing an

increase in the cooling rate at 25 ± 3 Ma. This event correlates well with the contemporaneous deformation to the north described in the previous sections.

2.4.4 Interpretation

AFT ages and thermal modeling of the Talas Range samples show that the range was rapidly being exhumed by the latest Oligocene, both near the TFF and at its northern termination. Based on this data and the geometrical relation of the TFF and the structural lineaments of the Talas Range (Fig. 2.3), we interpret the zone to be a pop-up structure kinematically-related to the TFF. Many of the NE-vergent thrust faults in the Talas Range, including the frontal thrust, might be curvilinear concave-down reverse faults that steepen at depth (e.g. *McClay & Bonora*, 2001) rooting into the TFF. Similar structures are described in the Central (Kyrgyz) Tien Shan (e.g. *Selander et al*. 2012; *Macaulay et al*. 2013). This relation implies that the exhumation of the Talas Range is mostly controlled by a coupled strike-slip/thrust system.

The form of the Shandalash Range vertical profile (SH, Fig. 2.1 and 2.5A) suggests a rapid exhumation event commencing near the Oligo-Miocene boundary. In this sector, the geometrical relationship of the reverse faults with the main TFF (Fig. 2.3) supports the interpretation that the eastern Chatkal Ranges formed as horsetail splays connected to the TFF. Moreover, the timing of exhumation given by vertical profile SH is contemporaneous with the deformation in the Talas area, suggesting that strike-slip movement along the TFF is responsible for the uplift of the Talas pop-up structure and the development of horsetail splays in the Ugam, Shandalash and Chatkal Ranges.

In the Chatkal area the maximum exhumation is found close to the TFF. AFT ages and thermal modeling from the Ugam Range samples show that only the structural depth corresponding to the PAZ has been exhumed; no fully reset samples representing larger amounts of exhumation have been analyzed from this area. Moreover, comparing samples along strike, we can conclude that the amount of exhumation decreases while moving away from the TFF. This might be related to a lateral gradient of slip on the horsetail splays, with only limited slip to the SW and increasing towards the NE. This gradient is actually an exhumation gradient. The further from the rotation pivot point, the more shortening needed to accommodate in the Chatkal ranges.

In the Chatkal Range itself, AFT ages become relatively younger towards the southern side of the range (65 and 51 Ma), representing progressively deeper portions

of an exhumed PAZ, similar to the Ugam Range. Like the Ugam and Shandalash, the Chatkal Range is bounded to the south by a north-dipping fault. As expected, exhumation is higher close to the faults. Structurally deeper rocks on the southern side of this range are exhumed to the surface, while to the north, the preserved erosion surface with late Mesozoic AFT ages (120 and 124 Ma) records far less Cenozoic exhumation.

In turn, the Fergana Range sampling site is located near the junction of active strike-slip and thrust faults (Fig. 2.1). Just from this structural setting and the sample locations, it is clear that the exhumation recorded by this vertical section should reflect the combination of strike-slip and dip-slip mechanisms. Furthermore, the timing of exhumation in this area suggested by the AER (Fig. 2.6A) is contemporaneous with the Talas and Shandalash Ranges.

Integrating all of the evidence presented above, we conclude that the north Western Tien Shan experienced a regional deformation episode near the Oligo-Miocene boundary, in which a linked strike-slip\thrust system developed. Strike-slip displacement along the TFF induced several changes: it exhumed the Talas Range as a positive flower structure, exhumed the northern Fergana Range with a combination of strike-slip and reverse faulting, and developed the Ugam, Shandalash and Chatkal horsetail splays with higher exhumation close to the main strike-slip fault, as expected from a linked strike-slip\thrust system. In comparison, exhumation further to the west along the strike of the Chatkal ranges must be dominantly compressional. However, deformation in the entire range should be a response to the same geodynamic driver.

2.5 Discussion

2.5.1 Talas-Fergana Fault Cenozoic chronology

According to *Thomas et al*. (1993), the Fergana basin experienced significant Cenozoic vertical-axis rotation. Paleomagnetic samples from the Oligo-Miocene Massaget Formation sampled at four localities around the basin show 20 ± 11° of counter-clockwise rotation in relation to the stable Issyk Kul area, located to the NE (*Thomas et al.* 1993). This implies that the change in declination happened during or after deposition of the coarsening-upwards Massaget Formation. Certainly the extreme tilting of Massaget beds in the northern sector of the basin suggests a strong tectonic event during deposition of the unit or shortly thereafter. Although the available age

constraints for the Massaget Fm. are limited, the suggested depositional time interval overlaps with the rapid exhumation period proposed for the TFF horsetail splays. Therefore, the published paleomagnetic data and field relations lead us to consider the Massaget Formation as a syn- or pre-tectonic unit. Interestingly, the sediments on top the unconformity are subhorizontal, implying that syn-rotational deformation was almost finished before deposition of the Baktriy Formation or has continued at slower rates since then. This latter interpretation is consistent with modern GPS vector data (*Zubovich et al.* 2010).

The counter-clockwise sense of rotation is consistent with the right-lateral slip of the TFF. Since the Fergana basin is bounded by the TFF, we concur with *Thomas et al*. (1993) that the rotation was absorbed by right-lateral slip along the TFF coupled with shortening in the Chatkal ranges. Our new data suggests that much of this slip occurred during the late Oligocene - early Miocene. The documented onset of exhumation in the STS at ca. 25 Ma (*Sobel et al.* 2006a; *Glorie et al.* 2011) was synchronous with the exhumation that we have constrained at the Talas and Shandalash ranges. Even though the NW Tien Shan lies ca. 400 km away from the Kokshal and At-Bashi Ranges, they all have a synchronous Cenozoic onset of exhumation. This situation could be explained if the localities are kinematically connected. We propose that both the north Western Tien Shan and STS east of the TFF are horsetail splays connected to the main strike-slip fault. We suggest that slip along the TFF was responsible for inducing exhumation at the proposed horsetail splays (Fig. 2.7). Moreover, the coincidence of pre-existing Paleozoic and Mesozoic structures with Cenozoic activity of the TFF implies that reactivation of favorably oriented structures must play a substantial role in how deformation was accommodated and how efficiently it was transmitted to the north.

Frequently, the initiation of horizontal strike-slip motion is hard to date because it does not produce substantial exhumation. However, in this case, the small size of the rotating block and the close proximity of the rotational pivot-axis (Fig. 2.1) mean that strike-slip movement and compression are expected to be synchronous with the onset of rotation. This local configuration allows us to date the initiation of strike slip displacement at ca. 25 Ma.

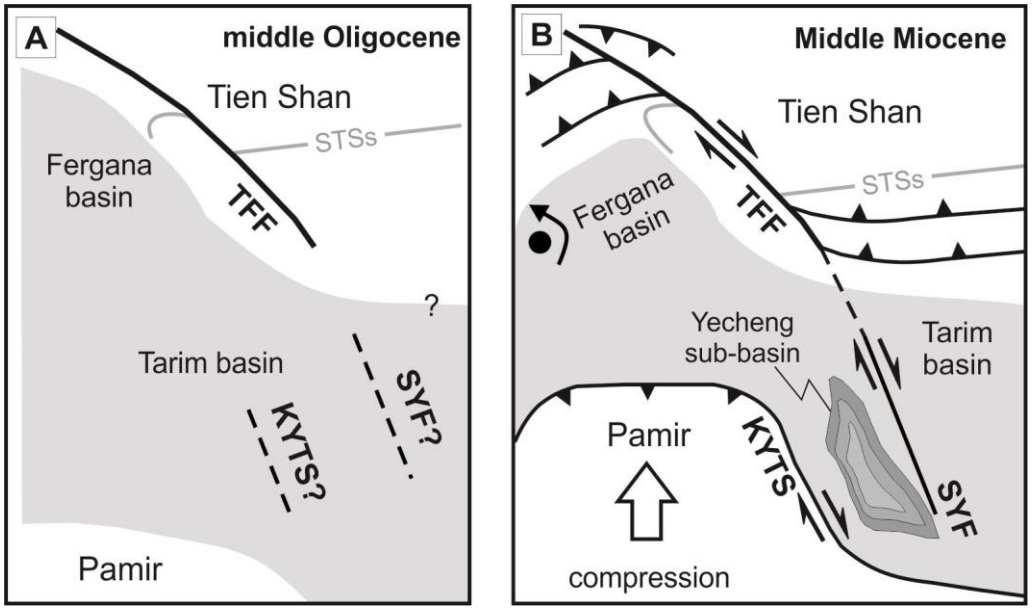

Figure 2.7 Schematic cartoon showing the tectonic evolution of the region. Grey, areas of active sedimentation; white, uplifted areas; dark grey line, South Tien Shan suture (STSs). (a) Early Cenozoic location of the TFF, displaced STSs and speculative location of the KYTS and SYF. (b) Commencing c. 25 Ma, Pamir indentation driven shortening provoked compression and strike-slip displacement along the KYTS and SYF. Between these structures a pull-apart basin developed (Yecheng subbasin). Simultaneously, compression is absorbed by the TFF, transpressive horsetail splays develop in both ends of the fault and the Fergana Basin experienced counter-clockwise rotation.

2.5.2 Connection to Pamir indentation

Indentation of the Pamir was underway by ~20 Ma based on AFT ages along the Kashgar Yecheng Transfer System (KYTS) (*Sobel & Dumitru* 1997). Recent stratigraphic work (*Klocke et al.* 2015) in the northern Tajik basin suggests late Oligocene uplift of the northern Pamir. Those changes are consequence of a south-dipping subduction zone at the northern margin of the Pamir, which is proposed to have initiated during the latest Oligocene- early Miocene (*Burtman & Molnar* 1993; *Sobel et al.* 2013). The northward indentation of the Pamir salient was accommodated not only by the right-lateral KYTS (*Cowgill* 2010) but also by the Shache-Yangdaman Fault (SYF) (*Wei et al.* 2013). The latter structure lies in the subsurface of the Western Tarim basin and was recently highlighted in an international journal for the first time (*Wei et al.* 2013). Moreover, these authors propose that a right stepover between these two faults formed the Yecheng pull-apart basin. Based on the spatial distribution, the SYF can be connected to the TFF, representing the southernmost portion of a major right-lateral strike-slip system. Following this interpretation, this regional strike-slip system was able to transfer shortening driven by Pamir indentation as far north as the northern portion of the Western Tien Shan (Fig. 2.7). The connection between the TFF and the

SYF worked efficiently during the Oligo-Miocene. However, Late Miocene deformation in the STS (*Sobel et al.* 2006a; *Heermance et al.* 2008) was responsible of shaping the actual Kokshal Range and Tarim basin foothills. Moreover, the active Miocene and Pliocene deformation of the STS and the Pamir triggered younger sedimentation in the NW Tarim basin keeping in the subsurface the SYF and the connection with the TFF.

We propose that the observed vertical-axis rotation of the Fergana basin which is coupled with the dextral slip TFF (*Thomas et al.* 1993) was driven by Pamir indentation. The transtensional Yecheng subbasin was filled with up to 6 km of Wuqia Group sediments (*Wei et al.* 2013). The basal age of this unit is apparently contemporaneous with the basal Massaget Formation, which we describe as a syn-rotational unit in the Fergana Basin (Fig. 2.2). Therefore, both units are syn-tectonic units genetically-related by the same tectonic driver. Magnetostratigraphy shows that shortening in the Kokshal range propagated rapidly southward into the Tarim basin between 16.3 and 13.5 Ma (*Heermance et al.* 2008). Therefore, relatively rapid slip along the TFF persisted from ca. 25 Ma until at least 13.5 Ma. This timing appears to agree well with the formation of the transtensional Yecheng depression in the SW Tarim basin (*Wei et al.* 2013), supporting our contention that the SYF and TFF are kinematically linked. Younger tectonic episodes affecting the STS and Pamir triggered the deposition of large volumes of sediment in the western Tarim basin, leaving the SYF covered in the subsurface.

In the Western Tien Shan the maximum amount of Oligo-Miocene shortening and exhumation is located close to the TFF. Our thermochronologic data shows that exhumation significantly decreases to the west in the Chatkal Ranges. Furthermore, the topography of the Chatkal Ranges also reflects the higher amount of shortening close to the TFF. Higher peaks (~4000 m) are located in close proximity of the strike-slip fault while to the west elevation decreases gradually until reaching elevations close to 400 m. Significant Oligo-Miocene deformation in the Alai range, between the Alai and Fergana basins, has not yet been documented. Although a relatively small Oligo-Miocene exhumational event is described in the Central (Kyrgyz) Tien Shan, the majority of the exhumation there occurred since Mid-Late Miocene times (*Sobel et al.* 2006b; *Glorie et al.* 2011; *Macaulay et al.* 2013; 2014). Therefore, the TFF was able to efficiently transfer shortening driven by Pamir indentation far into the hinterland. This

shortening occurred even when the Alai intracontinental subduction zone was active and accommodating most of the shortening in this sector of the orogen. This explains why more shortening and exhumation was located near the dextral strike-slip fault and decreased both to the east and west during the late Oligocene – early Miocene.

2.6 Conclusions

It is widely accepted that deformation in Central Asia is a far-field effect of the India-Asia collision (e.g., *Molnar & Tapponnier* 1975; *Allen et al.* 1991; *Hendrix et al.* 1994). During the late Miocene, a strong deformational event was responsible of shaping the current structure of many of the Central Asian Ranges (e.g. *Bullen et al.* 2003; *Macaulay et al.* 2014; *Heermance et al.* 2008). However, a growing body of evidence (*Hendrix et al.* 1994; *Sobel & Dumitru* 1997; *Sobel et al.* 2006a; *Heermance et al.* 2008; *Amidon & Hynek* 2010; *Macaulay et al.* 2013, 2014; *Wei et al.* 2013) points to a smaller, but important deformational event in the late Oligocene – early Miocene. By dating the onset of Cenozoic strike-slip movement along the TFF and in adjacent linked structures which distribute shortening within the NW Tien Shan, we are able to better document and areally extend the footprint of this Oligo-Miocene event. Furthermore, we present a kinematic mechanism that explains how contraction related to Pamir indentation was propagated hundreds of kilometers north into the Chatkal, Talas and Fergana Ranges. The proposed connection of the KYTS, SYF and TFF would have formed an efficient system to transfer this shortening to the north. Finally, we suggest that the presence of pre-existing crustal discontinuities such as the TFF played a significant role in establishing, localizing, and efficiently transferring shortening far into the hinterland.

Acknowledgments

This study was supported by the Darius Programme, DFG-Graduate School 1364 and a fellowship from the German Academic Exchange Service (DAAD) to A. Bande. We thank Y. Rolland, J. Kley and corresponding editor M-F Brunet for constructive and conscious reviews that strengthened the paper. M.Wack and S. Gilder are acknowledged for detailed discussion and explanations about paleomagnetism. We also thank S. Sen, E. Macaulay, D. Melnick and M. Strecker for constructive discussion that improved earlier versions of the manuscript. We are grateful to the members of the Materials Research Department at the GSI Helmholtzzentrum (Darmstad, Germany) for heavy ions irradiations.

Chapter 3
Exhumation history of the western Kyrgyz Tien Shan: implications for intramontane basin formation

Submitted by Alejandro Bande, Edward R. Sobel, Alexander Mikolaichuk, Alexander Schmidt and Daniel F. Stockli (2016) to Tectonics.

Abstract

The dextral Talas Fergana Fault separates the western from the central Tien Shan. Directly south of the western Tien Shan lies the Pamir indentor while to the east the rigid Tarim block is present. Recent advances have shed light into the Cenozoic evolution of the eastern and central Tien Shan paying less attention to the western Tien Shan history. In this contribution we present new thermochronological ages for the Fergana and Alai ranges that, combined with the available dataset, will be used to constrain the Cenozoic exhumation history of the western Tien Shan. Following a tectonically quiet early Cenozoic period, an onset of exhumation can be placed at ~25 Ma. The early onset was followed by a period of reduced exhumation rate and in some areas minor reheating. A final, strong late Miocene rapid cooling event is well represented in the western Tien Shan as in other sectors of the range. The early onset of uplift of the western Tien Shan dissected the previously continuous Parathethyan Sea, building progressive isolated basins (e.g. Fergana, Tarim, Alai basins) in the Central Asian hinterland. Moreover, the coeval timing of late Miocene uplift and the lateral strength variation between Tarim and Pamir crusts suggest that neither of them can act as the sole driver for the entire Tien Shan exhumation.

3.1 Introduction

The collision of India with the southern margin of Asia at about 55 Ma (e.g., *Searle et al*., 1987) caused extensive intracontinental deformation in Asia (e.g. *Molnar & Tapponnier*, 1975) where preexisting zones of lithospheric weakness have caused synchronous deformation in the Asian hinterland (e.g. *Burtman*, 1975; *Hendrix et al*., 1992). The Tien Shan is the world´s largest active intracontinental mountain belt with an east-west extent of ~2500 km along strike. Directly south of the western Tien Shan, the northern edge of the Pamir indentor has moved 300-400 km north with respect to stable Asia, forming a first order feature in the Central Asia topography. Both the Tien Shan and Pamir uplifts have created many now-isolated intramontaneous basins (e.g. Tarim, Alai, Fergana) where during Eocene times the shallow Paratethian Sea covered the Central Asian interior (e.g. *Tang et al*., 1992; *Burtman*, 2010; *Bosboom et al*., 2015). Although the Eocene connection between basins is well-known, it is unclear how the Tien Shan and Pamir dissected the formerly-unified Central Asian foreland. As in other

intracontinental settings, deformation is strongly influenced by pre-existing crustal heterogeneities, causing irregular spatiotemporal distribution of deformation (e.g. *Allen & Vincent*, 1997; *Neely & Erslev*, 2009). In recent years, significant advances were achieved in the understanding of the Cenozoic deformation of the central Kyrgyz Tien Shan, NW Tarim basin and Pamir (e.g., *Bullen et al*., 2003; *Heermance et al.*, 2008; *Zubovich et al.*, 2010; *Sobel et al.*, 2013; *Macaulay et al*., 2014; *Schurr et al*., 2014; *Liu et al.*, 2015). However, the Cenozoic evolution of the western Tien Shan has received very little attention and, in consequence, understanding of the geodynamics of this area has been left behind. In this contribution we will try to decipher the evolution of the western Tien Shan and in the light of the results decipher the progressive dissection of the Paratethyan Sea and the early topographic growth of the southern Tien Shan.

In this study, we present new apatite fission track (AFT), zircon (U-Th)/He (ZHe), and zircon U/Pb ages to provide constraints on Cenozoic cooling in the western Tien Shan. We present new basement samples from the Fergana and Alai Ranges that, combined with all the available thermochronolgy ages from the area, will be used to infer the sequence of range construction and basin dissection.

Our constraints on the timing of uplift and spatiotemporal development of blocks provide new insight into the evolution of the southern Tien Shan. We are able to identify basin former connections and the timing of basin partition. Furthermore, our data provides a temporal framework for the deformation that can be linked to syn-tectonic sedimentation in intramontaneous basins and used to improve our understanding of similar units (e.g. Massaget Fm. and Wuqia Gr.) in different sedimentary basin records.

3.2 Tectonic setting

The western Kyrgyz Tien Shan has a distinct morphology when compared to other Tien Shan sectors. The triangular-shaped Fergana basin is bounded by ranges with different orientations; to the east, most of the major structures trend E-W (Fig. 3.1). The boundary between these two domains is the right-lateral Talas-Fergana Fault (TFF). This strike-slip fault is a long-living structure that played a fundamental role in accommodating deformation during Permian continental collision in Central Asia (*Burtman et al.*, 1996; *Rolland et al*., 2013; *Konopelko et al*., 2013). The ancient Tien Shan formed during the Paleozoic by the amalgamation of different terranes, creating

distinctive tectonic zones with a roughly E-W orientation (present geometry) (e.g., *Windley et al.*, 1990; *Biske*, 1995; *Burtman*, 2010).

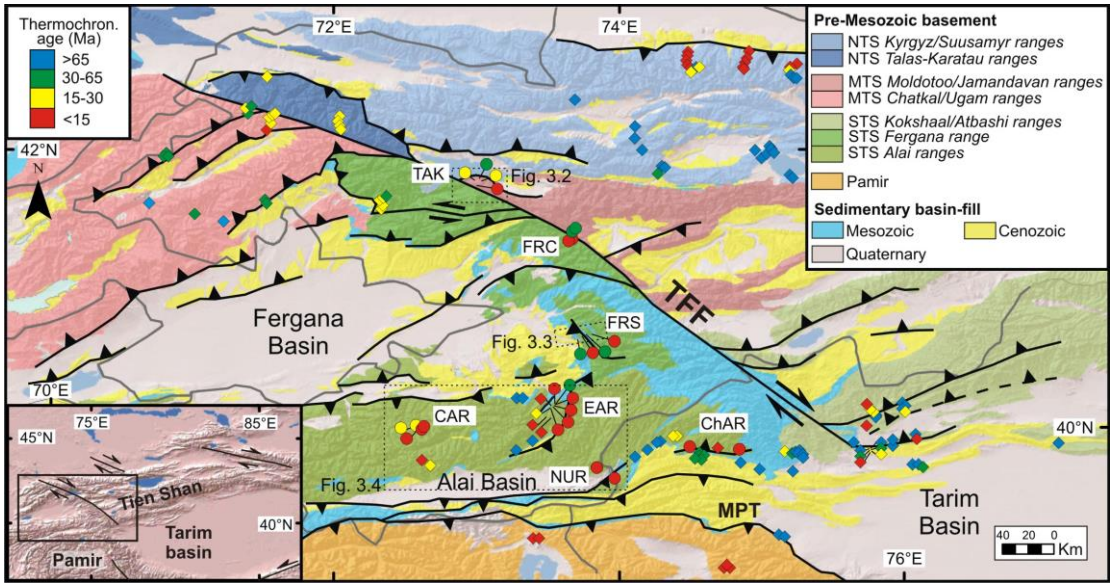

Figure 3.1 Geologic map of the Kyrgyz Tien Shan (modified after *Vlasov et al*., 1991 and *Bakirov et al*., 2001) superimposed on shaded relief image, showing regional structures in the western Tien Shan and thermochronological data. Solid circles show new AFT data and diamonds published AFT data; colours denote ages based on the shown scale. Labels in white are locations discussed in the text. Thermochronology ages are from *Sobel & Dumitru* (1997), *Bullen et al*. (2003), *Schmalholz* (2004), *Sobel et al*. (2006a), *Sobel et al*. (2006b), *Glorie et al*. (2011), *De Grave et al*. (2012), *Sobel et al*. (2013), *Thiede et al*. (2013), *Yang et al.* (2014), *Bande et al*. (2015a) and this study. Dashed boxes show location of Figure 3.2, 3.3 and 3.4. Country boundaries shown in grey. Inset map shows location of Figure 3.1 in the Tien Shan region. In the legend NTS is North Tien Shan; MTS is Middle Tien Shan and STS is South Tien Shan. In italics names of the ranges. TFF is Talas-Fergana Fault and MPT is Main Pamir Thrust

The northern Tien Shan (NTS), consisting predominantly of Precambrian and early Paleozoic metamorphosed sedimentary rocks (*Voytenko & Khudoley*, 2012), lies to the east of the TFF. On the west side of the TFF, the middle Tien Shan (MTS) presently has a NE-SW orientation. It is represented by the Chatkal Ranges and it is mostly composed of passive continental margin sedimentary sequences and Devonian-Carboniferous magmatic rocks (*Seliverstov & Ghes'* 2001; *Seltmann et al.*, 2011). The southern Tien Shan (STS) is represented by a late Paleozoic highly deformed accretionary belt (*Biske,* 1995*; Bakirov & Maksumova,* 2001). Ophiolites and related metamorphic rocks delineate a major suture zone along its northern margin (*Burtman,* 1975). A regional sigmoid formed and displaced the STS in the latest Paleozoic – early Triassic (*Bazhenov et al.*, 1993; *Alexeiev et al*., 2009). As a result, the Fergana and Alai Ranges formed the eastern and southern sectors respectively of the western Krygyz Tien

Shan. The Fergana range took a NW-SE orientation, while the Alai Range kept its E-W orientation but is disconnected from related units to the east.

During the early Mesozoic a quiescent tectonic environment affected most of the western Tien Shan region. Indeed, the region was affected by prolonged erosion, leading to the formation of a regional denudation surface (e.g. *Ruhin & Ruhina*, 1969; *Afonichev & Vlasov*, 1984; *Cobbold et al.*, 1996; *Sobel, et al*., 2006b) that is still preserved in the landscape. Thick transtensional basins formed along the TFF in the Jurassic, filled with sandstone and coal-bearing shales (*Sobel*, 1999). Unfortunately, the extent and magnitude of Cretaceous deformation remains poorly constrained in the western Tien Shan. However, the adjacent central Kyrgyz Tien Shan experienced >100 Myr period of tectonic quiescence in the late Mesozoic (*Bullen et al*., 2003; *Glorie et al*., 2011; *Macaulay et al*., 2013). During the early Cenozoic (Paleocene – Eocene), marine transgressions flooded Central Asia; these are well correlated across the Amu Darya, Tadjik, Fergana and Tarim basins (*Bosboom et al*., 2015). These marine incursions correspond to the Paratethys Sea, which was open to the west during that time. Around 25 Ma, the dextral TFF accommodated north-south contraction, which drove uplift and exhumation concentrated at its restraining bends (*Bande et al*., 2015a). A renewed period of deformation affected the Tien Shan in the late Miocene (e.g., *Sobel et al*., 2006b; *Chang et al*., 2012; *De Grave et al*., 2012; *Macaulay et al*., 2014). Pliocene deformation and related syn-sedimentary units are described in many basins throughout the Tien Shan (e.g., *Coutand et al*., 2002; *Heermance et al*., 2008, *Selander et al*., 2012; *Wei, et al*., 2013; *Bande et al*. 2015b, *Yang et al*., 2015).

3.3 Methodology and samples

3.3.1 Low-temperature thermochronology

This technique is based on temperature-dependant retention of radiogenic daughter products. Two commonly measured decay products are fission tracks, using the apatite fission track method (AFT), and ^{4}He using the Apatite and Zircon (U-Th-Sm)/He method (AHe and ZHe). Above certain temperatures, daughter products are not retained over geological timescales. This temperature is actually a zone: the partial annealing zone (PAZ) (*Gleadow & Duddy*, 1981) for AFT and the partial retention zone (PRZ) (*Wolf et al*., 1998) for AHe and ZHe. Within the PAZ, fission tracks are shortened and eventually removed, while ^{4}He progressively escapes by diffusion in the PRZ.

Temperatures for the PAZ and PRZ are dependant on the crystal kinetic characteristics and cooling rates (e.g., *Brandon et al.*, 1998; *Donelick et al.,* 1999; *Reiners & Farley*, 2001; *Ehlers & Farley*, 2003). Typically, the ZHe PRZ extends from 130 to ~200°C (*Wolfe & Stockli*, 2010), the AFT PAZ from ~60 to 120°C (e.g., *Ketcham et al*., 1999) and the AHe PRZ from ~40 to 85°C (*Wolf et al.,* 1998). Slowly cooled samples generally have lower closure temperatures and older ages (*Ehlers & Farley*, 2003). Since fission tracks form at a constant rate over time and initially have the same length (*Green et al*., 1989), the distribution of AFT lengths can be used to quantify the amount of annealing a sample has experienced (e.g., *Ketcham et al*., 1999); thermal modeling can be used to identify possible cooling pathways (e.g., *Ketcham et al*., 2007).

3.3.2 Apatite fission track (AFT) methodology

AFT analysis was carried out on 27 samples; horizontal confined fission track lengths were measured in 15 of them. Kinetic properties were assessed for every grain counted or containing confined tracks by measuring at least 4 D_{par} lengths (*Donelick* et al., 2005) that were averaged and corrected following *Sobel & Seward* (2010). Complete fission track and length data, sample preparation and analytical procedures can be found in the supplementary material (Table DR1). AFT ages were calculated following the procedures of *Galbraith* (1981) using the MacTrackX software. Most AFT ages are based on ca. 20 grains. However, 2 samples contained less than 11 countable grains, resulting in AFT ages with large errors. Ages are reported as pooled ages (±1σ), unless they fail the chi-squared test (<5%) in which case the central age is reported (Table 3.1). As many horizontal confined fission tracks (tracks-in-tracks) as possible were measured. To increase the number of measured horizontal confined tracks, additional mounts of 7 samples were irradiated with ^{252}Cf (*Carlson et al*., 1999) or heavy ions (*Jonckheere et al*., 2007). The complete dataset is included in the supplementary material. Full analytical results are available in table A2.1.

Sample	Latitude (N°)	Longitude (E°)	Elev. (masl)	n[a]	**Age (Ma)**	**±1σ**	P(χ^2)[d] %	# lengths[b]	Length (μm)	SD[c] (μm)
Takhtalik Range										
10FR69	41,719	72,956	1844	21	25,5	2,4	78	49*	12,1	1,8
10FR71	41,710	72,999	2131	20	46,5	3,2	8	102*	12,8	1,6
10FR72	41,700	73,028	1939	20	22	3	95	16*	12	2,1
10FR73	41,689	73,015	1789	20	10,4	1	93	72*	12,2	2,2
Kaldama Pass										
11TS532	41,306	73,655	2758	20	**6,3**	**0,9**	8	21*	14	1,1
11TS533	41,294	73,636	2911	20	**8,2**	**1,2**	7	ND	ND	ND
11TS534	41,338	73,647	2036	20	**42**	**3,5**	60	25	11,8	1,7
11TS535	41,346	73,664	2122	20	**51**	**3,9**	0	102	12,7	1,4
Fergana Range										
12FE27	40,661	73,871	1947	11	**11**	**2,1**	36	ND	ND	ND
12FE28	40,660	73,793	1424	20	**38**	**2,9**	36	80	11,3	1,9
12FE29	40,659	73,788	3605	4	**11**	**3,3**	44	ND	ND	ND
12FE30	40,637	73,731	3605	20	**49**	**5,3**	0	24	11,2	2,2
Alai Range										
11T23	39,838	74,844	3117	20	**6,7**	**0,9**	100	5*	14,4	1,6
11T75	39,850	74,498	2800	20	**6,9**	**0,9**	100	2*	15,4	1,6
12KA21	40,003	72,582	3475	20	**14**	**1,3**	100	ND	ND	ND
12KA22	40,005	72,572	3860	19	**22**	**1,8**	100	63	12,4	2,0
12KA23	40,006	72,577	3660	20	**20**	**1,7**	35	ND	ND	ND
12KA24	39,998	72,606	3122	20	**11**	**1,1**	99	ND	ND	ND
12KA25	39,999	72,608	1297	21	**13**	**1,2**	65	58	13,3	2
12NU12	40,129	73,526	1838	20	**9,8**	**1,3**	100	ND	ND	ND
12NU13	40,166	73,557	2890	20	**37**	**2,7**	86	100	10,5	1,7
12NU14	40,166	73,553	2670	20	**9,5**	**1,1**	49	ND	ND	ND
12NU15	40,161	73,549	2500	20	**9**	**0,7**	92	ND	ND	ND
12NU16	40,152	73,543	2210	21	**6,9**	**1,1**	99	ND	ND	ND
12NU17	40,145	73,540	2056	20	**7,9**	**0,9**	100	6	12,9	2,2
Nura - Alai Basin										
12NU02	39,616	73,837	2930	20	**11**	**1,3**	92	ND	ND	ND
12NU11	39,675	73,778	2939	20	**12**	**1,3**	97	ND	ND	ND

Note: All samples counted by AB (zeta=369.5 ± 7.9, unpub. 2012)

[a] number of individual crystals dated.

[b] Asterisk (*) indicates track lengths measured from heavy ions irradiation slide.

[c] Standard deviation of measured lengths.

[d] P(χ^2) (%) is the chi-squred probability (*Galbraith*, 1981; *Green*, 1981). Ages that pass the P(χ^2) test (>5) are reported as pooled ages.

Table 3.1. Summary of apatite fission track data of the western Tien Shan

3.3.3 Zircon (U-Th-Sm)/He (ZHe) methodology

Zircon (U–Th-Sm)/He dating was carried out on 4 samples at The University of Texas at Austin using laboratory procedures described in *Wolfe & Stockli* (2010). At

least 3 single grain aliquots were measured per sample. Individual ages were calculated using standard alpha-ejection corrections and with FT corrections that assume a homogeneous U and Th distribution (e.g., *Farley et al*., 1996; *Farley*, 2002). Reported age uncertainties of 2σ are based on the reproducibility of replicate analysis of laboratory standards (*Reiners et al.,* 2004). Estimated analytical uncertainties are ~8%. Both uncorrected and alpha- ejection corrected ages are reported (Table 3.2).

Sample	Latitude (N°)	Longitude (E°)	Elev. (masl)	**Corrected age (Ma)**	**error (1σ) (Ma)**	U (ppm)	Th (ppm)	^{147}Sm (ppm)	He (nmol/g)	[U]e	Ft
12KA24-1	39,998	72,606	3122	**52,5**	**4,2**	276,6	104,8	0,5	66,0	300,7	0,8
12KA24-2	39,998	72,606	3122	**43,0**	**3,4**	197,5	77,0	0,4	36,7	215,2	0,7
12KA24-3	39,998	72,606	3122	**114,3**	**9,1**	299,9	393,6	4,2	186,3	390,5	0,8
12KA22-1	40,005	72,572	3860	**156,1**	**12,5**	325,5	113,2	0,4	229,5	351,6	0,8
12KA22-2	40,005	72,572	3860	**110,5**	**8,8**	567,8	388,4	1,3	300,0	657,2	0,8
12KA22-3	40,005	72,572	3860	**146,9**	**11,8**	295,7	80,9	0,4	194,0	314,3	0,8
12NU12-1	40,129	73,526	1838	**64,3**	**5,1**	321,2	71,7	1,3	97,1	337,7	0,8
12NU12-2	40,129	73,526	1838	**9,9**	**0,8**	1225,6	251,6	1,9	53,4	1283,5	0,8
12NU12-3	40,129	73,526	1838	**32,7**	**2,6**	745,5	142,2	2,0	112,7	778,3	0,8
12NU12-4	40,129	73,526	1838	**43,2**	**3,5**	1035,8	234,8	1,8	199,0	1089,8	0,8
12NU12-5	40,129	73,526	1838	**26,4**	**2,1**	1041,6	238,5	2,1	126,1	1096,5	0,8
12NU12-6	40,129	73,526	1838	**54,6**	**4,4**	914,7	159,1	1,7	238,6	951,3	0,8
12NU13-1	40,166	73,557	2890	**110,7**	**8,9**	803,9	336,8	14,7	431,7	881,4	0,8
12NU13-2	40,166	73,557	2890	**48,5**	**3,9**	1247,6	267,9	24,8	290,2	1309,4	0,8

Table 3.2. (U-Th-Sm)/He ages of zircon (ZHe) in the Alai Range

3.3.4 Age-elevation relationships and thermal inverse modeling

Age-elevation relationships (AERs) of samples collected at regular intervals along steep topographic profiles are commonly used to date increases in exhumation and quantify exhumation rates (e.g. *Gallagher et al*., 2005). Typically, an increase in exhumation rate will result in a break-in-slope on an age-elavation plot. When possible we sampled along vertical profiles. We also collected spot samples to extend the areal coverage and spatial distribution.

To determine the cooling history recorded by the samples we used two different thermal modeling approaches. We used the HeFTy software (v.1.8.3) (*Ketcham*, 2005)

to model forward and inverse time-temperatures path for individual samples, and the QTQt software (v.5.4.1) (*Gallagher*, 2012) to derive integrated cooling constrains from multiple samples within age-elevation profiles. HeFTy is effective for assessing the thermal history of a single sample. The output reflects the goodness of fit of the models, which allows for testing different cooling histories. However, this version of the program is not able to model multiple samples within an AER. For this task we used QTQt, which is well suited for the latter approach. The main aim of our modeling was to identify and date cooling rate variations. Models were initially run with minimal constraints. In cases where apparent inflection points were depicted, constraint boxes were set and shifted to test each model's goodness of fit and reliability.

3.3.5 Zircon U/Pb LA-ICP-MS methodology

Zircon U-Pb dating was carried out in 2 samples. Grains were handpicked, mounted in epoxy, polished and imaged with cathodluminescence. Sample introduction was accomplished by laser ablation of the zircon grain surface. Zircons chosen for U–Pb geochronology were measured using a Cetac LSX-213 laser ablation system coupled with a Thermo Scientific Element-2 ICP-MS at the Institute of Earth and Environmental Sciences, University of Potsdam, with a small spot size of 25 μm. To correct for laser-induced elemental fractionation and mass discrimination by the instrument all analyses were normalized to the GJ1 zircon standard (*Jackson et al*., 2004). Data reduction was performed with the software UranOS v. 2.02 (*Dunkl et al*., 2014) using a linear regression line fitting over time for the measured isotope ratios of the GJ1 zircon, and a t-zero intercept for the individual U/Pb ratios. Spot analyses of sample zircons were also corrected for common Pb contributions using the Hg-corrected ^{204}Pb signal. The U, Th and Pb concentrations of sample zircons were determined relative to the GJ1 reference. Analytical results are available in table A2.2

3.4. Results

3.4.1 Takhtalik Range

We collected four AFT samples in this range (Figs. 3.1 and 3.2A, location TAK), following a steep topographic slope over 350 m. The lowest and closest sample to the TFF yielded the youngest age (10.4 ± 1 Ma). Two samples located to the north and at medium elevation (~1900 m) showed Oligo-Miocene ages that overlap in error (22 ± 3

and 25.5 ± 2.4 Ma). Finally, the top sample has an age of 46.5 ± 3.2 Ma. All samples yielded similar mean track length values (~12.3 μm).

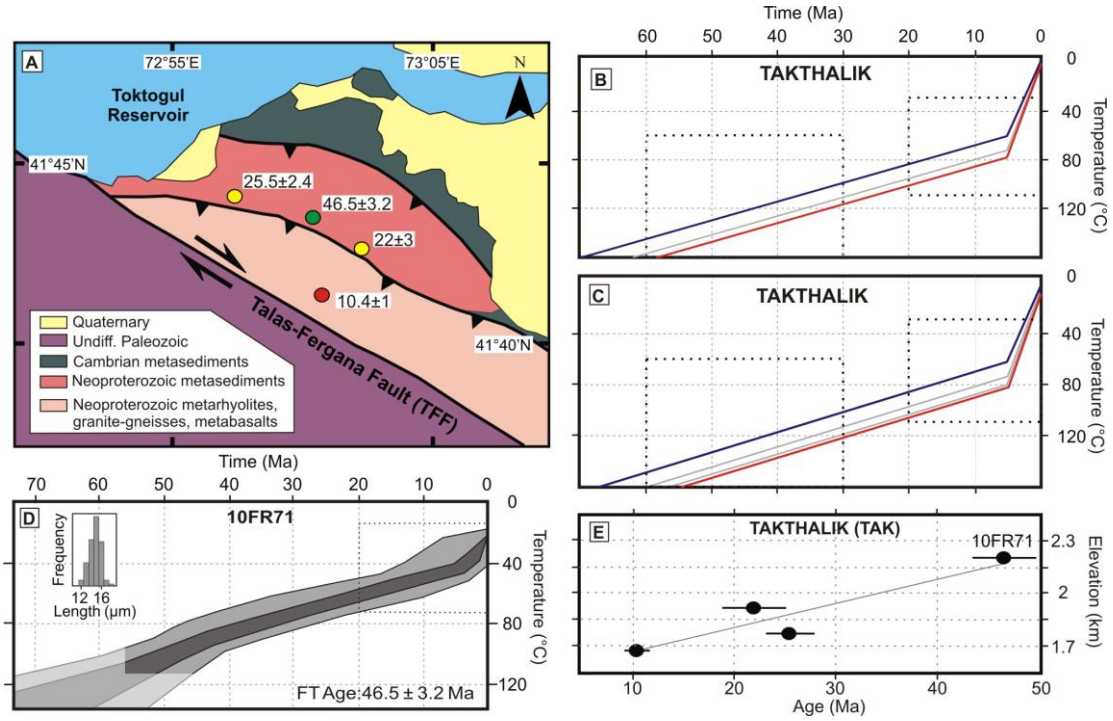

Figure 3.2(a) Geological and tectonic map of the Takthalik Range (modified after *Mikolaichuk et al.*, 2008) showing locations of new AFT samples; colours denote ages based on same scale as Figure 1; ages with 1 sigma errors (in Ma) are in white boxes. (b) AER from the Takthalik Range vertical profile. Age errors are 1 sigma. (c) Time-temperature histories obtained by thermal modeling using HeFTy software (*Ketcham*, 2005) of samples 10FR71. Unconstrained part of the models represented by transparent polygons. Dashed boxes are model input constraints. Inset shows histogram of track-length distribution. (d and e) Time-temperature histories derived from QTQt modeling (*Gallagher,* 2012). Dashed boxes are model input constraints. Blue and red lines correspond to the uppermost and lowermost samples, respectively.

Although we collected the 4 samples following a steep slope, an important thrust fault separates the bottom sample from the other 3 (Fig. 3.2A). If this fault was active during the Cenozoic, interpreting the entire profile in terms of an AER might be erroneous. In order to test the Cenozoic activity of the fault we performed two set of models using the QTQt software. In the first one we modeled only the 3 high elevation samples (Fig. 3.2B) and in the second we modeled the complete profile together (Fig. 3.2C). The results are conclusive; both model results show a rapid cooling event starting at 7-8 Ma, prior to a relatively slow cooling history. Single sample (HeFTy) modeling results for the higher sample (10FR71, Fig. 3.2D) is consistent with the multisample modeling that shows moderate slow cooling during most of the Cenozoic, interrupted by an abrupt increase in cooling rate at around 8 to 7 Ma. The AER relationship does

not show a clear break-in-slope (Fig. 3.2E). On the contrary, it shows a gentle slope probably related to prolonged time spent in the PAZ of the 3 upper samples, prior to the onset of rapid cooling.

3.4.2 Fergana Range

We sampled the Fergana Range (Fig. 3.1) in the central (FRC) and southern sectors (FRS). In the FRC we sampled on both sides of the TFF along the Kaldama pass. We collected 4 samples, two on each side of the fault. Interestingly the western samples are much younger (<10 Ma) than the ones located to the east (41 and 51 Ma). The oldest sample fails the chi square test. Moreover, the eastern samples have shortened lengths (~12.3 μm, Table 1), implying more annealing and non-reset ages. Mean track-length data from a western sample (11TS532) show longer lengths, suggesting less annealing.

In the southern sector (FRS) we sampled along the Karakulja River (Fig. 3.1 and 3.3A). We took four samples covering a horizontal distance of 13 km, distributed in two tectonic blocks. Interestingly, the results show two sets of ages, decreasing from west to east (Fig. 3.3B). The younger samples have a late Miocene age, while the older ones present Eocene ages (38 and 49 Ma). The oldest age fails the chi-square test. Confined track-lengths were measured in the Eocene samples and have a mean of 11.2 μm, suggesting substantial annealing and significant time spent in the PAZ. We interpret the Eocene samples as partially reset and the late Miocene as fully reset ages. Supporting this interpretation, thermal model of sample 12FE28 (Fig. 3.3C) shows slow cooling during most of the Cenozoic followed by an abrupt increase in the cooling rate by ~5 Ma.

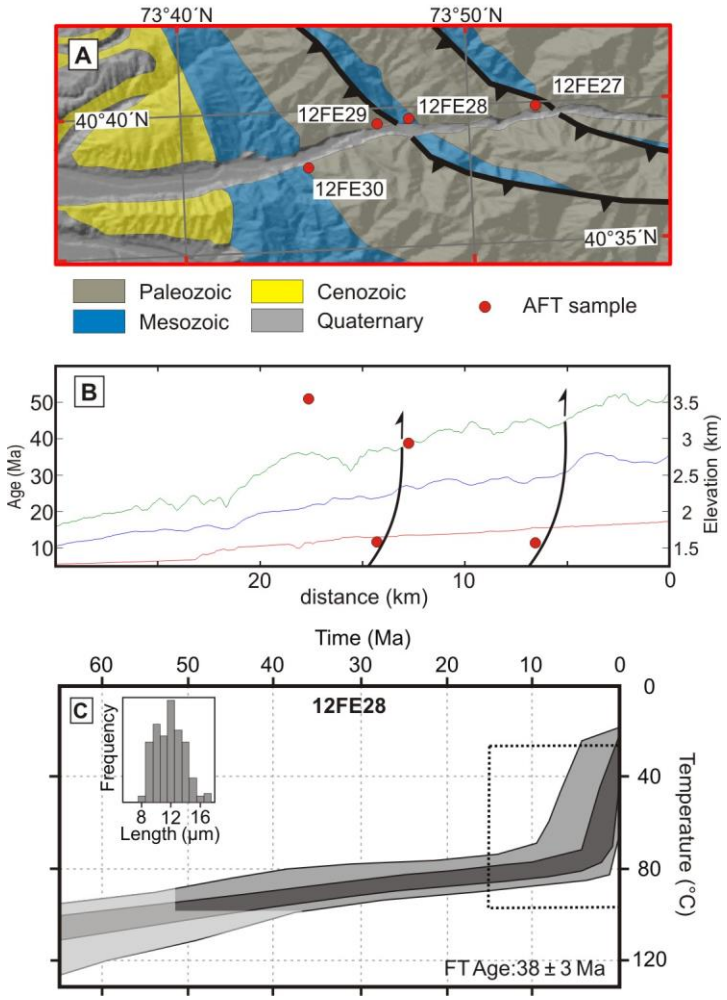

Figure 3.3(a) Geological and tectonic map of the Karakuldja valley (modified from *Bakirov et al.,* 2001) superimposed on shaded relief image showing locations of new AFT samples and interpreted structures. (b) Elevation swath profile through Karakuldja valley, showing minimum (red), mean (blue) and maximum (green) elevations. Solid circles are AFT ages; black lines are thrust faults determined in the field. (c) Time-temperature histories obtained by thermal modelling using HeFTy software (*Ketcham*, 2005) of samples 12FE28. Unconstrained part of the models represented by transparent polygons. Dashed boxes are model input constraints. Inset shows histogram of track-length distribution.

3.4.3 Alai Range

We sampled the southern range of the western Tien Shan in three sectors (Fig. 3.1): the central Alai Range (CAR), the eastern Alai range (EAR) and the Chinese Alai range (ChAR). In total we acquired 13 new AFT basement ages that we combine with 8 previously published basement and 30 detrital ages (*Sobel & Dumitru*, 1997; *Schmalholz*, 2004, *De Grave et al*., 2012; *Sobel et al*., 2013; *Yang et al*., 2014). In addition, we present 4 new ZHe ages and 2 U/Pb crystallization ages from this area (Fig. 3.4).

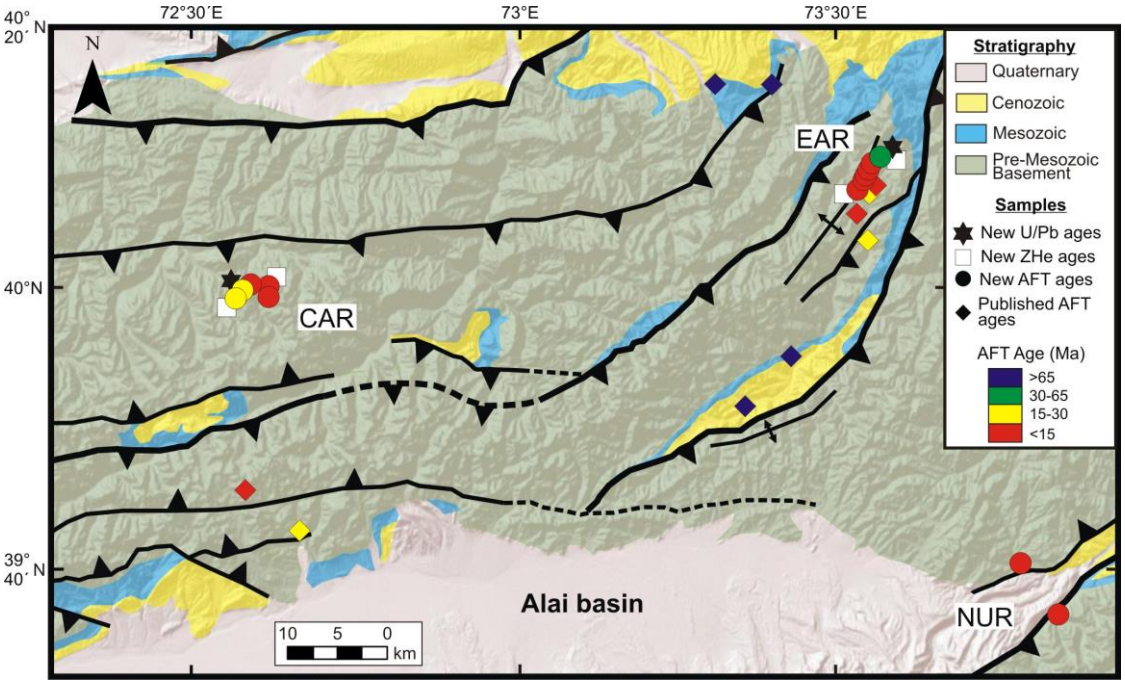

Figure 3.4 Simplified geologic map of the Alai Range (modified after *Bakirov et al*., 2001) superimposed on shaded relief image, showing regional structures and thermochronological data. Solid circles reflect new AFT ages, black stars new U/Pb ages, white squares new ZHe ages and filled diamonds available published AFT data; colours denote AFT ages based on the shown scale. Structures interpreted and modified after *Bakirov et al*. (2001) and *Coutand et al*. (2001). Colors of thermochronology ages same as in Figure 1. Labels in white are locations discussed in the text.

3.4.3.1 Central Alai Range

In the central part (Figs. 3.1 and 3.4, location CAR) we took samples near the headwaters of the Kyrgyz-Ata River. We collected 5 granitic samples distributed in a 738 m long vertical section. The $^{206}Pb/^{238}U$ ages acquired for sample 12KA23 are between 220 and 338 Ma (see Fig. 3.5A and Table DR2). Based on those results and using the *TuffZirc* tool of Isoplot (*Ludwig*, 2003) we extracted an age of 273 Ma (+7/-12 Ma) for a coherent group of 8 analyses for this sample. We used the *TuffZirc* algorithm to extract an age because is largely insensitive to both Pb loss and inheritance without entirely ignoring the analytical error information (*Ludwig*, 2003). The resulting age suggests Permian crystallization.

The AER (Fig. 3.5B) show younger AFT ages at lower elevations clustered at ~ 13 Ma and older ages at high altitude with a mean age of 21 Ma. The break-in-slope is hard to precisely mark, but the ages of the two set of samples are significantly different.

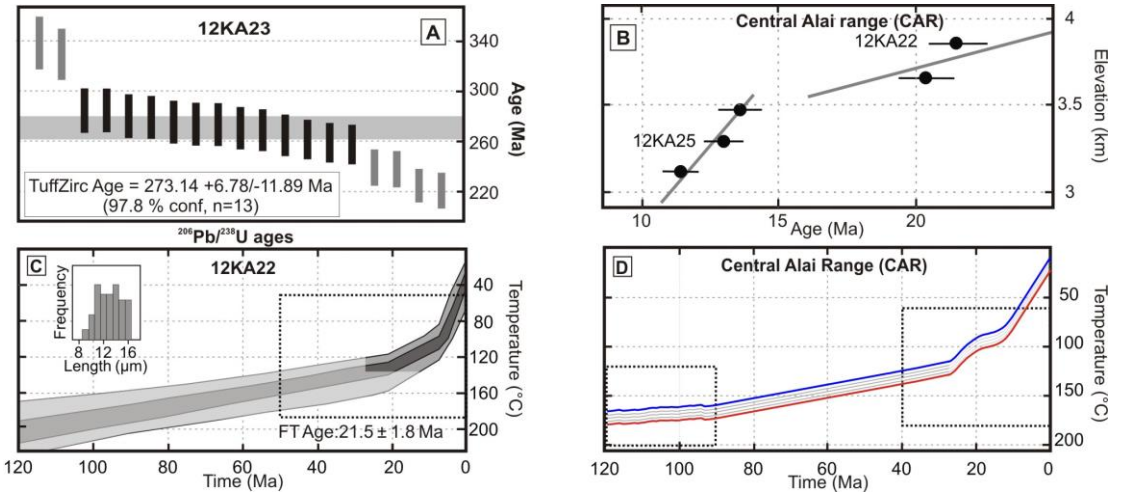

Figure 3.5(A) U-Pb *TuffZirc* age (*Ludwig*, 2003) calculated for sample 12KA23. Grey horizontal bar represent inferred age and uncertainty. Black rectangles are error bars of the analysis used to calculate the age (syngenetic), in grey error bars from the analysis discarded likely to experienced Pb loss. Box heights are 2 sigma. (B) AER from the Central Alai Range vertical profile. Age errors are 1 sigma. (C) Time-temperature histories obtained by thermal modeling using HeFTy software (*Ketcham*, 2005) of samples 12KA22. Unconstrained part of the models represented by transparent polygons. Dashed boxes are model input constraints. Inset shows histogram of track-length distribution. (D) Time-temperature histories derived from QTQt modeling (*Gallagher,* 2012). Dashed boxes are model input constraints. Blue and red lines correspond to the uppermost and lowermost samples, respectively.

As expected, the higher sample (12KA22; 3860 m) has a shorter track-length mean value (12.4 µm) than the lower sample 12KA25 (13.3 µm; 3297 m). We believe that the higher samples resided longer in the PAZ and might represent non-fully reset ages. However, the AER does not conclusively separate reset and non-reset ages. At the same location we analyzed 2 samples using the ZHe technique (Fig. 3.4, white squares). The highermost sample (12KA22) yielded 2 Jurassic ZHe ages (146.9 ± 11.7 and 156.1 ± 12.5 Ma) that overlap within error. The third aliquot has a significantly higher U concentration (57 ppm) that might reflect radiation damage (e.g. *Guenthner et al*., 2013), thus accounting for an anomalously younger ZHe age of 110.5±8.8 Ma. The bottom sample yielded two Eocene ZHe ages (52.5 ± 4.2 Ma and 43 ± 3.4 Ma) that were used in the models. A broken grain (12KA24-3) yielded an anomalous old age (227.5 ± 18.2 Ma) that was discarded. The fourth aliquot (12KA24-4) yielded an older Cretaceous age (114.3 ± 9.1 Ma) that might reflect different closure temperature given by variations in effective diffusion domain size (*Gautheron et al*., 2009).

In order to resolve the onset of Cenozoic cooling in this region, we performed both multi- and single-sample modeling. Single sample modeling of the highest sample using AFT as input (12KA22, Fig. 3.5C) shows a time-temperature path with a two-phase exhumational response. According to the model, the onset of Cenozoic cooling

happened at ~27 Ma, followed by a renewed acceleration of the cooling rate at ~9 Ma. The complete profile model (Fig. 3.5D) was built using 5 AFT ages, two of which have track-length data, and 2 ZHe samples (top and bottom). The output model shows a slow cooling rate (~0.75°C Ma^{-1}) from high temperatures (~120°C) until ~ 25 Ma. The inclusion of the Jurassic ZHe data might be responsible for the modeled high temperature when rapid cooling commenced. A short duration, relatively rapid cooling event is shown by modeling, followed by a period of renewed slow cooling until ~11 Ma. The final rapid cooling episode brought the samples to the surface. Although the models were built to decipher the pattern of Cenozoic cooling the output fits well with ZHe ages, suggesting the bottom sample was partially reset and top sample reflects slow cooling during the Cretaceous. Time-temperature paths modeled (Figs. 3.5C and D) show slow cooling during most of the upper Cretaceous until onset of rapid cooling at ~25 Ma

The complex Cenozoic history shown by the thermal models might be the reason that a simple, clear break in slope denoting the onset of rapid exhumation was not observed.

3.4.3.2 Eastern Alai Range

We collected a vertical profile in the eastern part of the Alai Range (Figs. 3.1 and 3.6, location EAR), accessing via the Pamir highway. The profile is composed of 6 granitic samples distributed over 1052 m of elevation and analyzed using the AFT method. As in the Kyrgyz-Ata profile, we also analyzed the top and bottom samples using the ZHe method.

Analysis of zircons in the highest sample (12NU13) yield $^{206}Pb/^{238}U$ ages in the range of 148 to 284 Ma (Fig. 3.6A and table DR2), however, these zircons have a much higher level of discordance than in sample 12KA23. The least discordant analysis (i.e. below 10%) have $^{206}Pb/^{238}U$ ages between 245 and 274 Ma and the *TuffZirc* age for the complete data set yields an age of 253 Ma (+2.2/-6 Ma). Based on the results we suggest that the crystallization of this pluton occurred near the Permian-Triassic boundary. In a nearby area, *De Grave et al*. (2012) reported two slightly older U/Pb Concordia ages of 283.7 ± 3.5 and 287 ± 38 Ma. The age difference is significant but both plutons might reflect the same tectonic event.

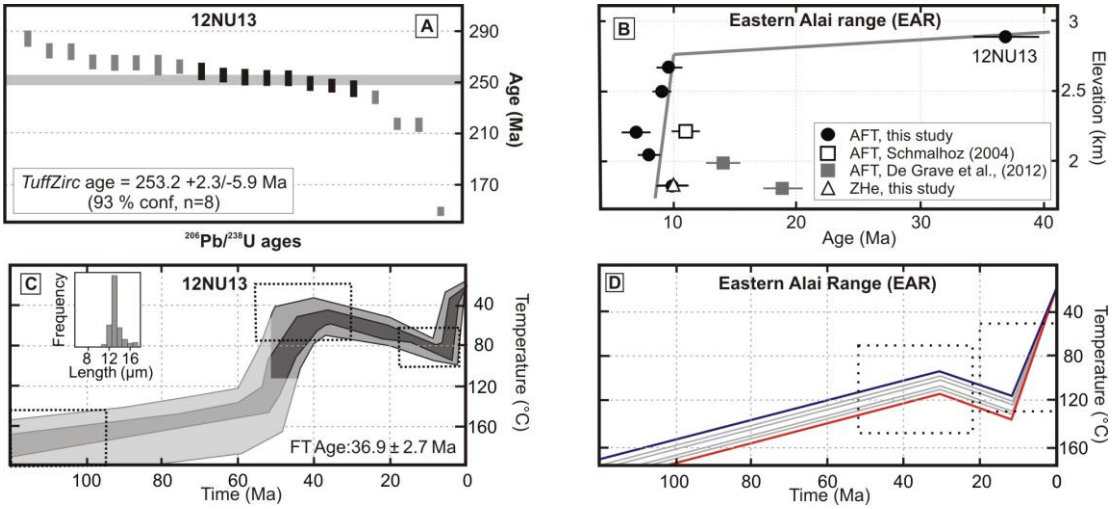

Figure 3.6(A) U-Pb *TuffZirc* age (*Ludwig*, 2003) calculated for sample 12NU23. Grey horizontal bar represent inferred age and uncertainty. Black rectangles are error bars of the analysis used to calculate the age (syngenetic), in grey error bars from the analysis discarded likely to experienced Pb loss. Box heights are 2 sigma. (B) AER from the Eastern Alai Range vertical profile. Age errors are 1 sigma. (C) Time-temperature histories obtained by thermal modeling using HeFTy software (*Ketcham*, 2005) of samples 12NU13. Unconstrained part of the models represented by transparent polygons. Dashed boxes are model input constraints. Inset shows histogram of track-length distribution. (D) Time-temperature histories derived from QTQt modeling (*Gallagher,* 2012). Dashed boxes are model input constraints. Blue and red lines correspond to the uppermost and lowermost samples, respectively.

The highest sample yielded a significantly older AFT age (36.9 ± 2.7 Ma) than the rest of the samples in the profile, which are between 7 to 9 Ma (Fig. 3.6B). This relation is clearly visible in the profile, enabling us to place the break-in-slope at ~10 Ma. The highest sample yielded a reliable ZHe aliquot of 110.7 ± 8.9 Ma, in good agreement with the high elevation sample 12KA22 from the previous vertical profile. The other aliquot (12NU13-2) has a significantly higher U concentration (1248 ppm) that might reflect radiation damage (e.g. *Guenthner et al*., 2013), thus accounting for the anomalously younger ZHe age. Interestingly, the bottom sample showed a youngest ZHe aliquot of 9.9 ± 0.8 Ma. The other 5 aliquots yielded older Paleogene ages. Interestingly, the resulting young age is similar to the AFT age for the same sample (see open triangle in Fig. 3.6B). The high U (1125.6 ppm) and [U]e concentration for the young aliquot might account for the young exhumation age.

In this area, *Schmalholz* (2004) obtained an AFT age of 10.9 ± 2.3, in good agreement with our dataset (open square in Fig 3.6B). However, 3 samples analyzed by *De Grave et al*. (2012) (Fig. 3.4) are slightly older than the results we obtained. The southernmost sample is located in a different tectonic block (Fig. 3.4) and the older AFT age might correspond to less exhumation. The other two ages came from within our profile and yield discordant results (grey filled squares in Fig. 3.6B). Our samples

12NU12 and 12NU16 were collected at similar elevations but yielded younger AFT ages than samples AI37 and AI38, reported by *De Grave et al.* (2012). Our samples have relatively small mean D_{par} value of 1.86 and 2.01 μm, suggesting faster annealing and relatively lower closure temperature (*Donelick et al*., 2005). Unfortunately, no kinetic parameters were reported by *De Grave et al*. (2012) to test if the ~8 Ma difference is related to different annealing properties between samples.

Although the AER is conclusive for constraining the onset of Cenozoic rapid cooling in this area, we modeled the thermal history of the samples in order to decipher the early Cenozoic history. Single-sample HeFTy modeling of sample 12NU13 (Fig. 3.6C) shows a relatively complex time-temperature history. The first models were run with minimum constraints and almost no acceptable paths were found. In order to get good and acceptable paths in the model output (Fig. 3.6C), we had to include a reheating episode prior to final uplift in the latest Miocene. The constrained part of the model (non-shaded area) shows a reheating episode from ~ 40 until 7 Ma, where a strong, fast cooling event occurred. The multisample QTQt model (Fig. 3.6D) was constructed using the 5 AFT ages, including 2 samples with track-length data and the two youngest ZHe aliquots of the 2 analyzed samples. We used the *Ketcham et al.* (1999) AFT annealing algorithm and *Guenthner et al.* (2013) ZHe diffusion algorithm. The resulting model show a relatively slow cooling rate until ~ 30 Ma, followed by a period of gentle reheating until around 10 Ma when a fast cooling episode commenced, exhuming samples to the surface. For this model we present the simplest plotting option in QTQt, the maximum likelihood model. Not surprisingly, the models do not provide tight constraints on the timing of reheating; however, the output models from both programs suggest that reheating occurred. This result is not unexpected, as the surface geology shows an uplifted and dissected sedimentary basin just south of the Gulcha profile (Fig. 3.4). As in the Kyrgyz-Ata profile, ZHe age (12NU13-1) of the highest elevation sample fits thermal models in Gulcha, suggesting slow cooling during most of the Cretaceous. The bottom sample in that profile was probably partially reset during Cenozoic reheating. Indeed, the aliquot with the highest U content (12NU12-2) yielded a late Miocene age (9.9 ± 0.8 Ma) in agreement with AFT data.

3.4.3.3 Chinese Alai Range

Finally, N of the Tierekesaki section (Fig. 3.1, location ChAr) we collected two spot samples at the southern boundary of the Alai Range and the deformed NW Tarim

basin sedimentary rocks. Both samples yielded a Late Miocene age (6.7 and 6.9 Ma) in agreement with a published age of 9.9 ± 1.0 Ma by *Sobel et al*., (2013). Mean track-length value show relatively long tracks (~14.9 μm) suggesting a fully reset age. Based on these results and the field reconnaissance, we propose that the exhumation in this area is driven by a south vergent structure.

3.4.4 Intramontane Alai Basin

In the eastern sector of the Alai basin close to the border between Kyrgyzstan and China and near the town of Nura, we collected two spot samples in Silurian sedimentary rocks with a Tien Shan affinity (Fig. 3.1, location NUR). Both samples yielded a Late Miocene AFT age (~11 Ma). *Coutand et al.* (2002) and *Strecker et al.* (2003) described important late Cenozoic tectonic activity in the Alai basin based on stratigraphic and geomorphic relations, but lack age control on their interpretation. We believe our cooling ages might reflect part of the tectonic activity described by those authors.

Moreover, based on our fieldwork we propose that the southernmost sample is located in the hanging-wall of a north-vergent thrust-fault and the northern sample in the hanging-wall of a south-vergent thrust (Fig. 3.5). In this scenario, we believe both faults might merge at depth with a major structure and are probably product of a more recent faulting. In any case, AFT ages represent single widely distributed late Miocene cooling event.

3.5. Interpretation of ages

LA-ICP-MS U/Pb crystallization ages span from Middle Permian to earliest Triassic for the emplacement of the granitic intrusions in the Alai Range. These ages are in agreement with previously published results (*De Grave et al*., 2012) in the Alai Range and correspond well with ages published in the Kokshaal Range (*Solomonovich & Trifonov*, 2002; *Konopelko et al*., 2007; *Seltmann et al*., 2011). For the Kyzylkum segment, *Seltmann et al*. (2011) report Early Permian post-collisional magmatism with emplacement ages of 293-276 Ma. The episode of post-collisional magmatism widely distributed across the entire Kyrgyz South Tien Shan is related to the final amalgamation of the Paleozoic Tien Shan orogen and the Central Asian Oceanic Belt (CAOB) as a whole (e.g. *Allen et al*., 1992, *Windley et al*., 2007, *Biske & Seltmann*, 2010).

Thermochronology results show two distinctive exhumation episodes during the Cenozoic: a widely distributed and robustly represented late Miocene exhumation event present in the Takthalik, Fergana and Alai Ranges and a smaller in magnitude Oligo-Miocene event in the central Alai Range. These two episodes are in good agreement with regional exhumation trends reported in the Western, Central and Eastern Tien Shan (*Macaulay et al*., 2014).

Based on our thermal modeling and AER results (Fig. 3.2), we can confirm that the Takthalik Range acted as a coherent block during Cenozoic deformation. The thrust faults in between the range are preexisting features that were not active during late Miocene exhumation. Combining all available information, we suggest that Cenozoic cooling commenced in the latest Miocene. Based on this interpretation and on our structural reconnaissance fieldwork, we interpret the Takthalik area as a pop-up structure bounded by reverse faults dipping to the south and the TFF. The S-dipping faults might merge at depth with the TFF. This configuration is similar to the Talas Range, located further north. Although the Talas Range experienced significant transpressional exhumation in the Oligo-Miocene, a younger reactivation is also present (*Bande et al*., 2015a). The late Miocene exhumational event found in the Tahthalik Range might be related to this latter history.

Moving south to the central part of the Fergana Range in the Kaldama pass, we interpret the younger, western samples as reset ages, based on the longer mean track-length and the regional extent of a late Miocene exhumation event. On the other hand, the eastern samples reflect partially reset ages. This pattern implies that the late Miocene exhumational event preferentially uplifted the western sector of the TFF. The young, late Miocene exhumation ages are in good agreement with exhumation in the Takthalik range and in most of the Central Kyrgyz Tien Shan as well as the Kyrgyz range (e.g. *Bullen et al*., 2003; *Macaulay et al*., 2013 and 2014). In the Karakuldja river section, the sampled tectonic blocks are separated by a thrust fault. Since the ages decrease to the east, we interpret the younger, late Miocene samples as reset ages. Consequencely, the vergence of the system must be towards the east. Furthermore, we have not identified a clear fault relation west of sample 12FE30 (Fig. 3.3A) that might suggest a west-vergent structure. In addition, we locate a clear fault contact between samples 12FE29 and 12FE28 (Fig. 3A). Based on these results, we interpret the structure as a backthrust, probably connected in the subsurface to a ramp or a major east-dipping fault.

This region coincides with the basin boundary of a thick transtensional Jurassic sedimentary basin (*Sobel*, 1999). We argue that, controlled by the sequence tapering to the west, the backthrusts are part of a thin-skinned deformational sequence. Unfortunately, subsurface data in this area is not available to further test our hypothesis. Regarding the timing of these structures, we propose a late Miocene exhumational event in the southern Fergana Range, based on exhumation along the Karaldja River and in conjuction with exhumation on the western side of the Kaldama pass.

In the Alai Range, ZHe ages and thermal modeling suggest slow cooling during the Cretaceous, as previously said by many authors (e.g. *Afonichev & Vlasov*, 1984; *Cobbold et al*., 1996, *Sobel et al*., 2006b). Both top profile samples (12KA22 and 12NU13) from high elevations yielded Mesozoic ages, fitting well with time-temperature modeled paths.

The Cenozoic exhumation history along this range has differences from west to east. In the Kyrgyz-Ata area (CAR), AFT and ZHe dating and thermal modeling suggest that exhumation started at around 25 Ma. Both single and multiple sample modeling (Fig. 3.5C and D) point to an Oligo-Miocene onset of exhumation and a late Miocene final, rapid uplift of the central Alai Range. In between rapid cooling segments, QTQt model (Fig. 3.5D) suggest a reduction in the exhumation rate, while the slow exhumation period is absent in the HeFTy model (Fig. 3.5C). However, the Oligo-Miocene onset and late Miocene final uplift are well constrained in both models and are well represented in other Tien Shan sectors.

In the eastern Alai range (EAR), the history is slightly different. The QTQt modeling results shows that the sampled block was reheated by 20 ± 7 °C between 30 and 11 Ma. We interpret the sampled granite as part of a NW-verging block that places Paleozoic basement on top of Mesozoic-Cenozoic sedimentary basin-fill. We suggest that the sampled block fomerly lay beneath an originally larger Gulcha basin that was inverted during late Miocene final uplift. *Hausburg et al.* (2012) measured 400 m of Neogene strata in the uplifted Gulcha basin, which is a minimum estimate for the thickness of the Neogene section. Indeed, the Neogene is up to 3.5 km thick in the Fergana basin to the north (*Khodjaev*, 1969; *Bande et al*., 2015b) and up to 2.5 km in the Alai basin to the south (*Coutand et al*., 2002). Assuming a geothermal gradient of 25° C km^{-1} we suggest that the Gulcha basin thickness during the Miocene was around 1 km. Finally, in the latest Miocene, starting at 11Ma, the basin was rapidly inverted at

a rate of 8°C Ma^{-1} (QTQt model estimate). The fast cooling was probably favored by the presence of partially consolidated sediments which are easy to strip off.

The third locality in the Alai Range (ChAR) also shows late Miocene AFT ages. Based on these reset ages and the well-mapped structural geology we suggest that a late Miocene south vergent thrust in the Chinese Alai Range was responsible for stacking Paleozoic basement sheets on top of Cenozoic sediments of the NW Tarim basin. This interpretation is consistent with previous ideas presented by *Sobel et al*. (2013) and *Yang et al.* (2014) in the same area. Our new cooling ages show that the size reduction of the NW Tarim basin suffered a peak of activity during the latest Miocene.

Finally, the samples located along thrust sheets in the eastern Alai Basin (Fig.3.1, location NUR), near the town of Nura, also show late Miocene exhumation ages. Based on the latter ages we interpret a late Miocene reduction in the size of the Alai and NW-Tarim basin between the north-vergent Pamir and south-vergent eastern Alai Range. Stratigraphic relations also show that the Pamir propagated northward during the middle Miocene – Pliocene (*Burtman & Molnar*, 1993; *Coutand et al*. 2002). Based on our ages we propose that the reduction is a long-living mechanism with a major event at ca. 10 Ma and still active based on recent seismicity data (*Feld et al.*, 2015). Probably, the blocks sampled in this area are limited by minor faults that merge at depth to a major structure responsible for the Pamir propagation (Main Pamir Thrust). *Teshebaeva et al.* (2014) argue that the main surface displacement and rupture of the Nura earthquake (2008, magnitude 6.6) occurred in the footwall of the minor Irkeshtam fault, a splay of the Pamir Frontal Thrust. We agree with their interpretation and probably most of the minor surface faults are connected to a deep major structure.

In summary of our new data, we conclude that the late Miocene rapid exhumation event is widespread and well represented along the southern western Tien Shan, as it is in the entire Tien Shan range. Moreover, we interpret an Oligo-Miocene onset of exhumation in localized sectors of the Alai Range. We also suggest that the Gulcha basin was broader than today and subsided around 1km between 30 and 7 Ma, acting as a connection within the Fergana and Alai basins.

3.6. Discussion

Based on our thermochronological data, we postulate three main stages of cooling during the Cenozoic: (1) low rates during a quiescent period during most of the

Paleogene, (2) onset of rapid cooling near the Oligo-Miocene boundary followed by a decreased rate of cooling and in some areas minor reheating and (3) final rapid cooling and exhumation starting in the latest Miocene. Based on geological, thermochronological and biostratigraphical data, many authors (*Ruhin & Ruhina*, 1961; *Afonichev & Vlasov*, 1984; *Maksumova et al*., 2001; *Bullen et al*., 2003; *Sobel et al.*, 2006a; *De Grave et al*., 2012; *Macaulay et al.,* 2013; *Bosboom et al*., 2015) have postulated a period of tectonic quiescence in the Kyrgyz Tien Shan extending from the late Mesozoic through much of the Early Cenozoic. In agreement, our well-constrained thermal models and ZHe ages from the western Tien Shan support a period of low cooling rate through the Cretaceous and much of the Paleogene. Following the quiet period, we find compelling results concerning the Neogene evolution of the western Kyrgyz Tien Shan that will be discussed in the next sections.

3.6.1 Spatio-temporal distribution of Neogene deformation in the western Tien Shan

Our thermochronological results show two distinctive groups of fully reset ages in the late Cenozoic: an Oligo- early Miocene group and a late Miocene one. Although both groups are distributed within the western Tien Shan, different groups are better represented in different zones. The ages obtained in the NW Tien Shan correspond mainly to the Oligo-Miocene group. In a recent publication (*Bande et al.*, 2015a) we propose that the Chatkal, Talas and northern Fergana Ranges experienced an episode of fast exhumation at 25 ± 5 Ma. Furthermore, we proposed that the exhumation episode is closely related to strike-slip movement along the TFF and has a geodynamic connection to Pamir indentation (*Sobel, et al*. 2013; *Bande et al*, 2015a). New results from the central Alai Range (CAR) also depicted an onset of cooling at the Oligo-Miocene boundary, meaning that this early event is also present in the SW Tien Shan. However, this age group has only been found in two areas so far; therefore, the extent is presently considered to be limited to a small portion of the Alai Range.

In contrast, in the southern sector the majority of reset ages are much younger, reflecting a second, widely distributed deformation episode. At the western side of the Kaldama pass, AFT analysis yield an age between 6 to 8 Ma (Fig. 3.1, Table 1). We found similar ages at the Karakulja River (~11 Ma, Fig. 3.3), implying that the central and southern part of the Fergana Range also experienced a rapid exhumation event in the late Miocene. In contrast, the northern Fergana Range experienced the onset of rapid exhumation in the Oligo-Miocene (*Bande et al*., 2015a), related to restraining bend

exhumation of the Chatkal Range. Samples from the Alai Range mostly yield ages consistent with a ~ 10 Ma event. In the central part (Fig. 3.1, CAR), as previously stated, exhumation commenced at ~25 Ma. At this locality, a final strong event is modeled starting at 11Ma; this is responsible for bringing samples to the surface. In this central region, both events are represented in the Kyrgyz-Ata profile and in samples analyzed by *De Grave et al*. (2012) (Fig. 3.4). New and published samples located in the eastern Alai Range (EAR) support a ~10 Ma event in that area. Our Gulcha AER (Fig. 3.5D) clearly shows an onset of exhumation around that time. Pamir-related thrust faults located in the easternmost Alai basin (Fig. 3.1 and 3.4) also shows the late Miocene event with ages <10 Ma. This strong event is also recorded in the Chinese sector of the Alai Range (ChAR, Fig. 3.1), based on 2 new results and a sample reported by *Sobel et al*. (2013). Northward propagation of the Pamir might be the driver of cooling in this region and was probably active until at least 7 Ma.

Our new data show that much of the Alai and southern Fergana Range suffered a period of rapid cooling in the late Miocene (10-12 Ma). Moreover, samples along the TFF showed exhumation ages in the same time interval, implying that exhumation was not circumscribed to the SW Tien Shan. Indeed, during the late Miocene, exhumation intensified along the entire Tien Shan Range (e.g. *Bullen et al.*, 2003; *Sobel et al*., 2006b; *Jolivet et al*., 2010; *Glorie et al*., 2011, *Macaulay et al*., 2014) Stress transfer along the rigid Tarim block has been proposed as a driver for late Miocene exhumation in the central Tien Shan (e.g., *Avouac et al.*, 1993; *Yin et al.,* 1998). However, based on the new regional areal extent of the late Miocene event a different mechanism is needed. Directly south of the study area, the Pamir is presently colliding with the Tien Shan. It has been proposed that the north Pamir has moved 300-400 km north with respect to stable Asia (e.g., *Burtman & Molnar*, 1993) and much of that movement was accommodated by subduction (e.g., *Hamburger et al*., 1992; *Sobel et al*., 2013). Although the nature of the crust subducting beneath the Pamir is still not clear, the relative strength when compared to the rigid Tarim crust should be lower. In consequence, we expect lateral strength variation between Tarim and Pamir crust and neither of them can act as the sole driver for the entire Tien Shan exhumation during the late Miocene.

3.6.2 Basin partitioning and exhumation

It is widely accepted that the Tarim, Fergana, Alai and Tadjik basins were part of a continuous shallow marine basin (Parathethyan sea) in the early Cenozoic (*Brookfield & Hashmat*, 2001; *Burtman*, 2010; *Wei et al*., 2013; *Bosboom et al*., 2015) and were subsequently dissected; these now form four separate depocenters. However, little is known about the timing and mechanisms of the physical partitioning of the Parathethyan basin. Thermochronological data from the Chatkal and Kokshal ranges (*Sobel et al*., 2006a; *Bande et al*., 2015a) point to a late Oligocene – early Miocene onset of exhumation, implying that the shortening around the margins of the Fergana and Tarim basins started around that time. Our new data from the Alai Range also suggest that its central sector has an onset of exhumation at around 25 Ma, coeval with exhumation in the Chatkal and Kokshal ranges. The early exhumation of the CAR might have created a topographic barrier (proto Alai range) that separated the Fergana and the Alai basins, starting the actual basin partitioning. Interestingly, to the east, in the Gulcha sector, thermal modeling of the sampled profile requires a reheating stage between 30 and 11 Ma. Crustal thickening produced by exhumation of the CAR might have enabled subsidence in the Gulcha sector, favoring reaheating of the Gulcha samples.

The Massaget Fm. is a 1 – 3 km thick Oligo-Miocene unit composed of red sandstones, siltstones, claystones and minor conglomeratic layers described in the Fergana, Gulcha and Alai basins (*Artyomova, et al*., 1971; *Coutand et al*., 2002; *Hausburg et al*., 2012; *Bande et al*., 2015b). It has been interpreted as a syn-tectonic unit in many areas within the western Tien Shan, although its age does not appear to be correlated with the main tectonic event that occurred at ~10 Ma. Based on our thermochronological results, we believe the Massaget Fm. is the syn-tectonic unit related to the ~25 Ma onset of exhumation. Erosion produced by block uplift filled the Fergana and Alai basins with locally-sourced detritus from the different adjacent ranges (Chatkal, Alai or Pamir). In the Tarim basin, the Oligo-Miocene Wuqia Group is also composed of red nonmarine mudstone, sandstones and sporadic comglomerates (*Meng*, 1997; *Hao et al*. 2002; *Wei et al*., 2013). Interestingly this unit is also interpreted as tectonically-related. The lithological description and timing of both units suggest coeval deformation and depositional environment. However, the mineralogical composition might be different since are sourced from different ranges uplifted at the same time. Based on our exhumation data and thermal models we suggest that the Wuqia Group

and the Massaget Fm are equivalents and show contemporaneous sedimentary basin margin deformation and early physical separation of the Paratethyan Sea.

3.7. Conclusions

An Oligo-Miocene onset of fast exhumation was observed in the central Alai range. In the western Tien Shan, we have previously postulated (*Bande et al*., 2015a) that Pamir indentation acted as a tectonic driver and the TFF provided the link transferring stress to the Chatkal Ranges around that time. The presence of a coeval event in the Alai Range suggests that Pamir indentation also affected the southwestern Tien Shan.

Based on our thermochronological results, we conclude that the Gulcha basin was wider during most the Miocene, connecting the Fergana and Alai basins, while to the west, the Kyrgyz Ata sector acted as an uplifted block in the early stages of dissection. Our new data shows a complex temporal pattern of basin partitioning in the Alai sector, suggesting that the range was not uplifted as a complete and coherent block in a single stage rather, an earlier stage of dissection started around 25 Ma. During most of the Miocene the Alai, Gulcha, Fergana and Tarim basin were only partially dissected. We suggest that only after the late Miocene the main four basins were separated and formed independent depocenters. This is particularly clear in the Gulcha basin, which today is an uplift basin surrounded by topographic highs composed of Tien Shan basement

The widespread late Miocene cooling event found through much of the central and eastern Tien Shan is also well represented in the western sector. New thermochronological ages and thermal modeling in the Fergana and Alai ranges show that this event was also intense in the western Tien Shan. The presence of late Miocene exhumation ages west of the TFF and directly north of the Pamir indenter suggest that timing of deformation for the entire Tien Shan is coeval. However, stress transfer along the rigid Tarim block or Pamir indentation might not be the single driver for Tien Shan late Miocene exhumation.

Acknowledgments

This contribution was supported by the Darius Programme and a fellowship from the German Academic Exchange Service (DAAD) to A. Bande. We are grateful to the members of the Materials Research Department at the GSI Helmholtzzentrum (Darmstad, Germany) for heavy ion irradiations. The data for this paper are available by emailing the corresponding author: aebande@googlemail.com.

Chapter 4
Cenozoic palaeoenvironmental and tectonic controls on the evolution of the northern Fergana Basin

Published by Alejandro Bande, Shukrat Radjabov, Edward R. Sobel and Tatyana Sim in Brunet, M.-F., T. McCann and E.R. Sobel (eds): Geological Evolution of Central Asian Basins and the Western Tien Shan Range. Geological Society, London, Special Publications, 427, doi:10.1144/SP427.12

Abstract

The least well-documented intramountain basin within the Tien Shan is the Fergana basin. Cenozoic deformation is localized along thrusts on the northern and southern flanks, and by transpressive deformation associated with the dextral Talas-Fergana fault on the eastern margin. We use sedimentologic and stratigraphic observations from well-exposed Cenozoic outcrops to describe depositional environments, provenance and sources. These results are combined with interpreted seismic reflection lines and geologic cross-sections are extended laterally based on outcrop geology to the north and east. Following a tectonically-quiet early Cenozoic period, a progressive change in palaeocurrent indicators suggests Oligo-Miocene uplift of the hinterland, coupled with an increase of higher energy facies in the Massaget Formation. A renewed pulse of deformation tilted Massaget strata and deposited a considerable volume of coarse sedimentary rocks (Baktriy Formation). The younger episode moved progressively basinwards, as imaged by growth-strata relationships in the subsurface. Published work shows that the accumulation of an impressive ~8 km of Cenozoic deposits cannot be accommodated only by lithospheric flexure produced by a tectonic load. We agree with the hypothesis that the thick sediments preserved in the basin are accommodated by lithospheric folding and propose that this is driven by compression associated with south-vergent Pamir subduction.

4.1 Introduction

The triangular Fergana basin in the Western Kyrgyz Tien Shan (Fig.4.1) has a different morphology and thus potentially a different structural evolution compared to the other Cenozoic intramountain basins within the Tien Shan, which are typically bounded by north or south vergent faults (e.g. *Cobbold et al*. 1996; *Burbank et al*. 1999; *Macaulay et al*. 2015). The position of this basin directly north of the Pamir provokes speculation of a tectonically-linked connection, but to date, no convincing mechanism has been proposed. The Fergana basin is bounded on the eastern side by the dextral Talas Fergana fault (TFF); the basin experienced 20 ± 11° of counter-clockwise rotation since the Paleogene (Thomas *et al*. 1993). This rotation is predicted to have been

compensated by significant south-southeast vergent thrusting in the Chatkal ranges, located on the northern margin of the basin. Such faults are often drawn on structural maps (e.g., *Khodjaev* 1969). However, the 200,000 scale geological maps show Quaternary sediments onlapping the Palaeozoic range in many places (*Artemova & Brodskiy* 1963; *Sidorenko* 1972); seismicity is sparse (*Kalmetieva et al*. 2009) and geodetic GPS shows slow rates of shortening (~5 mm/yr) across this basin margin (*Zubovich et al*. 2010), making definitive statements about the deformation style challenging. To date, published basin-scale cross-sections have not been supported by high resolution seismic reflection data. The lack of well-documented structures coupled with poor chronologic control on the depositional history of the ca. 8 km of late Cenozoic strata have led to a range of models including tectonic block rotation, lithospheric buckling and crustal thickening for the Cenozoic evolution of the region (e.g., *Akramhodjaev & Saidalieva* 1971; *Gridnev* 1971; *Clarke* 1984; *Burov & Molnar* 1998; *Cobbold & Davy* 1988; *Bazhenov* 1993; *Cobbold et al*. 1996).

In order to illuminate this history, we first present sedimentologic and stratigraphic observations from the well-exposed Cenozoic outcrops to the east, near Tash-Kumyr in Kyrgyzstan (Fig. 4.1). These are used to describe the depositional environments, provenance and sources for these strata. These results, together with a lithological description of a well (WN-1) drilled in the northern part of the basin (Fig. 4.1), are used to help interpret a suite of seismic reflection lines acquired by BGP, Integra-Geophysica and Uzbekgeophysica in Uzbekistan. The cross-sections based on subsurface data are extended laterally by combining mapped and observed outcrop geology in the Chatkal range to the north and east. With this database, we can address the deformation style and timing and ultimately, make inferences about how the basin has evolved from the late Palaeozoic through the Cenozoic. We combine the analysis of stratigraphy and subsurface data to address the role of pre-existing structures, areal distribution of depositional facies, possible subsidence mechanism, and prominent late Cenozoic growth strata. Finally, we discuss possible interactions between the Fergana basin and the Pamir indentor to the south.

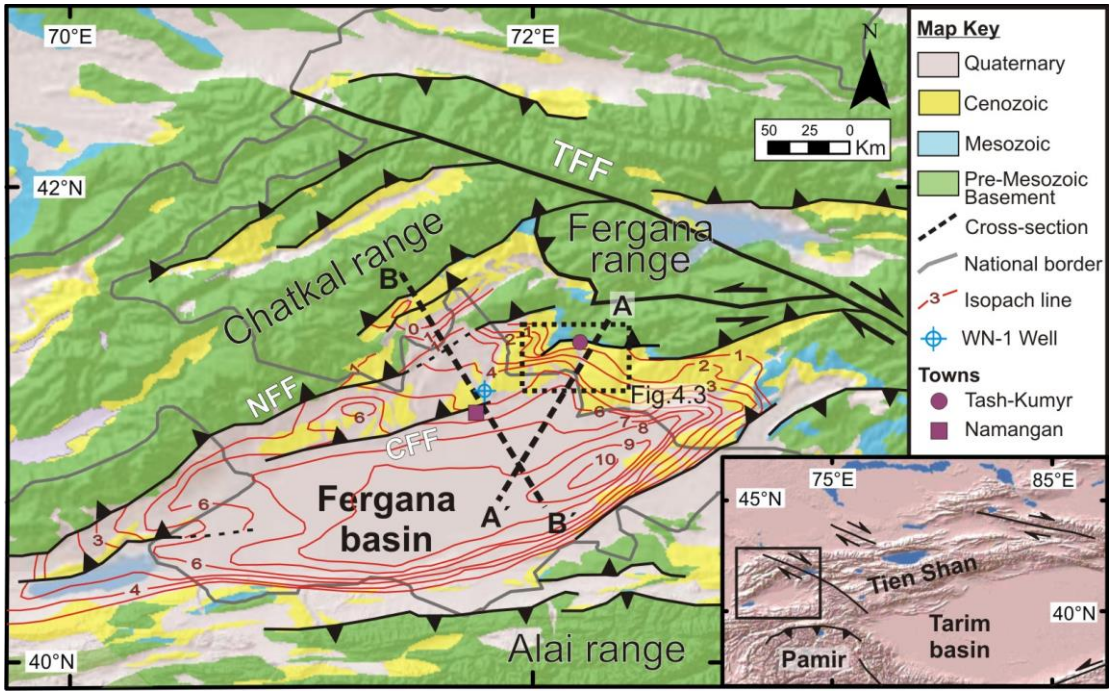

Figure 4.1Geological map of the Kyrgyz Tien Shan (modified after *Vlasov et al.* 1991 and *Bakirov et al.* 2001) superimposed on shaded relief image, showing regional structures in the western Tien Shan, location of interpreted cross-sections and isopach contours of the Mesozoic–Cenozoic Fergana Basin-fill. Dashed box shows location of Figure 4.3. Isopach contours show the depth below the surface in kilometres from the top of the Palaeozoic (*Vlasov et al*. 1991). Inset map shows location of Figure 4.1 in the Tien Shan region. TFF, Talas–Fergana Fault; NFF, North Fergana Fault; and CFF, Central Fergana Fault.

4.2 Geologic setting

The triangular Fergana basin lies in the Western Kyrgyz Tien Shan, which is part of the Central Asian Orogenic Belt (CAOB). This belt is composed of several microcontinents, magmatic arcs, ophiolitic units and accretionary wedges that underwent several periods of amalgamation during the Early Palaeozoic (*Bakirov & Maksumova*, 2001; *Burtman* 2010; *Kröner et al*. 2013), giving shape to the Palaeozoic Kazakh continent. Upper Devonian red clastic beds, outcropping in the Middle Tien Shan, formed as a result of erosion and deposition in the southern margin of the Kazakh continent (*Ges′ & Seliverstov* 1995). Subsequently, a marine passive carbonate margin evolved from an attached to an isolated platform during the early Carboniferous (*Alexeiev et al.* 2015). On the other hand, South Tien Shan units outcropping in the Alai and Fergana Ranges represent oceanic deepening and deep-water clastic facies reflecting the widespread regional extension of the Upper Palaeozoic oceanic basin (Turkestan Ocean) (*Biske & Seltmann* 2010). Bashkirian (~320 Ma) deformation reflects the onset of a convergent margin while the basin reached the maximum width

in the latest Carboniferous with an asymmetric shape thicker to the south (*Alexeiev et al*. 2015). Marine deposition stopped at the Carboniferous-Permian boundary (298 Ma) followed by folding and granitoid plutonism reflecting the onset of collision (*Biske & Seltmann* 2010). For more detailed descriptions of the Palaeozoic Kyrgyz Tien Shan please refer to *Alexeiev et al*. 2015 and *Loury et al*. 2015

A hiatus during the Triassic points to a subaerial environment at this time; indeed, there is little evidence for significant relief in the area surrounding the basin during much of the Mesozoic. Most of the latter region was affected by long-lasting erosion leading to the formation of a regional denudation surface (*Makarov* 1977; *Chediya* 1986; *Cobbold et al.* 1996; *Bullen et al.* 2003; *Sobel et al.* 2006a; *De Grave et al.* 2011; *Macaulay et al.* 2013). This surface is still preserved and is possible to follow in the Tien Shan landscape. During the Jurassic, sandstones and coal-bearing shales of nonmarine origin were deposited in assymetric transtensional basins bounded by the TFF (*Sobel* 1999); these basins are thick close to the fault and thin rapidly away. Similar although thinner Jurassic deposits are noted in the Karatau range at the northern end of the TFF, related to dextral slip (*Allen et al* 2001). Jurassic deposits in the subsurface of the Fergana basin appear to be much thinner than the strata deposited along the TFF (*Clarke* 1984); seismic data presented in this study suggests that lateral thickness variations are minor, pointing to a different style of basin formation. Cretaceous red beds (from conglomerates to mudstones) outcrop sporadically in the Fergana basin foothills. A branch of the Cretaceous Tethyan Seaway left a marine depositional record in the basin (*Ruhin & Ruhina* 1961). An Albian to Turonian shallow marine tongue entered from the east to the basin triggering the deposition of marginal marine to lagoonal facies during the Upper Cretaceous.

The calm tectonic environment continued into the Paleogene, enabling deposition of low-energy clastic sedimentation interspersed with sporadic marine incursions. These marine progradations are well-correlated (e.g., *Bosboom et al*. 2015) and have a regional distribution along the Central Asian interior. During the Cenozoic, the India-Asia collision stresses reached the Tien Shan and tectonic movements occurred in the area. The Tien Shan Ranges, favored by the presence of pre-existing discontinuities, were uplifted and intramountain basins developed, thus shaping the present topography (e.g., *Macaulay et al.* 2014).

4.3 Stratigraphy of the northern Fergana Basin

4.3.1 Subsurface lithological description

The well West Namangan-1 (WN-1) drilled in the hanging wall of the Central Fergana fault (CFF) reached the Eocene section of the basin with a total depth (TD) of 4140 m (Fig. 4.2). The upper 820 m correspond to the Baktriy Formation and coarsen and thicken upwards. The Pliocene section is composed of clastic beds; conglomerates are relatively more abundant than in deeper units. Underlying the Baktriy Fm., a thick interval of 3100 m is attributed to the Massaget Fm. The lithology of this unit is composed of sandstones, siltstones, claystones and minor conglomeratic layers. The unit is subdivided into two sections (suites) that are widely used in the subsurface description of the Fergana basin. Most of the Massaget Fm. is represented by the Pale Pink Suite, with a thickness of 2790 m. The lower part of the unit corresponds to the Brick Red Suite (310 m). At 3920 m the well reached the top of the Fergana Group, represented by a sandstone layer. The upper part of the unit is composed by the Sumsar, Isfara and Rishtan Fms and is mostly composed by clastic fine-grained rocks (claystones and siltstones). The first limestone levels are described at 4060 m and have an Eocene age, representing the top of the Turkestan Fm. Interbedded with the limestones are fine-grained clastic rocks. A second carbonatic interval appears at 4107 metres below kelly bushing and is interpreted as the Alai Formation. With a TD of 4140 m the well drilled a partial thickness 220 m of the Fergana Gr. and did not reach the Paleocene section.

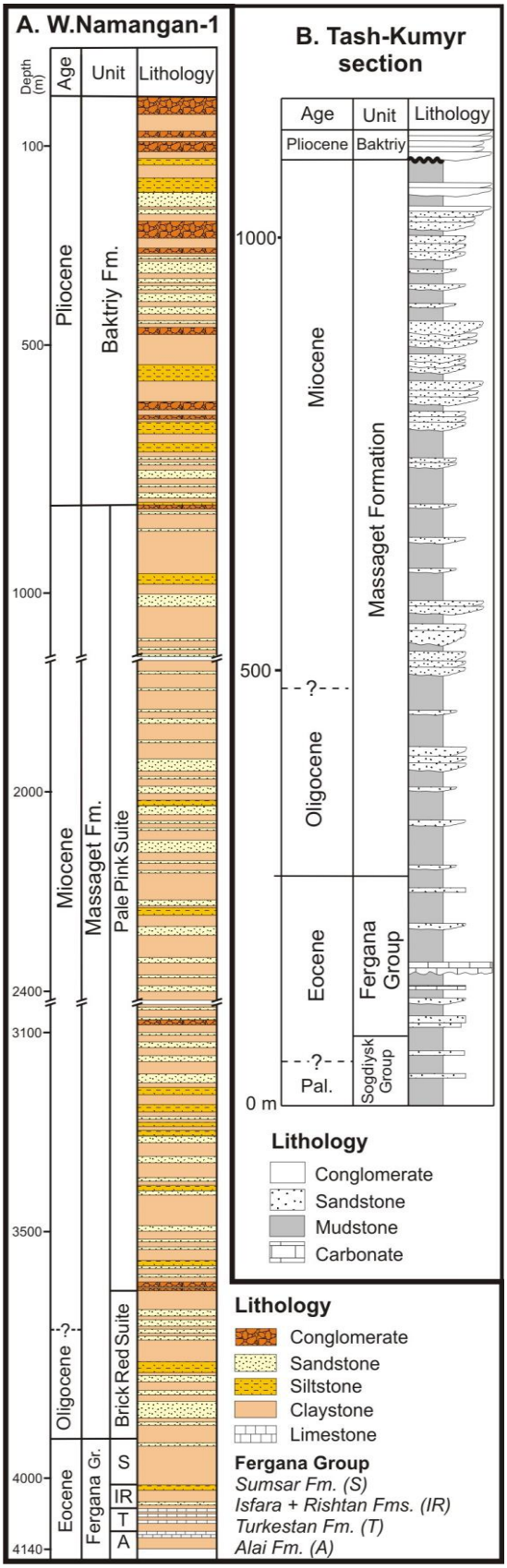

Figure 4.2(A) Lithological description of the West Namangan-1 (WN-1) well drilled in the hanging-wall of the CFF to the left. (B) Simplified logged section located east of the Naryn river near Tash-Kumyr.

4.3.2 Sedimentology and facies analyses of the Tash-Kumyr section

The Cenozoic succession of the Fergana basin is exposed along the foothills of the Chatkal, Fergana and Alai Ranges with a complex structural configuration. In the northeastern part of the basin, the southern limb of the Karagunday anticline (Fig. 4.3) offers key exposures of the sedimentary beds with dips ~65°. In that area, we documented sedimentological characteristics from a continuous 1100 m thick section (Fig. 4.4), which provides the foundation for the following descriptions of sedimentary lithofacies and interpretations of depositional processes. A total of 17 lithofacies (modified from *Miall* 1996), detailed in Table 1, are defined based on lithology, texture, grain size, bedding geometry and thickness, stacking patterns and sedimentary structures. They have been grouped into 7 sedimentary lithofacies associations, summarized in Table 2 and described below, that are interpreted to reflect processes characteristic of depositional environments.

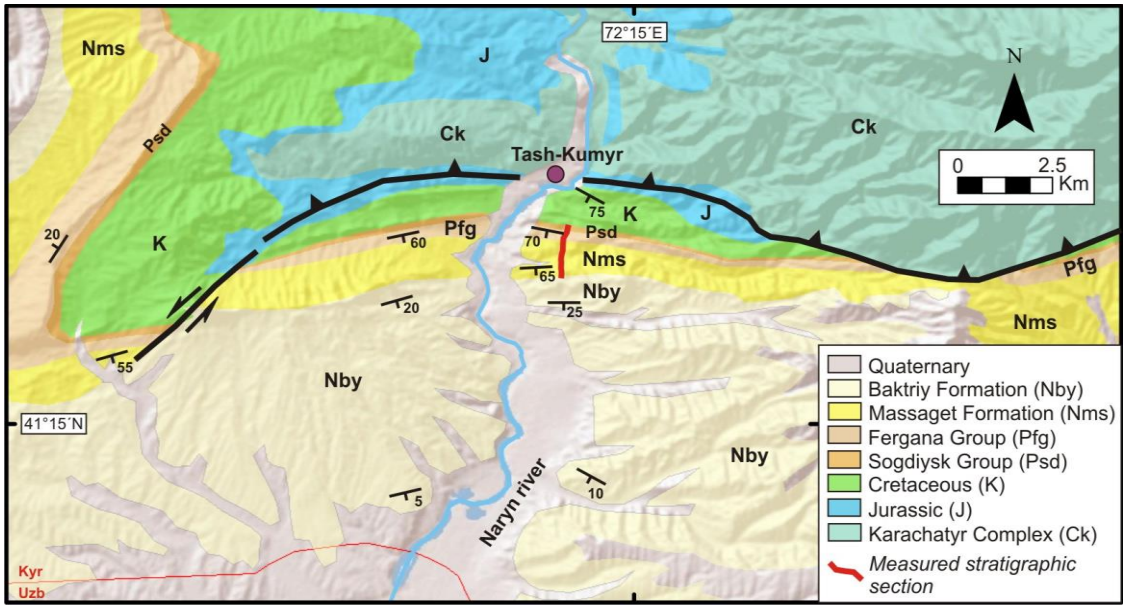

Figure 4.3 Geological map of the northern Fergana Basin foothills (modified after *Artyomova et al.* 1971) near the town of Tash-Kumyr, showing location of measured stratigraphic section. For location, see Figure 4.1.

The section (Fig. 4.4) spans from the Paleocene to the Pliocene, with at least one regional angular unconformity. The base of the section is represented by the Sogdiysk Group, which is formed by the Bukhara and Suzak Formations. *Bosboom et al.* (2015 and references therein) correlated these units with the Qimugen Formation in the Tarim Basin and assigned an Upper Paleocene – Lower Eocene age based on fossil assemblages. The Fergana Group overlies the Sogdiysk Group, and is composed of the

Alai, Turkestan, Rishtan, Isfara, Hanabad and Sumsar Formations. Based on bivalve assemblages, *Bosboom et al*. (2015) correlated these units with marine incursions spread over Central Asia and assigned them a Middle to Upper Eocene age. The Massaget Formation was deposited on top of this sequence. The age of this non-marine unit was traditionally considered to be Oligo-Miocene (Pg^3_3 -N_1ms) (*Artyomova et al*. 1971). The overlying Baktriy Formation is separated by a regional angular unconformity; at Tash-Kumyr, it is ~ 65°. This unit has been assigned a Pliocene age (*Artyomova et al*. 1971) based on fossil assemblage and lithostratigraphic correlation.

Lithofacies	Description	Interpretation
Fm	Massive mudstone to siltstone	Suspension deposits disrupted post-depositionally
Fl	Laminated mudstone to siltstone	Suspension deposits in shallow standing water
Fps	Massive mudstone with development of pedogenic calcretes	Suspension deposits or abandoned channel affected by pedogenic alteration (palaeosol)
M	Finally laminated alternation of mudstone and limestone layers.	Suspension deposits in shallow water alternating with precipitation of carbonates.
Sm	Massive sandstone	Rapid deposition. Alternatively, post-depositional perturbation of sand deposits.
Sh	Horizontally laminated sandstone	Deposition during upper flow regime conditions.
Sr	Ripple cross-stratified sandstone	Deposition of sand ripples
Shc	Convoluted bedded sandstone	Deformation by different loading
St	Trough cross-stratified sandstone	Deposition by migrating 3D dunes
Sp	Planar cross-stratified sandstone	Deposition by migrating 2D dunes
Sc	Shell-dominated sandstone	Deposition by suspension after storm events
Sb	Bioturbated sandstone	After deposition organism disturbed the primary structures
Gco	Clast supported organized conglomerate	Deposition by traction currents
Gct	Clast supported trough cross stratified conglomerate.	Deposition by traction currents in migrating subaqueous 3D dunes
Gcp	Clast supported planar cross stratified conglomerate.	Deposition by traction currents in migrating subaqueous 2D dunes
Gch	Clast supported horizontally bedded conglomerate	Deposition by traction currents in migrating longitudinal bedforms
Gci	Clast supported imbricated conglomerate	Deposition by traction currents in migrating subaqueous bar
Gm	Matrix supported polymictic conglomerate	Deposition by mass flows from hyperconcentrated or turbulent flows.

Table 4.1 Lithofacies codes, descriptions and interpretations.

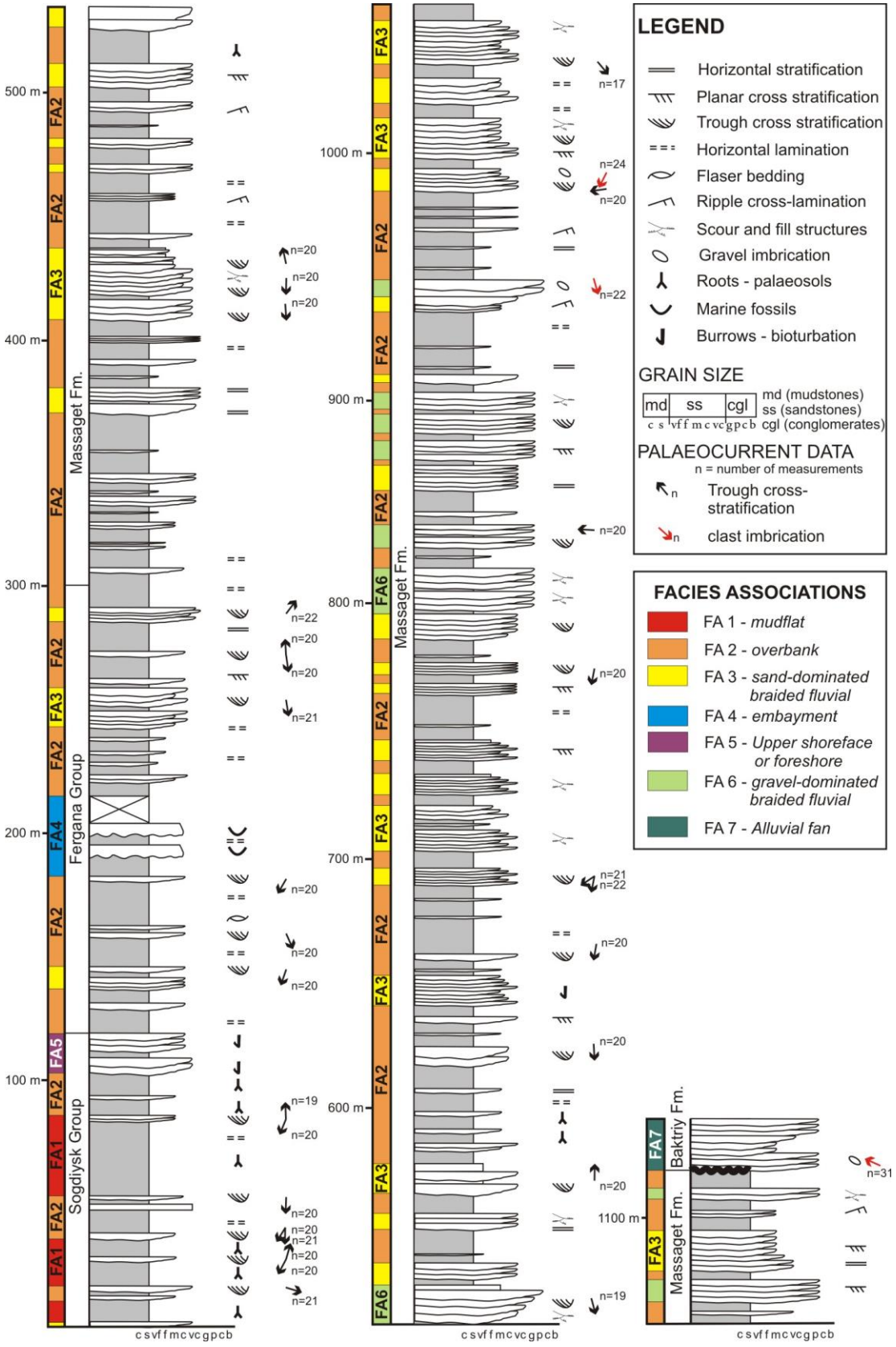

Figure 4.4Measured stratigraphic section with facies associations (FA) interpretation of the Sogdiysk, Fergana, Massaget and Baktriy units in the northern Fergana Basin foothills. For location of the section see Figure 4.3.

4.3.3 Lithofacies associations (FA)

FA1. Interbedded mudstones and sandstones with abundant palaeosols (Fm, Fl, Fps, Sm)

This association is composed of red to pink, laterally extensive, tabular, laminated or massive mudstone with development of palaeosol layers (Table 1). Thin sandstone beds are interbedded with the mudstones. Palaeosol layers are composed of white to light grey calcareous nodules and occur in isolated, clustered or coalescent bodies (Fig. 4.5A). Their forms vary from spherical to irregular, blocky and massive. Palaeosol layers range from 1 to 5 m thick. Some levels are characterized by desiccation cracks filled with medium-grained sandstone. This facies association is exclusive to the Sogdiysk Group.

This facies assemblage represents a mudflat or a distal low-energy fluvial system (Table 2). The presence of carbonate nodules with sharp boundaries may reflect a pedogenic origin, having formed by downward leaching or precipitation of calcium carbonate (e.g. *Alonso-Zarza & Wright* 2009). Overall the palaeosol layers indicate reduced sedimentation rates for long periods of time on surfaces in an arid or semi-arid palaeoclimate.

FA2. Interbedded mudstones and sandstones (Fm, Fl, Sm, Sh, Sr, Shc)

Light brown, fine- to medium-grained, fining and coarsening upward sandstones occur in sheet-like and rarely lenticular geometries of 0.5 to 1.5 m thickness interbedded with mudstones (Table 1). Sandstone layers extend laterally for hundreds of metres and are massive, horizontal laminated and ripple cross-laminated. Occasional small-scale soft-sediment deformation disrupts the primary sedimentary fabrics. Red-, yellow- and brown-colored, laterally very extensive, horizontally laminated or massive mudstone beds separate the sandstone beds (Fig. 4.5B). This FA is present in all the units except for the Baktriy Formation.

Strata of this facies association are interpreted as overbank and floodplain deposits of a meandering river produced by the waning flow strength of crevasse splays or sedimentation in standing floodplain water (Table 2). In particular, sand bodies are interpreted to represent crevasse splays and levee deposits because of occasionally observable fining- and coarsening-upward trends, respectively (*Farrell* 2001). Laminated and massive mudstone beds mark suspended-load deposition. In addition, floodplain sedimentation is indicated by soft-sediment deformation structures.

Facies Association		Lithofacies	Description	Thickness (m)	Interpretation	Ocurrence
FA1	Interbedded mudstone and sandstone with palaeosols	Fm, Fl, Fps, Sm	Laterally extensive, tabular mudstones with palaeosols layers, intebedded with thin sandstone beds. Palaeosol layers range from 1 to 5 m thick.	< 20	Mudflat or distal low energy fluvial system. Palaeosols layers indicate reduced sedimentation in arid paleoclimate.	Sogdiysk Gr.
FA2	Interbedded mudstone and sandstone	Fm, Fl, Sm, Sh, Sr, Shc	Fine- to medium grained, fining and coarsening upward sandstone sheets interbedded with mudstones. Sandstone beds occur in sheet like or lenticular geometries, while mudstones are tabular and laterally extensive.	5 to 30	Overbank and floodplain deposits produced by crevasse splay, levee and suspended-load deposition.	Sogdiysk Gr. Fergana Gr. & Massaget Fm.
FA3	Sandstone	Sm, Sh, St, Sp	Medium- to very coarse- grained sandstone with lenticular geometry, fining upward tendency and erosive bases. Form channelized stacked sand bodies.	5 to 20	Sand-dominated braided fluvial system	Sogdiysk Gr., Fergana Gr., Massaget Fm. & Baktriy Fm.
FA4	Varicolored mudstone interbedded with coquinas	Fl, Fm, M, Sr, Sh, Sc	Repetitive, thickening and coarsening upward sets of mudstones and fine-grained sandstones interbedded with coarse-grained shell hash coquinas.	< 30	Embayment or protected lagoon	Fergana Gr.
FA5	Massive bioturbated sandstone	Fm, Fl, Sr, Sb	Coarsening upward sucession capped by a highly bioturbated massive sandstone.	30	Upper shoreface or foreshore	Fergana Gr.
FA6	Granule to cobble conglomerate	Gt, Gp, Gh, Gci	Organized, polymict, clast-supported granule to cobble conglomerate. Presence of traction sedimentary structures.	< 20	Gravel-dominated braided fluvial system	Massaget Fm.
FA7	Cobble to boulder conglomerate	Sp, St, Gm, Gci, Gp	Sharp-based, lenticular to sheet-liked shaped, matrix- and clast-supported cobble to boulder conglomerate.	> 30	Alluvial fan high-energy stream flows in poorly confined channels.	Baktriy Fm.

Table 4.2 Facies associations and related lithofacies

FA3. Sandstone (Fm, Fl, Sm, Sh, St, Sp)

This association is characterized by 1 – 15 m thick, light brown to light red, moderately sorted, medium- to very-coarse-grained sandstone (Table 1). They show lenticular geometry, extend laterally for hundreds of metres, have a fining upward tendency, are moderately channelized and show sharp erosive bases. They form channelized stacked sand bodies. Normally the sandstone grades upwards into the interbedded mudstone and sandstone facies association (Fig. 4.5B). Outcrop observations include trough cross-beds, planar, massive and horizontal stratification (Table 1). Occasional pebble trains define cross-bed and planar cross-stratification (Fig. 4.5B). This facies association is present throughout the entire section in all the units.

We attribute this facies association to deposits of a fluvial braided system composed of mixed-load channels (Table 2). The presence of pebble trains indicate that bedload transport of clasts occurred simultaneously with saltation and "wash-load" suspension fallout of sand grains (*Uba et al*. 2005). Several layers of interbedded gravel suggest fluctuations in flow strength during a single flow event. The fining upward trend and change in bedforms represent a decrease in flow velocity or depth as flood intensity waned. Trough cross-bedded lithofacies and planar cross stratification (Table 1) represent 3-D and 2-D dunes, respectively, within shallow channels and bars (*Miall* 1996). The lack of lateral accretion surfaces suggests limited lateral migration of point bars.

FA4. Varicolored marls interbedded with coquinas (Fm, Fl, M, Sr, Sh, Sc)

This facies association is characterized by numerous repetitive, thickening and coarsening upward 40-80 cm thick sets of laminated, red to green to purple mudstone and fine-grained limestone (Fig. 4.5C). Thin-bedded sandstone layers are sporadically intercalated, showing horizontal cross-lamination and symmetrical ripples. Two of the cycles are capped by a well-sorted, coarse and very-coarse-grained shell hash coquina (Table 1). The detrital coarse-grained limestone show high abundance of Ostrea fossils and are only represented in the middle section of the Fergana Group. The majority of the fossils found have been described as *Sokolowia buhsii* (*Grewingk* 1853). This fossil confirms the correlation to the Turkestan Formation (*Vialov* 1948). This species is typical of the Wulagen Formation in the southwest Tarim Basin which has been magnetostratigraphically dated as Lutetian (*Bosboom et al*. 2015). It points to normal

saline, warm and turbulent, subtidal shallow marine water conditions (*Grewingk* 1853; *Vyalov* 1937).

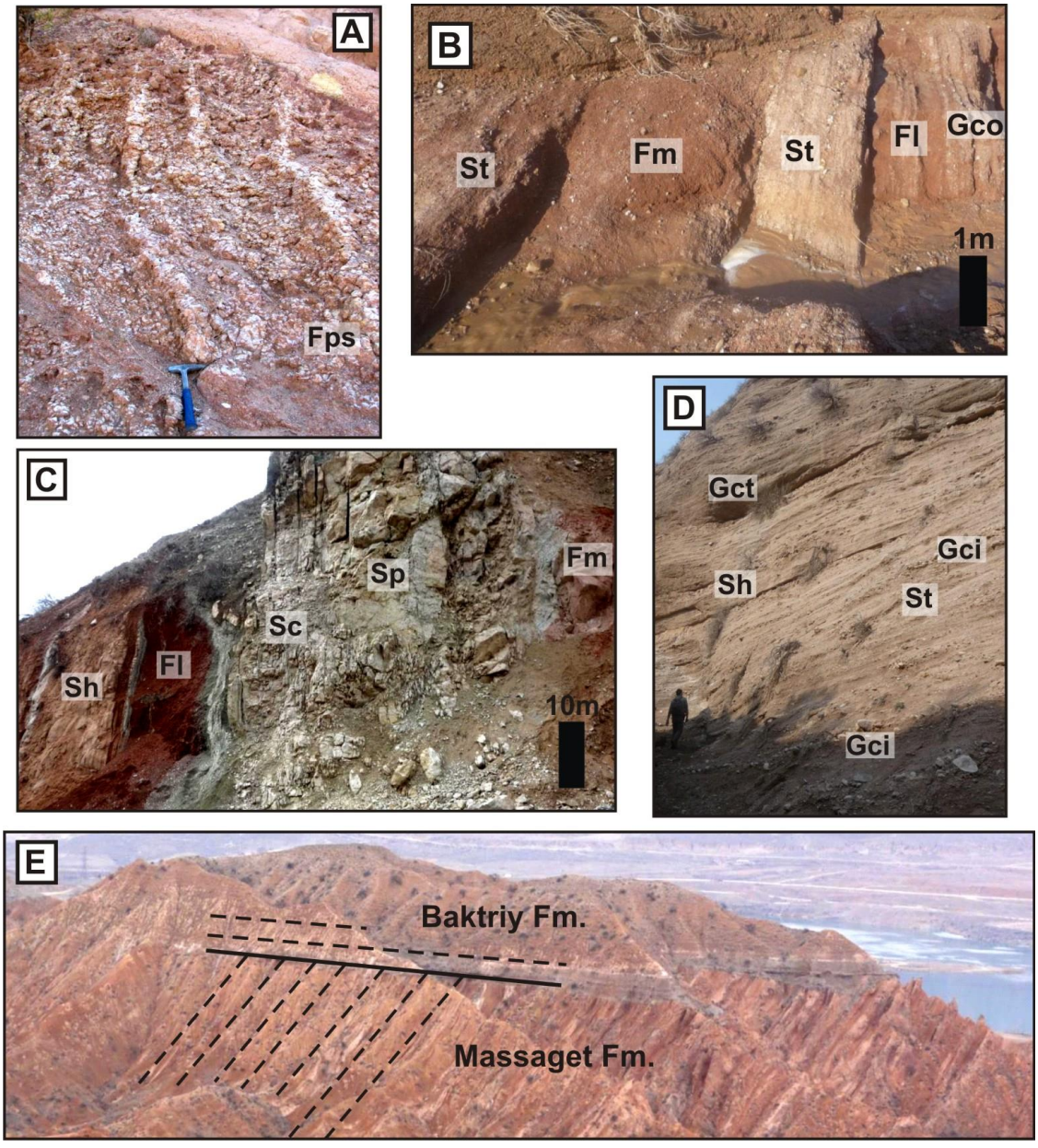

Figure 4.5 Photographs of described lithofacies, facies associations and strata relations. (a) Fine mudstones with abundant carbonate palaeosols (Fps). Geological hammer for scale. (b) Fine massive (Fm) and laminated mudstone (Fl) with sandstone intercalations (St). Photograph represents interplay of FA2 and 3. (c) Shell-abundant (Sc) and stratified (Sp) sandstone immersed in mudstone layers. Image shows the position of FA4 with respect to FA2. (d) Sandstone beds (Sh and St) with conglomeratic beds (Gci) intercalated. Person for scale. Photograph representative of FA6. (e) Angular unconformity between the Oligo-Miocene Massaget and the Pliocene Baktriy formations, near Tash-Kumyr. Tilting of Massaget beds is c. 65° to the south.

The internally continuous, thickening- and coarsening-upward mudstone-sandstone-coquina sets are likely related to periodic fluctuations in water depth, whereas the mudstone color variations suggest frequent changes between oxidizing and

reducing conditions. The presence of Ostrea indicate a marine influence. Overall, this facies association appears to have formed in a protected lagoon or embayment setting (Table 2).

FA5. Massive bioturbated sandstone (Fm, Fl, Sr, Sb)

The main element of this facies association are 5-15 m thick, massive, highly bioturbated, medium-grained sandstone beds (Table 1). Bioturbated beds occur at the top of a coarsening and thickening upward succession starting with laminated and massive mudstones followed by symmetrical cross-ripple stratified fine-grained sandstones. The total thickness of the sequence is ~30 m. High amount of *Cruziana* ichnofacies completely overprint the primary structures. This facies association was observed at the top of the Sogdiysk Group.

The thick, massive, tabular sandstone of this facies association together with its extensive lateral extension suggest the presence of a marine parasequence. On the basis of tabular bedding geometries, upward coarsening grain size trend, presence of horizontal burrows and lack of storm deposits we interpret this association as upper shoreface or foreshore environments (*Reading & Collinson* 1996). The extensive bioturbation at the top of the succession indicates a period of slow deposition favoring the development of burrows.

FA6. Granule to cobble conglomerate (Gt, Gp, Gh, Gci)

This facies association consists of organized, moderately to well sorted, polymict, mostly clast-supported granule to cobble conglomerate (Table 1). The conglomerate comprises rounded to well rounded clasts showing normal grading. Imbricated clasts together with horizontal, planar and trough cross-stratification are common. Individual sharp-based beds reach up to 8 m in thickness and extend laterally for several tens to hundreds of metres (Fig. 4.5D). This facies association changes upsection to the sandstone facies association (FA3) and is common in the Massaget Formation.

This facies association is interpreted as representing deposition by stream flows in low sinuosity, gravel-dominated braided system in which transportation occurred largely by bedload and deposition occurred under waning flow conditions (Table 2). The interpretation is supported by the presence of erosional surfaces, imbrications and dominance of organized lithofacies. The fining upward sequences indicate waning flow velocities of individual events.

FA7. Cobble to boulder conglomerate (Sp, St, Sh, Gm, Gci, Gch)

Clasts of this FA are subangular to well rounded and moderately sorted. The clast size distribution is polymodal and shows inverse to normal grading; imbrications and planar cross-stratification are moderately developed. Individual beds are up to 5 metres thick. Interbedded, 0.5 to 2 m thick, subordinated, sheet-liked geometry, medium- to coarse-grained sandstone layers show planar and trough cross-stratification (Table 1). Conglomerate bases are sharply erosive, showing lenticular to sheet-like geometries laterally extending for several tens of metres. The conglomerates consist of disorganized, matrix supported, organized and imbricated lithofacies within a very coarse-grained sand matrix. This facies association is exclusive to the Baktriy Formation.

This FA is interpreted as resulting from high-energy streamfloods in poorly to moderately confined channels in an alluvial fan setting. The interpretation is consistent with clast-supported fabric, basal erosion surfaces, moderately developed clast imbrications and cross-stratification (*Blair & Mc Pherson* 1994). The organized clast-supported lithofacies with moderately developed imbrications may be a result of gravel bed-load sedimentation under waning energy flows (Table 2). This interpretation is supported by the presence of thick vertically accreting conglomerates and erosive surfaces. In contrast, the disorganized bedforms suggest high sedimentation rates and/or shallow flow depth (*Blair & Mc Pherson* 1994). The cross-bedded sand bodies represent deposits in channels under waning flow.

4.3.4 Depositional summary and tectonic implications

Paleogene (Bukhara and Suzak Formations) deposition in the northern Fergana Basin occurred in a distal, fluvial, low-energy environment (FA1 and 2). The presence of pedogenic layers (Fig. 4.5A; FA1) supports the interpretation of a reduced rate of sedimentation for long periods of time, as such rates enable the development and growth of palaeosols. The presence of gypsum and anhydrite in these formations in the western part of the basin (e.g. *Clarke* 1984) points to an arid or semi-arid palaeoclimate. Upsection of the distal non-marine environment, a deltaic setting (FA5) is interpreted with a limited thickness of less than 40 m. This marginal marine environment might represent the distal remanents of the 3rd marine transgression documented in Central Asia (e.g., *Burtman* 2010; *Tang et al*., 1989; *Bosboom et al*. 2015). A renewed distal, low energy nonmarine environment is interpreted upsection based on the intercalation

of FA 2 and 3 (Fig. 4.5B). On top, marine deposits (Fig. 4.5C; FA 4) with a restricted thickness of < 20 m succeed the low energy association. Marine fossils found in these beds at Tash-Kumyr and carefully documented by *Bosboom et al.* (2015) provide a middle Eocene (Lutetian) age for these beds. Based on bivalve fossil assemblages, *Bosboom et al.* (2015) correlate these deposits to the Wulagen Formation in the Tarim Basin and the 4th Paratethys transgression in Central Asia. Upsection, a 50 m thick sequence represented by the upper Fergana Group is interpreted as representing a distal low-energy nonmarine environment (Fig. 4.5B; FA2 and 3). Overall, the interpretation of the lithofacies assemblages comprising the Sogdiysk and Fergana Groups points to a distal low-energy environment with sporadic thin, regionally correlatable marine incursions. At Tash-Kumyr, ~ 300 m of strata were deposited during the Paleocene and Eocene, implying an accumulation rate of ~ 9.4 m/Ma. Therefore, the sedimentological observations corresponding to this interval do not support important tectonic changes with introduction of proximal sources. Rather, during the early Cenozoic the northern Fergana basin represented a tectonically quiet area with sporadic thin, coastal incursions of the Paratethys sea.

After retreat of the palaeo-sea in the middle to late Eocene (*Bosboom et al*. 2015), continued accumulation took place in fluvial environments under different energies regimes, which might extend to the Fergana basin. The overall trend of the Massaget Fm. fluvial succession is upward thicken- and coarsening, showing a transition from distal to more proximal and higher energy fluvial facies. This trend is clearly seen in the constant increase in grain size of the sandstone beds and the appearance of the granule to cobble conglomerate facies association (FA 6) in the upper part of the Massaget Formation (Fig. 4.5D). The lower portion of the unit is represented by an alternation of FA 2 and 3, while towards the top FA 6 develops and become abundant. One plausible interpretation of this trend is a change in the source area. Tectonic uplift in a nearby area could have triggered deposition of proximal fluvial facies in the northern Fergana Basin. Palaeomagnetic studies (*Thomas et al*, 1993) and new thermochronologic data (*Bande et al*. 2015a) postulate strike-slip displacement along the Talas-Fergana Fault (TFF) and associated crustal shortening in the Chatkal and Fergana Ranges. The onset of this tectonic episode is placed near the Oligo-Miocene boundary (*Bande et al*. 2015a), in agreement with the traditional age (Pg^3_3 - N_1ms) of the Massaget unit (*Artyomova et al*. 1971). Exhumation in the Chinese portion

of the south Tien Shan, west of the TFF, was underway by 18 Ma (*Yang et al.* 2015). The Alai range south of the Fergana basin also began to be exhumed by ~20 Ma (*De Grave et al*. 2012). In consequence, we interpret the Massaget Formation to be a syn-tectonic unit related to the Oligo-Miocene tectonic episode occurred along the TFF

In outcrop, the base of the Baktriy Formation is marked by a well-developed angular unconformity (Fig. 4.5E) and sedimentary facies in this unit depict a high energy, very proximal environment. This unit is the only one having the highest energy lithofacies association (FA 7), interpreted as poorly confined streamflows that suggest very proximal source areas. Based on the structural relations with the underlying units and the lithofacies analyses, we propose a new tectonic event creating a more proximal sediment source by the latest Miocene – Pliocene. Moreover, palaeocurrent indicators, described below, suggest a change in the location of the source area with the new uplifted zone located more to the east.

4.3.5 Sediment dispersal

4.3.5.1 Methods

Palaeocurrent indicators were measured systematically throughout the Tash-Kumyr section (Fig. 4.3). We took a total of 667 measurements, divided between the Sogdiysk and Fergana Groups and the Massaget and Baktriy Formations. The palaeocurrent database consists of 590 trough-cross limb measurements (method I of *DeCelles et al*. 1983) at 29 locations (Fig. 4.5). Most of the locations correspond to fluvial facies. However 2 locations are interpreted as marine deposits and were removed from the rose diagrams (Fig. 4.6). A total of 77 conglomerate clast imbrications measured at 3 sites complete the data set.

4.3.5.2 Results and interpretation

Cenozoic palaeocurrent indicators in the Tash-Kumyr section show a gradual change of flow direction from south directed to west directed (Fig. 4.6). Grouped measurements for the Sogdiysk and Fergana Groups show variable directions but display a general southward directed flow (Fig. 4.6A). This variability and palaeo-flow pattern is consistent with a low energy fluvial environment with source area to the north; sporadic marine transgressions that flooded the area might be responsible for the variable directions.

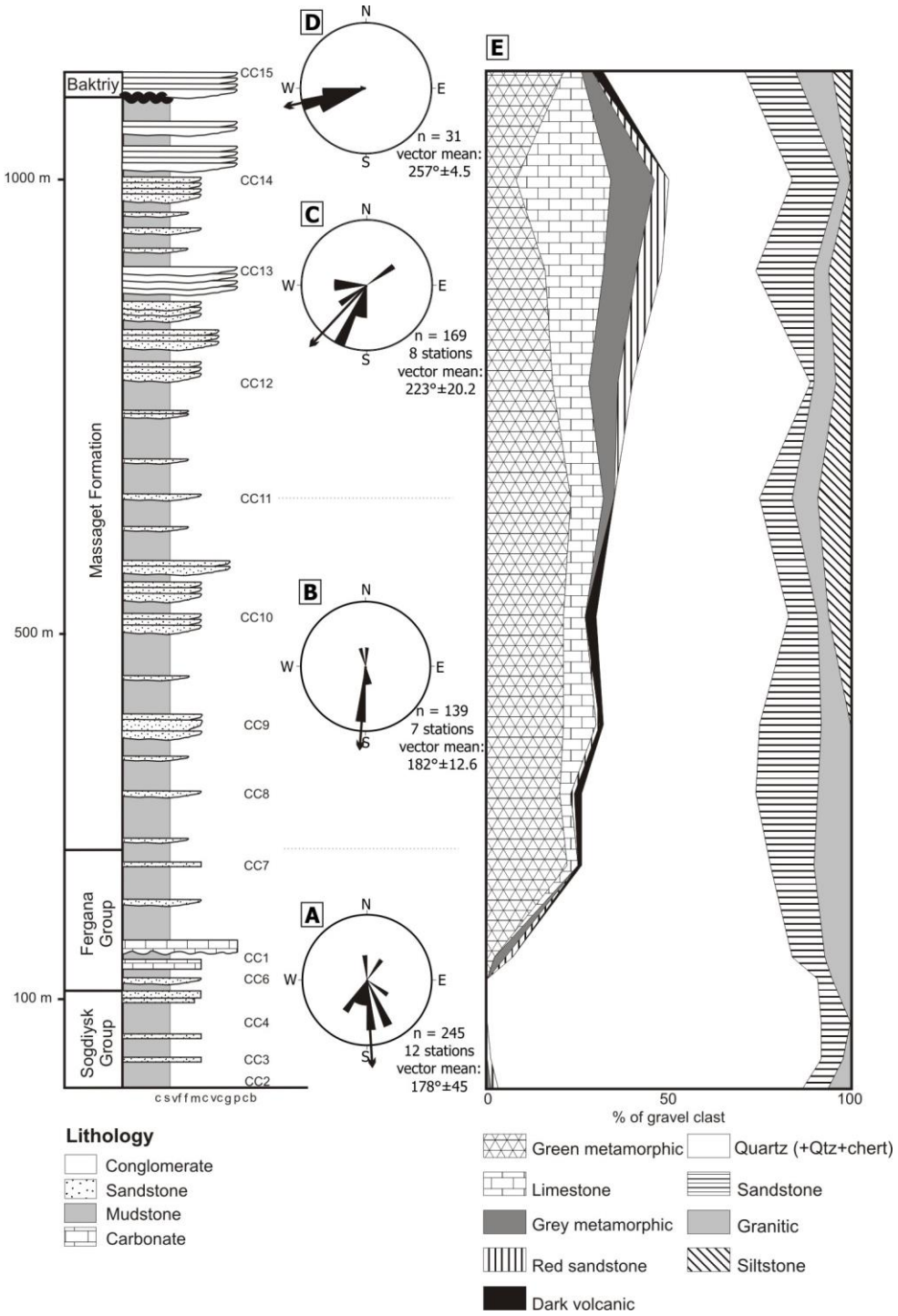

Figure 4.6 Generalized stratigraphic section of the northern Fergana Basin foothills showing: palaeocurrent data for (a) the Sogdiysk + Fergana Group, (b) the lower Massaget Formation, (c) the upper Massaget Formation and (d) the Baktriy Formation, arranged stratigraphically. Mean palaeocurrent vector, number of measurements, and stations are listed for each rose diagram, and (e) conglomerate clast compositional data (14 locations), also arranged stratigraphically. Horizontal axis represents percentage of modal composition.

The lower Massaget Fm. shows a similar dispersal pattern (Fig. 4.6B) with a well defined trend to the south (dir. azimuth 182°). Upsection, the upper Massaget Fm. (Fig. 4.6C) show a minor change with an overall palaeoflow to the SW (dir. azimuth

223°). This progressive south to southwestward palaeoflow change might be interpreted as a gradual change in source area. During deposition of the Massaget Fm., the Talas Fergana fault became active, as documented by exhumation of restraining bends (*Bande et al*. 2015a). The uplift of the northern restraining bend, located to the NE of Tash-Kumyr, might be responsible for the shift to a southwestward directed palaeoflow. Above the angular unconformity that separates the Massaget and Baktriy Formations, a new gradual shift is observed, with palaeoflow direction to the west (Fig. 4.6D, dir. azimuth 257°). This change implies a more proximal source and in consequence proximal deposits, consistent with the palaeoenvironmental interpretation of the Baktriy Formation. This change might be interpreted as reflecting a renewed tectonic event to the east that propagated deformation westwards.

4.3.6 Conglomerate clast-counts

4.3.6.1 Methods

Conglomerate compositional data were obtained at 14 outcrops localities along the Tash-Kumyr logged section (Fig. 4.4). Square grids of at least 30 cm length were drafted on the outcrop, and at least 100 clasts were counted at each location. Compositional data are available from the Sogdiysk and Fergana Group and the Massaget and Baktriy Formations (Fig. 4.6). Although many clasts cannot be identified with confidence at the formation level, some are indicative of specific intervals or source areas. In order to address that we will briefly present the stratigraphy of the Western Tien Shan Ranges as a framework to interpret provenance data.

The Ordovician and Silurian are represented by granite and granodioritic units and related sedimentary units both in the Chatkal Range and in STS Ranges (Alai and Fergana). According to *Maksumova et al.* (2001), by Givetian times (382 – 387 Ma) the arc located at the southern edge of the Kazakh continent became inactive and fluvial and marginal marine environments occupied the present Fergana basin area. The upper Devonian units are dominated by shallow marine carbonates (*Cook et al*. 2002). During Mississipian times, the northern Fergana basin continued to host a relatively shallow marine environment, including the formation of reef-facies and the deposition of mud-rich carbonates. On the other hand, the STS units represent oceanic deepening and dark laminated mudstones and shales outcrop in the Alai and Fergana Ranges (*Biske & Seltmann* 2010). Near the Mississipian-Pennsylvanian boundary, sedimentation stopped and andesites and granitic rocks were emplaced (*Ges´& Seliverstov* 1995) to the north

of the Fergana basin (Chatkal-Kurama Belt). Pennsylvanian sedimentation is characterized by fluvial and shallow marine clastics in the region of the modern Chatkal Range (*Ges´& Seliverstov* 1995), forearc facies (sedimentary breccias and turbidites) and deep marine units (laminated dark shales) in the Alai Range and carbonate units in the Fergana Range (*Biske & Seltmann* 2010). In the STS, the black shales and turbidite facies rest unconformably on ophiolite and metamorphic rocks (*Biske* 1996). Middle Permian and younger red sandstones and related rocks represent nonmarine sedimentation together with a widespread emplacement of post-collisional granitic plutons (*Seltmann et al.* 2011).

4.3.6.2 Results and interpretation

The composition of the Sogdiysk and lower Fergana Groups (Fig. 4.6E) is dominated by ca. 85 % quartz-related (quartz, quartzite and chert) clasts, with subordinate granitic and sandstone grains. This is expected in a mature and marine environment where physical and chemical weathering enhances the concentration of quartz grains (e.g., *Johnsson et al*. 1991). Similar quartz enrichment in this interval is observed in the southwest Tarim basin (*Sobel* 1995). Moreover, a widespread regional unconformity together with a prolonged hiatus occurred in the Cretaceous throughout much of the Tien Shan (e.g., *Afonichev & Vlasov* 1984; *Jolivet* 2015). This prolonged episode of weathering also contributed to the concentration of quartz-related components. Consequently, we interpreted these units as sourced from a long-lived, mature landscape with sporadic marine incursions.

The uppermost counted site (CC7) of the Fergana Group shows a notable change in composition with the inclusion of 22% of green metamorphic grains and ~8% of limestone clasts. This change is well defined and permanently established in the lower Massaget Fm. (Fig. 4.6E). Moreover, in this section ~2% of dark volcanic grains appear in the mode together with an increase in sandstone and granitic clasts. The modal composition of this section clearly reflects erosion of a Tien Shan source, probably the Chatkal Range zone. This compositional change might reflect either a definite retreat of marine-influence and landscape rejuvenation in the source area or a drainage basin reorganization together with a capture of different source area.

In the upper part of the Massaget Formation, the composition becomes less quartzitic (~33%) and the red sandstone grains and grey metamorphic clasts both form distinctive modes, 5% and 10% respectively (Fig. 4.6E). In this section, the abundance

of limestone clasts increases significantly (~17%) and the abundance of green metamorphic clasts remains relatively constant (~15%). Also, the dark volcanic mode is absent. This change is accompanied by a modification of the palaeocurrents (Fig. 4.6C) from south- to southwestward directed flow. The increase of limestone grains and disappear of dark volcanics could be interpreted as reflecting a higher participation of Middle Tien Shan units in the source area. A tectonic episode might be responsible for this change, exposing Palaeozoic red-beds and carbonaceous units which presently outcrop to the north of Tash-Kumyr.

The uppermost sample (CC15) represents the Baktriy Formation (Fig. 4.6E) and shows a dominant quartz-related composition (39%), but with a high proportion of metamorphic grains (24%), relatively large limestone mode (5%) and a distinctive dark volcanic signal (3%). The presence of an angular unconformity (Fig. 4.5E) and a change in palaeocurrent indicators (Fig 4.5D) lead us to interpret the minor change in composition as a change in source area caused by a younger (late Miocene?) unroofing event east of Tash-Kumyr or a capture of a different source area.

4.4 Seismic reflection data of the northern Fergana basin

4.4.1 Methodology

We obtained and interpreted three NW-SE trending dip lines (lines LN005, LN006 and LN009) and one strike line (line 12CH03) in the northern part of the basin and one NE-SW trending dip line (12CH02) in the northeastern sector of the basin (Figs. 4.7 and 4.8); these were measured during seismic surveys carried out in 2010-2012 by Integra-Geophysica and Uzbekgeophysica. The stacking method used during processing is from Paradigm Geophysical. Borehole logging from well Isp-1 allowed us to define formation tops and make stratigraphic correlations between the different lines. The stratigraphic identification and ties of reflecting horizons in the seismic data within the study area were based on sonic log and VSP data from deep wells located in the Isparan, Namangan, Iskovat, Shorbulak prospects. The reflectivity function was calculated using an acoustic impedance curve for the well, which is the product of the P-wave velocity, derived from the sonic log, and density data ($\rho = Const$). Ties of seismic horizons in the interval above Brick Red Suite (BRS) and below Turkestan (Paleogene) were based on geological and structural concepts of the area, using interval times from the VSP data. The seismic lines shown (Figs. 4.7 and 4.8) are not migrated

in depth and the well WN-1 is projected to the seismic section without a time-depth conversion. This is important since these two pieces of data correspond to different domains (depth and time) and cannot be directly compared using the data we have.

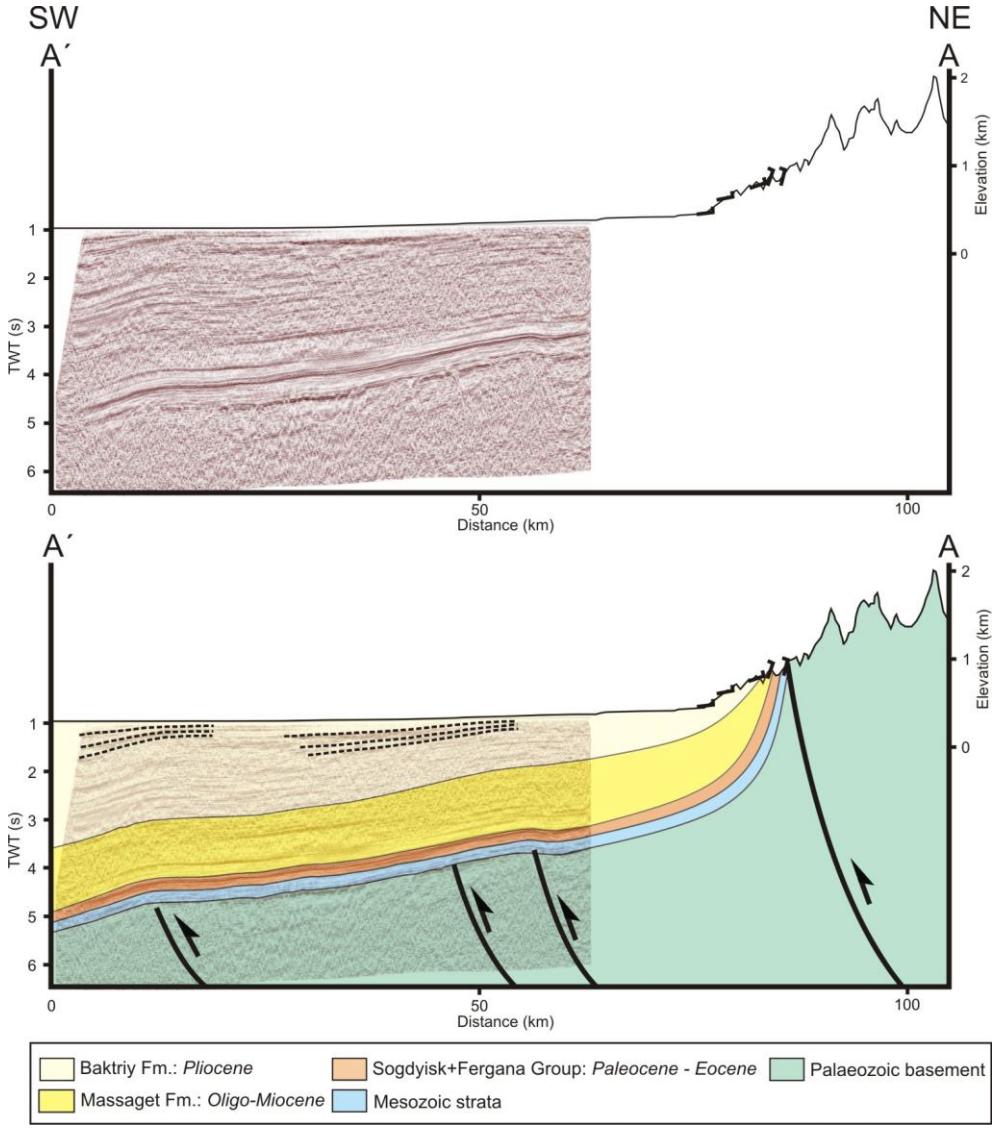

Figure 4.7 Cross-section A–A′ showing 2D seismic reflection line (12CH02) and field data above and interpreted geological cross-section below. Vertical scale in kilometres is only valid for the topographic cross-section. Dashed lines in Baktriy Formation represent growth-strata. For location, see Figure 4.1.

Using the interpreted seismic lines as a foundation and adding our own field data and previous geological mapping (*Vlasov et al*. 1991; *Bakirov et al*. 2001), we constructed two regional profiles from the basin center to the Chatkal Range and North Fergana Range respectively (Figs. 4.7 and 4.8). Strike and dip data from outcropping units in the ranges foothills were placed and projected into the regional profiles, enabling subsurface interpretation where no seismic reflection data is available.

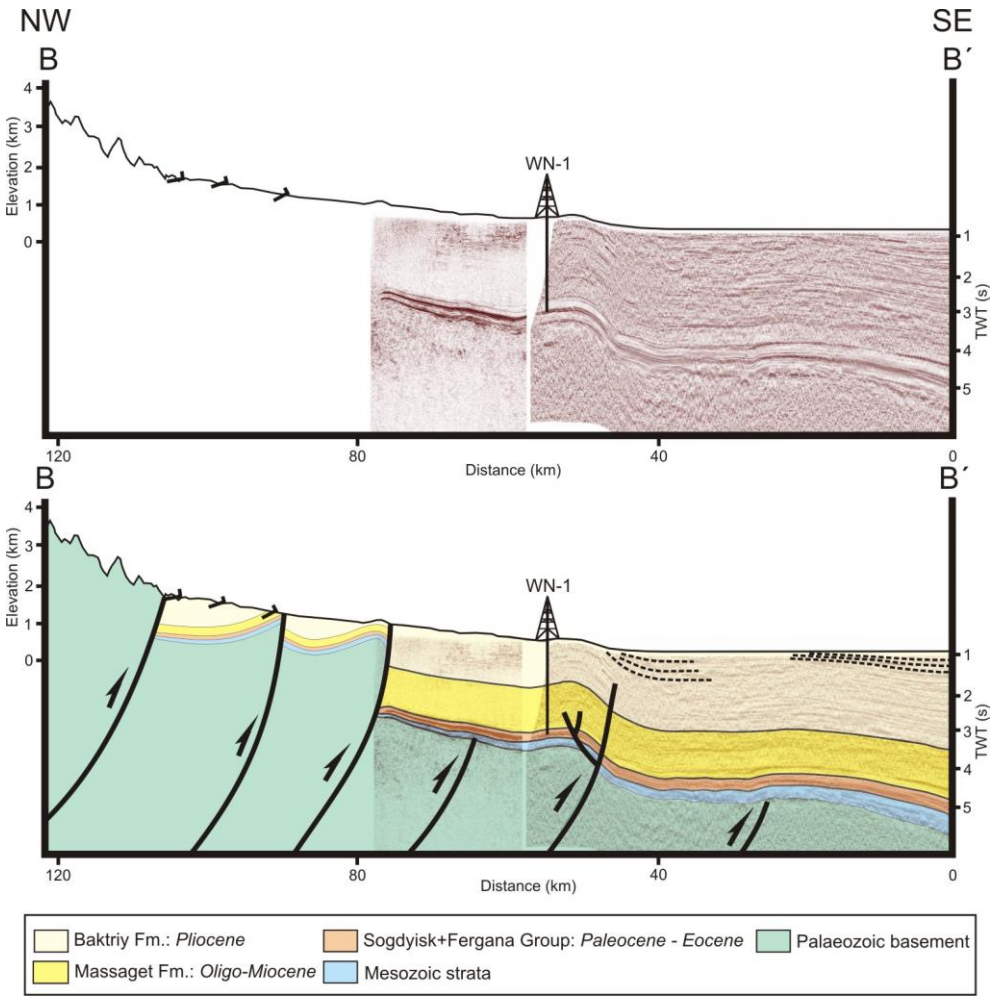

Figure 4.8 Cross-section B–B′ showing 2D seismic reflection lines (LN006 and 12CH03) and field data above and interpreted geological cross-section below. Vertical scale in kilometres is only valid for the topographic crosssection. Total depth of well WN-1 is 4135 m. Dashed lines in Baktriy Formation represent growth-strata. For location, see Figure 4.1.

4.4.2 Observations

The Baktriy Fm. is up to 2.5 s TWT thick in the basin center and 1.2 s TWT at well WN-1. The reflectors are closely spaced in the northwest and progressively diverge to the southeast (Figs. 4.7 and 4.8), building a wedge-shaped unit thinning towards the basin borders. The uppermost 0.5 s TWT shows well-developed growth-strata architecture in at least four sectors of the basin. Reflections in the Baktriy Formation appear disconnected, typical of a fluvial non-marine environment of deposition (*Simm & Bacon* 2014).

According to the seismic characteristics, the Massaget Fm. can be divided into three sections. The top of the unit matches the well-defined Pale Pink Suite (PPS) marker. The uppermost one shows a similar seismic response as the Baktriy Fm. with low continuity reflections and relatively high contrast of acoustic impedance (high

amplitude). In the middle, it is possible to define a zone with low continuity that is seismically transparent. Finally, the lowermost section shows higher continuity reflections with higher amplitude. This lower section corresponds to the Brick Red Suite (BRS). At depth, the contrast of acoustic impedance is lower, but the reflections are still continuous. The thickness of the Massaget Formation is up to 1.3 s TWT in the center of the basin (Fig. 4.8), while it is 1 s TWT thick in the footwall of the North Fergana fault (NFF).

Below, the Turkestan, Alai and related units are imaged with high frequency content and regionally laterally-continuous, subparallel and high amplitude reflections (Figs. 4.7 and 4.8). Their thickness reaches a maximum in the basin center with ca. 200 ms of continuous high amplitude reflections, while at the northern border of the seismic sections the thickness is around 125 ms. The Mesozoic section has relative lower amplitudes and partially continuous reflections. Finally, the Palaeozoic basement is imaged as partially continuous to discontinuous reflectors in some areas; these are truncated by high-angle faults.

Near the city of Tash-Kumyr, in the Karagunday anticline (Figs. 4.2 and 4.6), the outcropping Paleogene units and the Massaget Fm. dip steeply (60-70°) towards the S. Upsection, the Massaget Fm. is bounded by an angular unconformity and the Baktriy Fm. was deposited on top with dips < 25° to the S. From that location to the south only the Baktriy Fm outcrops, with low angle dips (5 - 10°) to the S and SW.

North of the city of Namangan (Fig.4.1), the Baktriy Fm. outcrops define a gently dipping NE-SW trending anticline. This anticline correlates with the location of the Central Fergana fault (CFF). To the north, the trace of the North Fergana fault (NFF) runs parallel to the Chatkal Ranges (Fig.4.1). The fault exhumes Palaeozoic units to the surface. Although along the trace of the cross-section (Fig. 4.8) the location of the NFF is covered by Quaternary deposits, a gentle hill is apparent in the topographic profile. Continuing north along the cross-section a new fault is interpreted that places Massaget Fm. rocks in contact with Quaternary deposits. Massaget layers lie in the hanging-wall of the fault with dips of ~30° to the NW. In the same block, the Baktriy Fm dips from 8° to 20° to the NW. Continuing to the north, the Chatkal Fault exhumed Palaeozoic basement to the surface and it is the main fault uplifting the Chatkal Range.

4.4.3 Interpretations

The Sogdiysk and Fergana Groups have a seismic pattern that thins towards the basin borders located to the north, implying that the depocenter was located to the south, roughly matching the present topography. The subparallel layout of the reflections suggests a conformable stacking of the different units in the Paleogene (Figs. 4.7 and 4.8). The high contrast of acoustic impedance confirms the presence of distinctive lithologies (limestone vs. siltstone) throughout the basin. Considering the exposures in the outcrop belt, the high frequency content can be interpreted as sporadic, short marine incursions followed by progradation of siliciclastics.

The Massaget Fm thickens towards the basin center, implying that the source area of the unit was located to the north of the present basin margin (Figs. 4.7 and 4.8). Two lithologically-defined markers are included in the Massaget Fm: the Pale Pink Suite (PPS), which corresponds to the top of the unit and the Brick Red Suite (BRS), located at the basal part of the unit. According to its seismic character, the upper portion of the Massaget Fm. appears more discontinuous with relative low frequency reflectors and might reflect the stacking of fluvial non-marine strata (*Simm & Bacon* 2014). This environment might be related to higher energy facies, implying syn-deposition deformation at the source area. On the other hand, the seismic response of the layers below the BRS is more laterally-continuous and has higher frequency. This response could reflect low energy depositional environments with a distinct horizontal stacking of laterally continuous units; this is consistent with the absence of conglomerates in the well description (WN-1) for the BRS (Fig. 4.2).

The seismic data image a southward-thickening wedge (Figs. 4.7 and 4.8) primarily composed of reflections related to the Baktriy Fm. The lower Baktriy Fm. is truncated by basement faults near the basin borders. This relation is well-developed in the seismic line 12CH03, where the truncations appear at the footwall of the CFF (Fig. 4.8). There, the CFF truncates and deforms units as young as the lower Baktriy Fm.; growth-strata develop in the upper Baktriy Fm. The growth-strata relationships appear to be younger towards the south, implying deformation migrated from the surrounding ranges to the basin center (Figs. 4.7 and 4.8). Although the seismic definition is not the best, an incipient piggy-back basin can be imaged in the back limb north of the CFF in the upper Baktriy Formation (Fig. 4.8). This interpretation is correlated with field strike

and dip data. In the back-limb zone dips of 8° to the north are measured, while the front limb has an inclination of 6-8° to the south.

To construct cross-section A-A' (Fig. 4.7), we interpret the outcropping section at Tash-Kumyr as the front limb of the Karagunday anticline. Then we connect this limb to the subsurface section of the seismic section. We choose this simple interpretation since we have no other data that suggests a more complex geometry.

Along cross-section B-B' (Fig. 4.7), the geometry is more complex. In the seismic section we interpret the CFF to cut and displace the entire section up to the lower Massaget Fm. Growth strata are clearly imaged in the front limb of the surface anticline. Although in the back limb the seismic quality is poor, growth relations are also interpreted. A gentle anticline at the surface in the outcropping Baktriy Fm. matches this interpretation. Following the backlimb to the north, a young piggy-back basin of upper Baktriy and Quaternary deposits is interpreted (Fig. 4.7). Although the constructed profile runs through a Quaternary covered area when crossing the NFF, we interpret the formation of an anticline in the hanging-wall of the NFF. Palaeozoic units outcrop in the hanging-wall of the NFF ~15 km to the NE and SW of the section trace. Based on that observation we interpret the presence of Palaeozoic basement close to the surface, even where the section runs through Quaternary cover. This interpretation is supported by the abrupt ending of the basin-fill isopach contours against the NFF (Fig. 4.1). Another basement-involved thrust is interpreted 15 km to the north. This structure puts Massaget strata in contact with Baktriy and Quaternary deposits (Fig. 4.8). A syncline is interpreted in the hanging-wall of this fault, matching the strike and dip of the surface geology in the Chatkal foothills. The northernmost thrust of the profile corresponds to the Chatkal fault that exhumed Palaeozoic units up to the surface (Fig. 4.1) and is responsible for much of the topography in the Chatkal range.

4.5 Basin evolution

4.5.1 Pre-Himalayan History

The Mesozoic is represented by thin, laterally continuous deposits in the subsurface. Published stratigraphic data suggest that the Triassic is largely absent (*Akramhodjaev & Saidalieva* 1971; *Abidov et al.* 1992). Thin Jurassic and lower Cretaceous continental deposits are overlain by a sequence of Albian to Turonian and Paleogene shallow marine transgressions and non-marine regressions. Numerous

studies have previously characterized much of the Tien Shan during the Mesozoic as a small amount of exhumation interrupted by periods of limited deposition (e.g. *Hendrix* 2000; *Bullen et al*. 2003; *Sobel et al*. 2006b; *Jolivet et al*. 2010; *Macaulay et al*. 2013). The generally low energy facies, slow accumulation rates, low amount of erosion and regionally lateral continuous reflections of these deposits point to a lack of tectonic activity. The exception to this pattern are thick Jurassic sediments along the TFF, particularly in the southern portion of the Fergana Range; these are not representative of the Fergana basin. Instead, these thick sediments are associated with an apparent pull apart basin along the TFF (*Sobel* 1999) which continues north into the Leont'yev basin and finally joins the Turgay basin (*Allen et al*. 2001; *Alexeiev et al.* 2009; *Wei et al.* 2012). Other exceptions to this pattern are far to the east, where more extensive depocenters bound the Tien Shan in the Tarim and Junggar basins (e.g., *Hendrix et al.* 1992).

Gravity, seismicity, and heat flow data imply that the Fergana basin has an effective elastic thickness of ~15 km; this has been explained as being related to a significant Jurassic thermal event (e.g., *Burov & Molnar* 1998). However, the stratigraphic record that we observe in outcrop and interpret in the subsurface are incompatible with the latter interpretation. Steeply-dipping faults deep in the basin are more reasonably assigned a Permian age, corresponding to the period when the entire Tien Shan experienced significant transpressional deformation (e.g., *Burtman* 1975; *Bazhenov & Mikolaichuk* 2004; *Alexeiev et al*. 2009; *Konopelko et al*. 2013; *Rolland et al.* 2013). In the Fergana basin, the entire Mesozoic sequence is relatively thin and laterally continuous. Shifting the age of the thermal event from 175 to 275 ± 25 Ma and using the same 200-250 km folding wavelength implies that the deformation plots in the field corresponding to lithospheric mantle folding rather than the undefined area between that and whole lithosphere folding (*Cloetingh et al.* 1999; *Cloetingh & Burov* 2011). Recently, *De Grave et al.* (2012) suggested an Early Cretaceous (~140 - 110 Ma) cooling event in the Alai Range, based on thermochronology ages. The interpretation is based on one basement sample and a detrital signature on Cenozoic-aged samples. We believe this event likely reflects a spatially-limited deformation event south of the Fergana basin and might not have a regional expression.

The Early Cenozoic record in the basin is composed of low-energy, distal, nonmarine depositional environments. The Palaeo-Tethys Sea sporadically flooded the basin, depositing thin marginal marine facies in the northern Fergana basin (Fig. 4.9A). These marine incursions are well-correlated across western Central Asia. According to our interpretation, sedimentation occurred in a calm tectonically-quiescent environment as seen by the regional lateral continuity of the Paleogene reflectors in the subsurface and the low estimated rate of deposition for the Eocene – Paleocene section.

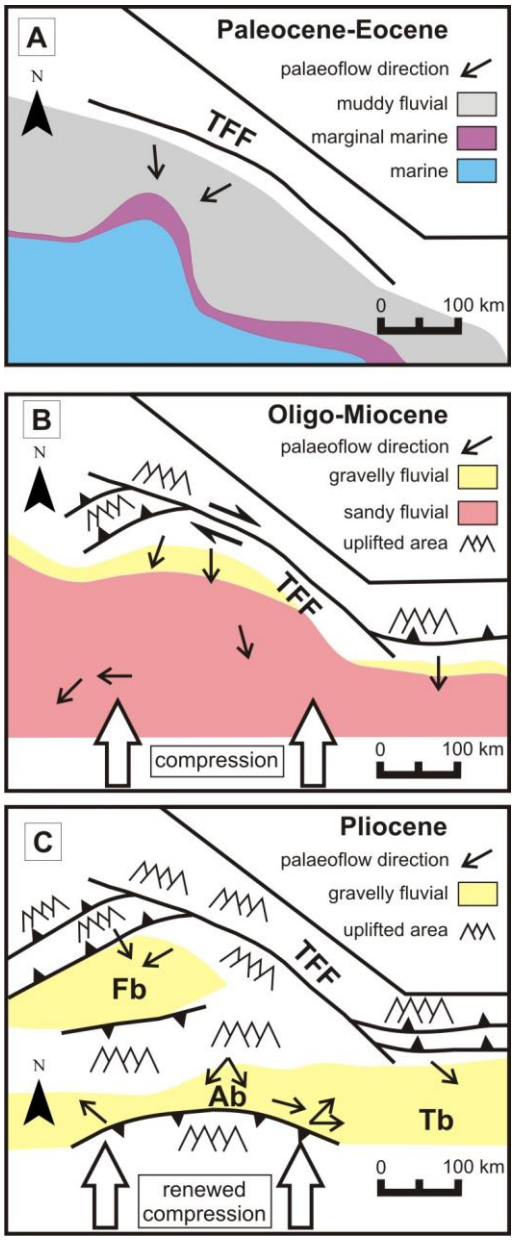

Figure 4.9 Schematic palaeogeographic basin evolution sketch reconstructions. Palaeo-flow indicators from *Meng* (1997), *Heermance et al*. (2007), *Hausburg et al.* (2012), *Thompson et al.* (2015), *Klocke et al.* (2015) and this study. TFF, Talas–Fergana Fault; Fb, Fergana Basin; Tb, Tarim Basin; and Ab, Alai Basin.

4.5.2 Syn-Himalayan History

In contrast to the older strata, the Oligocene to Recent section in the basin is represented by thick packages of non-marine sedimentary rocks. Most of the rock volume corresponding to this period is in the basin subsurface (Figs. 4.7 and 4.8). The scarce availability of subsurface data might explain the rough knowledge of the Fergana basin Neogene section. According to *Gotfrid & Puchkov* (1980) the Neogene section is ~ 5 km thick in the western part of the basin. The well WN-1 reached the top of the Fergana Gr. at 3920 metres below kelly-bushing (mbkb), constraining the thickness of the Neogene in the hanging-wall of the CFF. A gradual shift in palaeocurrent indicators is apparent in the upper section of the Massaget Formation (Fig. 4.6C), together with an increase in higher energy depositional facies (Fig. 4.4). This new data together with the results presented by *Bande et al.* (2015a), suggest a ~ 25Ma onset of exhumation located along the northern sector of the TFF. The Oligo-Miocene event (~ 25Ma) triggered the uplift of the eastern Chatkal and northern Fergana ranges, leading to a reduction in basin size (Fig. 4.9B). If we assume that the base of the Massaget Fm has an age around 25 Ma, the approximate sedimentation rate for the Massaget Fm is ~ 0.15 mm/y^{-1}.

The seismic sections show no significant angularity between the Massaget and Baktriy Formations in the basin center (Figs. 4.7 and 4.8). However, in the logged section we recognized a significant angular unconformity (Fig. 4.4 and 4.5E) between these two units. This suggests that the basin was more extensive than its present configuration and that an important tectonic episode happened prior to the deposition of the Baktriy Formation. *Bande et al.* (2015a) propose that a rapid exhumation event commenced at ~25 Ma along the eastern and northern flanks of the Fergana basin. This age is within the poorly constrained depositional time-span of the Massaget Formation, implying that the event responsible for forming this unconformity should be younger. Many authors (e.g. *Bullen et al*. 2003; *Sobel et al*. 2006b; *Macaulay et al*. 2014) suggest that there was a significant increase in tectonism at ~10-12 Ma in the Central Kyrgyz Tien Shan, east of the TFF. We suggest that a late Miocene tectonic event was also present in the Western Kyrgyz Tien Shan and that it is responsible for folding the Massaget Formation in the foothills and subsequent erosion, leading to the formation of the angular unconformity.

This younger deformational episode extended in time through the Pliocene and continued to affect the basin, as documented by the numerous examples of Baktriy

growth strata (Figs. 4.7 and 4.8) in the interpreted seismic sections. Moreover, if we assume a Pliocene age for the Baktriy Formation we can estimate a relatively high sedimentation rate of ~ 0.18 mm/y^{-1} at least for the hanging-wall of the CFF. This rate is presumably higher basinwards where the Baktriy Fm. is clearly thicker (Fig. 4.8). In both cross-sections, growth-strata are interpreted as being related to the growth of anticlines, as shown in the hanging-wall of the NFF (Fig. 4.8). Younger growth-strata relations are found basinwards that correspond to the position of basement-related faults (Figs. 4.7 and 4.8). The stratigraphic position of the growth strata clearly indicates that deformation shifted basinwards with the deposition of younger sediments. Moreover, the good correlation between the growth strata and the presence of basement-involved faults points to Neogene reactivation of previously formed discontinuities. Continued exhumation affected the basin borders, reducing the size of the depocenter; therefore, we suggest that the Alai range was uplifted during this period, disconnecting the Fergana basin from the Alai and Tarim basins (Fig. 4.9C). Thermochronological ages from the Alai Range confirm a late Miocene cooling event (*De Grave et al.* 2012). Thick Pliocene conglomeratic units are described in both the subsurface and outcrop of the adjacent Alai (e.g. *Coutand et al.* 2002) and Tarim basins (e.g. *Heermance et al.* 2008; *Li et al.* 2012; *Wei et al.* 2013).

From the subsurface data, we interpret most of the reverse fault in the basin to be steeply-dipping, basement-involved structures (Figs. 4.7 and 4.8). This interpretation is consistent with other intermountain basin within the Tien Shan (e.g. Issyk-Kul, Turpan basin; *Hendrix et al*. 1992; *Avouac et al.* 1993; *Greene et al.* 2000; *Jolivet et al.* 2010; *Macaulay et al.* 2014). The geometrical relationships of the faults suggest minimal horizontal displacement and consequently low amount of shortening, at least in the northern Fergana area. As proposed by *Thomas et al.* (1993), this subsurface data favors the interpretation that much of the north-south shortening was compensated by dextral strike-slip motion along the TFF; probably the shortening in the Chatkal ranges is greater to the NE and diminishes to the SW. Moreover, we can conclude that the amount of crustal thickening produced by basement-involved faults should be minor and will not significantly contribute to the formation of flexural subsidence in the basin.

4.5.3 Basin formation

An important question concerns the mechanism responsible for creating the accommodation space for the extremely thick late Cenozoic sequence. As shown by the

seismic images and isopach map (Figs 4.1, 4.7 and 4.8) the basin does not show the typical wedged-shaped depositional geometry expected for flexurally-formed foreland basin. As carefully explained by *Burov & Molnar* (1998), the large negative gravity anomaly over the basin (~120 mGal) cannot be explained solely as the result of flexural subsidence caused by basin-vergent thrusting and accumulation of low-density sediment in the resulting depression. The basin-fill also cannot be explained purely as a flexural consequence of south-vergent subduction to the south. This gravity anomaly is similar in both the Soviet-era data which these authors used and in the more recent GRACE data (*Smit et al*. 2013). The preferred interpretation of *Burov & Molnar* (1998) is that the Moho is about 10 km deeper beneath the basin than beneath the adjacent ranges. Seismic tomographic imaging of the crust and upper mantle also shows the Moho under the Fergana basin at greater depth than surrounding areas (*Lei* 2011). In turn, this is interpreted to have been caused by folding or buckling of the lithosphere due to north-south compression (*Burg et al*. 1994; *Burov & Molnar* 1998; *Cloetingh & Burov* 2011). Based on the stratigraphic record presented above, we interpret the thermotectonic age of the crust to be late Palaeozoic rather than the previous (*Burov & Molnar* 1998) interpretation of a Jurassic age; this would suggest lithospheric mantle folding rather than folding of the entire lithosphere (*sensu Cloetingh & Burov* 2011). In such a buckling system, the upper crust is decoupled from the weaker lower crust, allowing for the accumulation of thick sedimentary sequences without requiring significant shortening within the basin, as is indeed observed. Numerical modeling shows that significant faulting can occur in the up-folded basin-bounding ranges while the basin is being folded (*Burov & Molnar* 1998).

The deep basin which was rapidly formed by lithospheric folding was filled by sediment. The early sediment fill was derived from the uplifted Chatkal ranges. The younger basin fill, represented by the Baktriy Fm., was derived from sources to the east. Today the Tash-Kumyr section is cut by the Naryn river, which drains the eastern portion of Kyrgyzstan. We suggest that the large thickness of the Baktriy Fm is the depositional expression of an expansion of the drainage basin at this time. Much of the upstream portion of the Naryn river lies in the Central Tien Shan; therefore, although the drainage area is now immense, the composition is not dramatically different from that of the Chatkal ranges.

The Pamir orogen is located south of the Fergana basin. Northward indentation of the Pamir seems to have commenced at about the same time as deposition of the Massaget formation in the late Oligocene to early Miocene (see *Bande et al*. 2015a and *Sobel et al*. 2013 for a more complete discussion). Although neither history is well dated, the spatio-temporal similarities encourage a search for a link between the two systems.

A recent 2-D thermomechanical model of the Pamir orogen using the finite element code SLIM2D by Tympel and Sobolev and reported in *Sippl et al*. (2013) and *Tympel* (2015) focused on regional lithospheric deformation. Interestingly, their results show the distal, northern portion of the south-dipping downgoing Pamir-Alai slab as having a large downward buckle beneath the location corresponding to the Fergana basin. This thermomechanically-modeled buckling is produced by north-south compression of this slab and is compatible with the large late Cenozoic subsidence of the basin. On the east side of the TFF, 4-6 km thick Cenozoic basins such as Naryn and Issyk Kul have similar late Palaeozoic and Mesozoic histories but lack such large negative gravity anomalies and have Cenozoic basin fill that appears to be isostatically-compensated (*Burov et al*. 1990); the Tien Shan is not bounded by a south-vergent subduction zone at these longitudes. Therefore, we suggest that lithospheric folding driven by subduction-associated compression provides a geologically-consistent explanation for the basin subsidence mechanism.

How could such a buckle evolve? The Fergana basin is bounded on the east by the dextral TFF. This lithospheric-scale fault had a multi-stage pre-Cenozoic history that presumably made it easier to reactivate during late-Oligocene - early Miocene compression (see *Bande et al*. 2015a for discussion). The geometry and magnitude of exhumation in the Chatkal ranges, to the north of the basin, document a westward decreasing amount of upper crustal shortening (*Cobbold et al*. 1996; *Bande et al*. 2015a). However, less late Oligocene - early Miocene shortening has been documented within the Tien Shan to the east of the TFF (e.g. *Macaulay et al*. 2014). This is compatible with the observation that the TFF extends southwards beneath the western Tarim basin and is linked to Pamir indentation (*Bande et al*. 2015a; *Wei et al*. 2013). Combining these observations, we suggest that when shortening commenced, it was largely bounded on the east by the TFF; in turn, the E-W shortening gradient lead to the observed counterclockwise Fergana basin rotation. It remains unclear whether

buckling-driven subsidence commenced synchronously with deposition of the basal Massaget formation or later in the Neogene basin evolution. Did the initial formation of a flexural / rotating basin focus a subsequent lithospheric buckle? Or did a buckle form initially, synchronously with initiation of vertical axis basin rotation and bounded on the east by the TFF? We favor the former scenario of delayed buckling because late Oligocene - early Miocene deformation associated with dextral slip along the TFF continues far south-southeast of the Fergana basin. In addition, buckling should be coeval with uplift and exhumation on both the north and south flanks of the basin; to date, there is little evidence for Oligocene-early Miocene exhumation in the south Tien Shan, south of the basin. Clearly more data are required to resolve this question; however, regardless of the exact timing, deformation associated with the TFF and buckling provide mechanisms for propagating deformation far north of the main deformation front at the northern margin of the Pamir.

4.6 Conclusions

During the Mesozoic, the Western Tien Shan was characterized by a lack of tectonic activity, which lead to the development of a regional erosional surface. Thin sedimentary strata outcrop in the basin borders and are imaged in seismic reflection data from the subsurface. The early Cenozoic section of the northern Fergana basin is characterized by a low-energy nonmarine depositional environment developed during a tectonic quiescent period. Sporadic marine incursion reached the area, depositing thin marginal marine beds that are widely correlatable.

Starting in the Oligocene, compressional stresses reached the western Kyrgyz and Uzbek Tien Shan. Shortening was transferred along the TFF and exhumation occurred in the Chatkal and Fergana Ranges by ca. 25 Ma. The basin bounding reverse faults (e.g. NFF and CFF) are imaged as steeply dipping planes, suggesting that the amount of shortening should be small; along strike, this was absorbed by lateral slip along the TFF. The upward coarsening and thickening arrangement of the Massaget Fm reflects this tectonic episode. Thick strata corresponding to the Massaget Fm are imaged in the basin center and thin towards the basin border. The geometrical relationship of the reflectors suggests that the basin should have been wider than its present configuration. A regional angular unconformity separates the Massaget from the Baktriy Fm., implying a younger tectonic episode, possibly dated as ~10 Ma based on

regional correlations. Many growth-strata relations are imaged in the Baktriy Fm., suggesting recent (< 10 Ma) basin-vergent deformation. Similarly to the Massaget Fm., thick Baktriy strata are present in the basin center, implying a young and efficient subsidence mechanism. We propose that this mechanism might be caused by lithospheric buckling related to the continental subduction occurring to the south beneath the Pamir.

Acknowledgements

This contribution was supported by the Darius Programme and a fellowship from the German Academic Exchange Service (DAAD) to A. Bande. We thank T. Voigt, R. Heermance and editor M.-F. Brunet for constructive and valuable reviews that strengthened the paper. We acknowledge C. Galarza for coordinate transformation and map handling, E. Micucci for geophysical suggestions and considerations and E. Macaulay for geological discussions that improved early interpretations made in the paper.

Chapter 5
Discussion and conclusions

The overall goal of this study was to establish a comprehensive chronology of tectonic events, changes in topography, and basin formation processes in the western Tien Shan. To achieve this objective, I have used a diverse set of data to constrain and infer exhumation, deformation, sedimentation and subsidence processes in most of the western Tien Shan ranges and in its adjacent intramontane basins. For the first time, a thorough chronology of related tectonic and sedimentary processes based on modern multi-method approach is available for the western Tien Shan. The preceding 3 chapters included results and interpretation from different ranges and basins. Nonetheless, a complete and time-ordered recap is needed. In the next sections, I will chronologically summarize the main findings and interpretations in order to achieve the main objective of the thesis.

5.1 Apparently calm Mesozoic record

U/Pb crystallization ages of Alai range granites suggest a Permo-Triassic emplacement of the intrusions in the southern Tien Shan. The ages agree with previous estimates (e.g., *Konopelko et al*., 2007; *Seltmann et al*., 2011), corresponding to post-collisional magmatism widely distributed across the entire Tien Shan. This event is related to the final amalgamation of the Paleozoic Tien Shan orogen and the Central Asian Oceanic Belt as a whole (e.g., *Windley et al*., 2007; *Alexeiev et al*., 2015).

According to the available stratigraphic data, the Triassic is absent (*Abidov et al*., 1992). Thin Jurassic and lower Cretaceous nonmarine beds are covered by a sequence of Albian to Turonian shallow marine transgressions and regressions. Numerous studies have previously characterized the Tien Shan Mesozoic history as a period with a small amount of exhumation interrupted by periods of limited deposition (e.g. *Hendrix* 2000; *Bullen et al*. 2003; *Sobel et al.* 2006b; *Jolivet et al.* 2010; *Macaulay et al*. 2013). Alai Range thermal models that include zircon (U-Th)/He data support the interpretation made by previous authors, suggesting a period with a very slow exhumation rate (~0.75°C Ma^{-1}) in the late Cretaceous (Fig. 4.5D). The thin, laterally continuous beds imaged in the subsurface suggest also a calm tectonic environment. The exception to this pattern are thick Jurassic nonmarine sediments distributed along the Talas-Fergana fault. These strata are associated with apparent pull-apart basin along

and restricted to the strike-slip fault (*Sobel*, 1999). This type of beds are present also to the north in the Leont'yev Basin and finally in the Turgay Basin (*Allen et al.,* 2001; *Alexeiev et al*., 2009; *Wei et al*., 2012).

It is important to note that amount of data available to constrain the Mesozoic history of the western Tien Shan is very scarce, even compared to the Cenozoic. Thus, the interpretations made account for the available pieces of information. Substantial work is still needed to delineate a more clear and unambiguous Mesozoic evolution.

5.2 Paleogene tectonic quiescence

The early Cenozoic record does not show a substantial change compared to the late Cretaceous history. The Fergana basin Paleogene outcrops described in chapter 4 show low-energy distal nonmarine facies and marginal marine strata. The Paratethys Sea sporadically flooded the basin, with the maximum expansion corresponding to the carbonate beds described in the Tash-Kumyr section (Fig. 4.4). *Bosboom et al*. (2015) correlated these beds to the third transgression, also present in the Alai, Tadjik and Tarim basins. According to the paleoenvironment interpretation presented in the thesis, sedimentation occurred in a calm tectonically quiescent environment in agreement with the regional lateral continuity of the Paleogene strata in the subsurface. Thin basin-wide laterally continuous seismic reflectors suggest a tectonically calm environment dominated by a low depositional rate (~9.4 m Myr^{-1}). The thermal models and thermochronologic ages presented in this thesis also suggest low cooling rates (<1°C/Myr) during most of the Paleogene in most of the western Tien Shan's mountain ranges. Similar estimates have been postulated by different authors (e.g. *Bullen et al*., 2003; *Sobel et al.,* 2006a; *De Grave et al*., 2012; *Macaulay et al*., 2013; *Jolivet*, 2015) also based on thermochronology data from other sectors of the Tien Shan.

5.3 Oligo-Miocene onset of deformation and basin partitioning

The tectonic quiescence was interrupted at ~25 Ma by a rapid cooling event. This is interpreted as reflecting increased erosion caused by surface uplift and active deformation. In the late Oligocene – early Miocene, a rapid exhumation episode determine the onset of deformation in the western Tien Shan (chapter 2). This event is recorded in samples collected in the Talas, Shandalash, northern Fergana and Alai Ranges. Based on the available results it is stronger in the northern ranges (Talas,

Shandalash and northern Fergana) than in the southern (Alai Range). Similar estimates have been proposed for the At-bashi Range (*Glorie et al*., 2011) and Kokshaal Range (*Sobel et al*., 2006a) suggesting synchronous exhumation. It is interesting that the Kokshaal-Atbashi Ranges lies ca. 400 km away from the NW Tien Shan. However, both areas are linked by the Talas-Fergana fault (TFF). The TFF formed in the late Paleozoic–early Mesozoic related to the final amalgamation of Pangea (*Burtman* 1980) and was reactivated in the Jurassic and Cenozoic (*Bazhenov* 1993; *Burtman et al.* 1996). The coeval exhumation of the Chatkal and At-bashi ranges suggests that they are not just linked; both regions are kinematically connected. Supporting the kinematic connection, *Thomas et al*. (1993) suggested that the Fergana basin experienced 20 ± 11° of counterclockwise rotation with respect to stable Eurasia. The rotation sense is consistent with right-lateral slip along the TFF and I concur with *Thomas et al.* (1993) that the rotation was absorbed by slip along the main strike slip fault and shortening in the TFF terminations. Based on the available data, I interpret both the Chatkal (NW Tien Shan) and the South Tien Shan east of the TFF as horsetail splays connected to the main strike-slip fault. Moreover, the coincidence of preexisting discontinuities with Cenozoic activity of the TFF implies that reactivation of favorably oriented structures must play a substantial role in how deformation was accommodated and how efficiently it was transmitted hundreds of kilometers.

In the central portion of the Alai Range, the Oligo-Miocene onset of deformation is also present. However, the magnitude and areal extent is restricted. As along the TFF, the initial deformation in this sector represents the first manifestation of tectonic forces related to the India-Asia collision. South of the Alai range lies the Pamir indentor, which has moved ~400 km north with respect to stable Asia. It is supposed that south-dipping subduction beneath the Pamir initiated during the latest Oligocene – early Miocene (e.g., *Burtman & Molnar*, 1993; *Sobel et al.*, 2013). This first order change in the geodynamic configuration of the India-Asia collision was probably the driver necessary to preferentially reactivate the frictionally weakest and most suitably orientated inherited structures available for accommodating north-south directed horizontal shortening. The Talas-Fergana fault acted as one of these preexisting discontinuities as well as E-W oriented structures located in the Alai Range.

The sedimentary response to the Oligo-Miocene event is represented by the first syn-tectonic unit described in the Fergana basin: the Massaget Formation. Although the

age-constraints for the Massaget Formation are not strong, it is traditionally interpreted to have been deposited during the Oligo-Miocene (e.g., *Artyomova et al.,* 1971). A gradual shift in paleocurrents is apparent in the upper part (Fig. 3.6c) of the unit together with an increase in higher-energy depositional facies (Fig. 3.4). The onset of deformation in the western Tien Shan triggered the uplift of the ranges surrounding the Fergana basin, creating topography, enabling erosion, changes in paleocurrents and bringing source areas closer. As a result, the syn-tectonic Massaget Formation was deposited. However, as previously mentioned, the onset affected many ranges in the Central Asia interior. Similar processes occurred coevally, resulting in equivalent units distributed in the Central Asian interior (e.g. Wuqia Group in the Tarim Basin; *Wei et al.,* 2013). Moreover, the Oligo-Miocene deformation event dissected the previously continuous Paratethyan Sea. In chapter 4, I suggest that early uplift of the Alai Range separated the Fergana and Alai basins, starting the actual basin partitioning. Interestingly, in the eastern Alai Range thermal models require a reheating period between 30 - 11 Ma. In that area, the Gulcha basin in presently uplifted. The result of these models (Fig. 3.5 C and D) suggests that Oligo-Miocene uplift was diachronous and spatially separated.

The TFF is a preeminent example of a Cenozoic reactivated fault that corresponds to a Permian subvertical strike-slip fault (e.g., *Burtman*, 1980; *Bazhenov & Mikolaichuk*, 2004). For these steeply dipping structures, even minor along-strike inherited geometrical differences would result in substantial changes in the ability to accommodate horizontal stresses. The Tien Shan is an ancient plate boundary (*Molnar & Tapponnier*, 1975); therefore a large number of preexisting discontinuities are expected. Himalayan stresses acting on this complex mosaic might explain the diachronous uplift produced in the Oligo-Miocene.

5.4 Late Miocene widespread Tien Shan deformation

Subsequently, in the late Miocene a new deformation episode started in most of the western Tien Shan ranges. The late Miocene event is represented in the northern sector (e.g. Shandalash and northern Fergana ranges, section 2.4), in the central part (e.g. central Fergana and Takthalik ranges), in the entire Alai Range (section 3.4) and even in basement thrust sheets immersed in the Alai basin (section 3.4, NUR). Clearly the late Miocene event was strong and well represented. Interestingly, most of the

ranges that show an Oligo-Miocene onset also show late Miocene rapid exhumation. For example, the northern Fergana range clearly show an Oligo-Miocene onset based on the AER (Fig. 2.6A) and thermal models of a sample (10SU62) included in the profile clearly show the late Miocene rapid event (Fig. 2.6C). The Central Alai range (CAR) models show a similar pattern (Fig. 3.6 C and D). Based on this information, I suggest that the locus of deformation has not shifted in the late Miocene and it is not possible to describe out-of-sequence deformation. The late Miocene event is recorded in most of the sampled ranges, suggesting that deformation has not simply migrated between ranges and instead an overall increase in shortening is needed. Although horizontal shortening started in the late Oligocene – early Miocene, rates should have significantly increased in the late Miocene. Therefore, it seems likely that the significant shortening increased identified in the western Tien Shan (chapter 3), central Kyrgyz Tien Shan (e.g. *Macaulay et al.* 2014) and eastern Chinese Tien Shan (e.g. *Charreau et al., 2006*) was part of a much larger geodynamical change that affected much of Central Asia.

Variably-sized strike-slip structures characterize many sectors of the western Tien Shan. The abundance of this kind of fault explains how shortening is distributed along the ranges. For example, in the Chatkal ranges exhumation is higher close to the Talas-Fergana fault and decreases along strike to southwest (Chapter 2). In other words, N-S shortening is not only absorbed by thrust faulting, but also by strike-slip displacement and block rotation. As shown in chapter 4, steeply-dipping range-bounding fault characterize the northwestern Tien Shan and might account for crustal thickening in that sector. Recent work on steeply dipping faults around the Issyk-Kul lake (e.g. *Burgette*, 2008; *Selander et al.* 2012; *Macaulay et al*. 2013) suggest that the inclination of these fault systems decreases with depth, causing block rotation or basement-involved fault-bend folding. A similar geometry might be present in the Chatkal ranges. Nevertheless, the impressive thickness (> 8 km) of the Fergana basin cannot be explained only by subsidence-caused crustal thickening. *Burov & Molnar* (1998) analyzed the large negative gravity anomaly over the basin and concluded that cannot be justified by basin-vergent thrusting and accumulation of low-density sediment in the resulting depression. The hypothesis of the previous authors is that the Moho is about 10 km deeper beneath the basin than beneath the surrounding ranges. This is interpreted to have been caused by folding or buckling of the lithosphere owing

to north-south subduction. In chapter 4, I agree with the hypothesis that the thick sediments preserved in the basin are accommodated by lithospheric folding (e.g. *Burov & Molnar*, 1998; *Cloetingh & Burov*, 2011) and propose that this is driven by compression associated with the south-dipping downgoing Pamir-Alai slab subduction (*Sippl et al*., 2013).

In the foothills of the Fergana basin the contact between the Massaget and Baktriy Formation is marked by an impressive angular unconformity (Fig. 4.5E). In chapter 4, I suggest that the unconformity was created during the late Miocene event and the Baktriy Formation is a younger syn-tectonic unit. However, deformation persisted during the Pliocene as documented by numerous examples of well-developed Baktriy Formation growth strata interpreted in the seismic sections (e.g., Fig. 4.7 and 4.8). The good correlation between growth-relations and the presence of steeply-dipping basement-involved faults points to continued reactivation of preexisting structures.

The rapid exhumation event described in both the western and central Tien Shan suggests that there have been an overall increase in the rate of horizontal crustal shortening across the entire Tien Shan range during the late Miocene. Increases in the magnitude of deformation have been proposed in numerous locations within the Tien Shan (e.g. *Abdrakhmatov et al*., 1996; *Sobel et al.*, 2006a; *Glorie et al*., 2011, *Macaulay et al*., 2014). Based on my revised definition of the regional extent of the late Miocene event, neither stress transfer along the rigid Tarim block or Pamir indentation can account for the overall increase in horizontal shortening causing synchronous Tien Shan exhumation. A singular driver for Tien Shan exhumation is needed and should be connected to the evolution of the India - Asia collision located further south.

5.5 Open research questions

Numerous insights and constraints on the tectonic evolution of the western Tien Shan are presented in this thesis. However, many important questions remain and some new ones arose from the research in this dissertation. In terms of the spatiotemporal evolution of deformation, modern data is still needed in the westernmost Tien Shan. My results are derived from an area that is in close proximity to the Talas-Fergana fault. The results presented in this thesis clearly show that exhumation in the Alai range varies along strike (Chapter 3). Moreover, as stated in the Introduction and in Chapter 2,

shortening and possible exhumation should decrease to the west in the Chatkal ranges. Research work in the Uzbek Chatkal range should confirm or modify the hypothesis. Changes in exhumation and deformation should be documented in the Turkestan and Gissar ranges, in the westernmost Tien Shan. The complete picture on the evolution of the Tien Shan will only be shown when the entire Tien Shan has been sampled and analyzed.

Additionally, I consider that the understanding of the Mesozoic evolution of the western Tien Shan is still far from complete. Although the focus of the study presented here focused on the Cenozoic evolution, some of the data have implications for the earlier history of the region. Time-temperature modeling shows that during Cretaceous times, the cooling rate was low. However, these results are constrained by only a few samples. A comprehensive study focused in the Mesozoic exhumation using higher temperature thermochronometers (e.g. zircon (U-Th)/He and zircon fission track) will result in interesting results and solve some of the remaining questions. Some authors (e.g. *Hendrix et al*., 1992; *Dumitru et al*., 2001; *De Grave et al*., 2012) already suggested exhumation and cooling episodes during the Mesozoic. However, there is no agreement on the timing and areal extent of the different episodes. The Mesozoic sedimentary record of the Tien Shan also needs further attention. Thick Jurassic deposits are described along the Talas-Fergana Fault (*Sobel*, 1999). Albian to Turonian shallow marine transgressions are intercalated with high- energy nonmarine Cretaceous strata (*Bakirov et al.,* 2001) in the Fergana basin foothills. Connecting those deposits to exhumation patterns and placing them in a tectonic evolution context is far from complete. Moreover, little is known about the subsurface distribution and abundance of Mesozoic strata in most of the Tien Shan intramontane basins. In the same way that little is known about exhumation and stratigraphy, a broad structural research project is also needed in the Tien Shan to test whether the same Cenozoic structures got previously reactivated and to determine the timing and magnitude of the Mesozoic deformation. A comprehensive Mesozoic analysis will clarify the extent of terrain accretions (e.g. Qiantang, Lhasa collision) to the southern margin of Eurasia during the Mesozoic and which of them affected the hinterland (*Hendrix et al*., 1992; *Jolivet et al*., 2010).

Only by having better constraints on the Mesozoic deformation can a complete understanding of fault reactivation emerge. One of the most significant questions

remaining is what makes a particular inherited structure more suitable to tectonic reactivation? In this thesis, I proposed that most of the deformation in western Tien Shan is localized in places where the susceptibility of preexisting discontinuities to reactivation is higher. However, the data presented here does not fully resolve why some structures are more prone to reactivation. Solving this question will produce a clear breakthrough in the understanding of intracontinental deformation.

Another potential research direction is the sedimentary record of intramontane basins, which remains poorly understood. In my opinion, future work should focus on defining reliable age controls for the Fergana basin deposits. The lack of detailed age constraints on the Fergana basin sedimentary units constitutes the biggest shortcoming in order to understand the evolution of the basin. Conscious and detailed paleomagnetic and/or biostratigraphic work might solve the problem, given the absence of pyroclastic layers in the Cenozoic section. After resolving the chronostratigraphic uncertainties, detailed provenance analysis, together with stable isotopes (or other climatic proxy) could be performed in the basin and tied to the main findings presented in this dissertation.

References

ABDRAKHMATOV, K. Y., S. A. ALDAZHANOV, B. H. HAGER, M. W. HAMBURGER, T. A. HERRING, K. B. KALABAEV, K. B. KALABAYEV, V. I. MAKAROV, P. MOLNAR, S. V. PANASYUK, M. T. PRILEPIN, R. E. REILINGER, I. S. SADYBAKASOV, B. J. SOUTER, Y. A. TRAPEZNIKOV, V. Y. TSURKOV, & ZUBOVICH, A. V. 1996, Relatively recent construction of the Tien Shan inferred from GPS measurements of present-day crustal deformation rates. *Nature*, **384**(6608) 450-453, doi: 10.1038/384450a0.

ABIDOV, A. A., KALOMAZOV, R. U. & PEDDER Y. G. 1992. New scheme of tectonic framework of the Fergana Depression. *J. Oil and Gas Geology*, ***11***. Nedra, Moscow. (In Russian)

AFONICHEV, N. A. & VLASOV, N. G. (eds) 1984. *Appendix to the geological map of the Kazakhstan and the Central Asia in scale 1:1 500 000*. Leningrad: Vsegei Publ., 234 tables (in Russian).

ALEXEIEV, D. V., COOK, H. E., BUVTYSHKIN, V. M. & GOLUB, L. Y. 2009. Structural evolution of the Ural-Tian Shan junction: A view from Karatau ridge, South Kazakhstan. *Comptes Rendus – Geoscience*, **341**, 287-297.

ALEXEIEV, D. V., COOK, H. E., DJENCHURAEVA, A. V. & MIKOLAICHUK, A. V. 2015. The stratigraphic, sedimentological and structural evolution of the southern margin of the Kazakhstan continent in the Tien Shan Range during the Devonian to Permian. In: BRUNET, M.-F., MCCANN, T. & SOBEL, E. R. (eds) *Geological Evolution of Central Asian Basins and the Western Tien Shan Range*. Geological Society, London, Special Publications, **427**, http://doi.org/10.1144/SP427.3

ALLEN, M.B., WINDLEY, B.F., ZHANG, C., ZHAO, Z. & WANG, G. 1991. Basin evolution within and adjacent to the Tien Shan Range, NW China. *Journal of Geological Society,* **148**, 369-378.

ALLEN, M.B., WINDLEY, B.F. & ZHANG, CH. 1992. Palaeozoic collisional tectonics and magmatism of the Chinese Tien Shan, Central Asia. *Tectonophysics,* **220**, 89–115.

ALLEN, M. B. & VINCENT, S. J. 1997. Fault reactivation in the Junggar region, northwest China: The role of basement structures during Mesozoic-Cenozoic compression. *Journal of the Geological Society*, **154**, 151-155, doi: 10.1144/gsjgs.154.1.0151.

ALLEN, M. B., ALSOP, G. I., & ZHEMCHUZHNIKOV, V. G. 2001. Dome and basin refolding and transpressive inversion along the Karatau fault system, southern Kazakstan. *Journal of the Geological Society*, **158**, 83-95.

ALLEN, M.B. & ARMSTRONG, H.A. 2012. Reconciling the Intertropical Convergence Zone, Himalayan/ Tibetan Tectonics, and the Onset of the Asian Monsoon System. *Journal of Asian Earth Sciences*, **44**, 36-47.

ALONSO-ZARZA, A. M. & WRIGHT, V.P. 2009. Calcretes. In: Alonso-Zarza, A. M & Tanner, L.H. (eds) *Carbonates in Continental Settings: Facies, Environments, and Processes*. *Developments in Sedimentology,* Vol. 61, Elsevier, Amsterdam

AMIDON, W. H., & HYNEK, S. A. 2010. Exhumational history of the north central Pamir. *Tectonics*, **29,** doi:10.1029/2009TC002589.

ARGAND, E. 1924, La tectonique de l'Asie, Congres Géologique International, Comptes Rendus de la XIII Session, Belgique, 1922,1, 171-371.

ARGUS, D. F., GORDON, R., HEFLIN, M. B., MA, C. R., EANES, J., WILLIS, P., PELTIER, W. R.,& OWEN, S. E. 2010. The angular velocities of the plates and the velocity of Earth's centre from space geodesy. *Geophys. J. Int*., **180**, 913–960. doi: 10.1111/j.1365-246X.2009.04463.x

ARTEMOVA, Z. N. & BRODSKIY, I. A. 1963. *Geological map of the USSR*, near Tashkent series. 1:200,000 (in Russian).

ARTYOMOVA, Z.P., BRODSKIY, I.L. & VNUCHKOV, V.I., 1971. *Geological map of the USSR. Aal- Kokshaal series*. Sheet K-43-XXV. 1:200,000 (in Russian).

AKRAMHODJAEV, A. M. & SAIDALIEVA, M. S. 1971. *Fergana oil-gas bearing basin*. Nedra, Moscow. 279 pp. (in Russian).

AVOUAC, J. P., TAPPONNIER, P., BAI, M., YOU, H. & WANG G. 1993. Active thrusting and folding along the northern Tien Shan and late Cenozoic rotation of the Tarim relative to Dzungaria and Kazakhstan. *Journal of Geophysical Research*, **98**, 6755-6804, doi: 10.1029/92JB01963.

BAKIROV, A., GHES, M., MAKSUMOVA, R. & GUSAK, L. 2001. *Geodynamic map of Kyrgyzstan.*1:500,000. Institute of Geology, National Academy of Science, Bishkek.

BANDE, A., SOBEL, E. R., MIKOLAICHUK, A. & TORRES ACOSTA, V. 2015. Talas-Fergana Fault Cenozoic timing of deformation and its relation to Pamir indentation. *In*: BRUNET, M.-F., MCCANN, T. & SOBEL, E. R. (eds) *Geological Evolution of Central Asian Basins and the Western Tien Shan Range*. Geological Society, London, Special Publications, **427**,doi.org/10.1144/SP427.1

BANDE, A., RADJABOV, S., SOBEL, E.R. & SIM, T. 2015b. Cenozoic palaeoenvironmental and tectonic controls on the evolution of the northern Fergana Basin. . In: BRUNET, M.-F., MCCANN, T. & SOBEL, E.R. (eds) *Geological Evolution of Central Asian Basins and the Western Tien Shan Range*. Geological Society, London, Special Publications, **427**, doi:10.1144/SP427.12

BAZHENOV, M.L., 1993. Cretaceous paleomagnetism of the Fergana Basin and adjacent ranges, central Asia: tectonic implications. *Tectonophysics*, **221**, 251-267.

BAZHENOV, M.L., & MIKOLAICHUK, A.V. 2004. Structural Evolution of Central Asia to the North of Tibet. A Synthesis of Paleomagnetic and Geological Data. *Geotectonics*, ***38*(5)**, 379–393

BISKE, Y. S. 1995. Late Paleozoic Collision of the Tarim and Kyrgyz-Kazakhstan Paleocontinents, *Geotektonika*, **30(1),** 31-39.

BISKE, Y. S. 1996. *Paleozoic structure and history of Southern Tien Shan*. Leningrad, LGU (in Russian).

BISKE, Y.S. & SELTMANN, R. 2010. Paleozoic Tian-Shan as a transitional region between the Rheic and Urals-Turkestan oceans. *Gondwana Research*, **17**, 602-613, doi:10.1016/j.gr.2009.11.014

BLAIR, T.C. & MC PHERSON, J.G., 1994. Alluvial fans and their natural distinction from rivers based on morphology, hydraulic processes, sedimentary processes, and facies assemblages. *Journal of Sedimentary Research,* **64 (3A)**, 450–489

BOSBOOM, R.E. 2013. *Paleogeography of the Central Asian proto-Paratethys Sea in the Eocene: controlling mechanisms and paleoenvironmental impacts*: PhD. Thesis, 223 p. Utrecht.

BOSBOOM, R., DUPONT-NIVET, G., GROTHE, A., BRINKHUIS, H., VILLA, G., MADIC, O., STOICA, M., KOUWENHOVEN, T., HUANG, W., YANG, W. & GUO, Z. 2014. Timing, cause and impact of the late Eocene stepwise sea retreat from the Tarim Basin (west China), *Palaeogeography, Palaeoclimatology, Palaeoecology*, **403**, 101–118. doi: 10.1016/j.palaeo.2014.03.035

BOSBOOM, R., MANDIC, O., DUPONT-NIVET, G., PROUST, J-N., ORMUKOV, C. & AMINOV, J. 2015. Late Eocene palaeogeography of the proto-Paratethys Sea in Central Asia (NW China, southern Kyrgyzstan and SW Tajikistan). *In*: BRUNET, M.-F., MCCANN, T. & SOBEL, E. R. (eds) *Geological Evolution of Central Asian Basins and the Western Tien Shan Range*. Geological Society, London, Special Publications, **427**, http://doi.org/10.1144/SP427.11

BRANDON, M. T., RODEN-TICE, M. K. & GARVER, J. I. 1998. Late Cenozoic exhumation of the Cascadia accretionary wedge in the Olympic Mountains, northwest Washington State, *Geol. Soc. Am. Bull*., **110**, 985-1009, doi: 10.1130/0016-7606(1998)110<0985:LCEOTC>2.3.CO;2

BROOKFIELD, M.E., & HASHMAT, A. 2001. The geology and petroleum potential of the North Afghan platform and adjacent areas (northern Afghanistan, with parts of southern Turkmenistan, Uzebekistan and Tajikistan). *Earth-Science Reviews*, v. 55, p. 41-71.

BULLEN, M.E., BURBANK, D.W. & GARVER, J.I. 2003. Building the Northern Tien Shan: Integrated thermal, structural, and topographic constraints. *Journal of Geology*, **111**, 149-165, doi: 10.1086/345840.

BURTMAN, V.S. 1975. Structural geology of Variscan Tien Shan, USSR. *American Journal of Sciences*, **275-*A***, 157-186.

BURTMAN, V. S., 1980. Faults of Middle Asia. *American Journal of Sciences*, **280**, 25-744.

BURTMAN, V.S., 2000. Cenozoic crustal shortening between the Pamir and Tien Shan and a reconstruction of the Pamir-Tien Shan transition zone for the Cretaceous and Palaeogene. *Tectonophysics*, **319**, 69-92.

BURTMAN, V. S., & MOLNAR, P. H. 1993. Geological and geophysical evidence for deep subduction of continental crust beneath the Pamir. *Geological Society of America Special Paper.* v. **281**.

BURTMAN, V.S., SKOBELEV, S.F., & MOLNAR, P. 1996. Late Cenozoic slip on the Talas-Ferghana fault, the Tien Shan, central Asia. *Geological Society of America Bulletin*, **108**, 1004-1021.

BURTMAN, V.S. 2010. Tien Shan, Pamir, and Tibet: History and Geodynamics of Phanerozoic Oceanic Basins. *Geotectonics*, **44(5)**, 388–404, doi: 10.1134/S001685211005002X

BURBANK, D.W., MCLEAN, J.K., BULLEN, M., ADBRAKHMATOV, K.Y. & MILLER, M.M. 1999. Partitioning of intermontane basins by thrust-related folding, Tien Shan, Kyrgyzstan. *Basin Research*, **11**, 75-92.

BURG, J.-P., DAVY, P. & MARTINOD, J. 1994. Shortening of analogous models of the continental lithosphere: New hypothesis for the formation of the Tibetan plateau. *Tectonics*, **13**, 475-483.

BUROV, E.B. & MOLNAR, P., 1998. Gravity anomalies over the Ferghana valley (Central Asia) and intracontinental deformation. *Journal of Geophysical Research*, **103**, 18,137-18,152.

BUROV, E.V., KOGAN, M.G., LYON-CAEN, H. & MOLNAR, P. 1990. Gravity anomalies, the deep structure, and dynamic processes beneath the Tien Shan. *Earth and Planetary Science Letter,* **96***,* 367-383.

CARLSON, W.D., DONELICK, R.A. & KETCHAM, R.A. 1999. Variability of apatite fission-track annealing kinetics: I. Experimental results. *American Mineralogist*, **84(9)**, 1213-1223.

CHANG, J., QIU, N., & LI, J. 2012. Tectono-thermal evolution of the northwestern edge of the Tarim Basin in China: Constraints from apatite (U–Th)/He thermochronology. *Journal of Asian Earth Sciences*, **61**, 187-198.

CHARREAU, J., GILDER, S., CHEN, Y., DOMINGUEZ, S., AVOUAC, J. P., SEN, S., JOLIVET, M., LI, Y. & WANG, W. M. 2006. Magnetostratigraphy of the Yaha section, Tarim Basin (China): 11 Ma acceleration in erosion and uplift of the Tianshan Mountains, *Geology*, **34(3)**, 181-184, doi:10.1130/G22106.1.

CHEDIYA, O.K. 1986. *Morfostruktury i noveishii tektogenez Tyan'-Shanya (Morfostructures and Neotectonics of the Tien Shan)*, 314 pp., Ilim, Frunze, Kyrgyzstan.

CHEN, J., HEERMANCE, R., BURBANK, D. W., SCHARER, K. M., MIAO, J. & WANG, C. 2007. Quantification of growth and lateral propagation of the Kashi anticline, southwest Chinese Tian Shan. *Journal of Geophysical Research*, **112**, B03S16, doi:10.1029/2006JB004345

CLARKE, J.W. 1984. *Geology and possible uranium deposits of the Fergana region of Soviet Central Asia*. USGS open-file report 84-513, p. 42. Reston, VA.

CLOETINGH, S., BUROV, E. & POLIAKOV, A. 1999. Lithosphere folding: Primary response to compression? (from central Asia to Paris basin). *Tectonics*, **18(6)**, 1064–1083, doi:10.1029/1999TC900040.

CLOETINGH, S. & BUROV, E. 2011. Lithospheric folding and sedimentary basin evolution: a review and analysis of formation mechanisms. *Basin Research,* **23**, 257-290.

COBBOLD, P. R. & DAVY, PH., 1988. Indentation tectonics in nature and experiment. 2. Central Asia. *Bulletin of the Geological Institute of Uppsala*, **14**, 143-162.

COBBOLD, P.R., SADYBAKASOV, E. & THOMAS, J.C. 1996. Cenozoic transpression and basin development, Kyrgyz Tien Shan, central Asia. In: ROURE, F., ELLOUZ, N., SHEIN V.S. & SKVORTSOV, I. (eds) *Geodynamic Evolution of Sedimentary Basins*, Editions Technip, Paris, 181-202.

COOK, H. E., ZHEMCHUZHNIKOV, V. G., ZEMPOLICH,W. G., BUVTYSHKIN, V.M., ZHAIMINA, V. YA., KOTOVA, E. A., GOLUB, L. YA., ZORIN, A. YE., LEHMANN, P. J., ALEXEIEV, D. V., GIOVANNELI, A., VIAGGI, M., FRETWELL, N., LAPOINTE, P., CORBOY, J. J., BOWMAN, M. & DE COO J. C.M. 2002. Devonian and Carboniferous carbonate platform facies in the Bolshoi Karatau, Southern Kazakhstan: outcrop analogs for coeval carbonate oil and gas fields in the North Caspian basin, Western Kazakhstan. *In:* ZEMPOLICH, W. G. & COOK, H. E. (eds) *Paleozoic carbonates of the Commonwealth of the Independent States (CIS): subsurface reservoirs and outcrop analogs*. SEPM Special Publication **74**, 81-122.

COUTAND, I., STRECKER, M.R., ARROWSMITH, J.R., HILLEY, G., THIEDE, R.C. KORJENKOV, A. & OMURALIEV, M. 2002. Late Cenozoic tectonic development of the intramontane Alai Valley, (Pamir-Tien Shan region, central Asia): An example of intracontinental deformation due to the Indo-Eurasia collision, *Tectonics*, **21(6)**, 1053, doi:10.1029/2002TC001358.

COWGILL, E. 2010. Cenozoic right-slip faulting along the eastern margin of the Pamir salient, northwestern China. *Geologial Society of America Buletin,* **122**, 145–161, doi:10.1130/B26520.1.

CUNNINGHAM, W. D. & MANN, P. 2007. Tectonics of Strike-Slip Restraining and Releasing Bends. *Geological Society, London, Special Publications*, **290**, 1–12.

DECELLES, P.G., LANGFORD, R.P. & SCHWARTZ, R.K. 1983. Two new methods of paleocurrent determination from trough cross-stratification. *Journal of Sedimentary Petrology*, **53**, 629–642.

DECELLES, P.G. 1988. Lithologic provenance modeling applied to the Late Cretaceous synorogenic Echo Canyon Conglomerate, Utah: A case of multiple source areas. *Geology,* **16**, 1039–1043, doi:10.1130/0091613(1988)016<1039: LPMATT> 2.3. CO;2.

DE GRAVE, J., GLORIE, S., BUSLOV, M. M., IZMER, A., FOURNIER-CARRIE, A., BATALEV, V. Y., VANHAECKE, F., ELBURG, M. & VAN DEN HAUTE, P. 2011. The thermo-tectonic history of the Song-Kul Plateau, Kyrgyz Tien Shan: Constraints by apatite and titanite thermochronometry and zircon U/Pb dating. *Gondwana Research*, **20**, 745-763, doi: 10.1016/j.gr.2011.03.011

DE GRAVE, J., GLORIE, S., RYABININ, A., ZHIMULEV, F., BUSLOV, M.M., IZMER, A., ELBURG, M., VANHAECKE, F. & VAN DEN HAUTE, P. 2012. Late Palaeozoic and Meso-Cenozoic tectonic evolution of the Southern Kyrgyz Tien Shan: constraints from multi-method thermochronology in the Trans-Alai, Turkestan-Alai Section and the Southeastern Ferghana Basin. *Journal of Asian Earth Sciences*, **40**, 149-168, doi: 10.1016/j.jseaes.2011.04.019.

DONELICK, R. A., KETCHAM, R. A. & CARLSON, W. D. 1999. Variability of apatite fission-track annealing kinetics: II. Crystallographic orientation effects, *American Mineralogist*, **84(9),** 1224-1234.

DONELICK, R.A., O'SULLIVAN, P.B., & KETCHAM, R.A. 2005. Apatite Fission-Track Analysis. *Reviews in Mineralogy & Geochemistry*, **58**, 49-94, doi: 10.2138/ rmg.2005.58.3.

DUMITRU, T. A. 1993. New computer-automated microscope stage system for fission-track analysis. *Nuclear Tracks and Radiation Measurements*, **21(4)**, 575-580. doi: 10.1016/1359-0189(93)90198-I

DUMITRU, T. A., ZHOU, D., CHANG, E. Z., GRAHAM, S. A., HENDRIX, M. S., SOBEL, E. R. & CARROLL, A. R. 2001. Uplift, exhumation, and deformation in the Chinese Tian Shan. *In* HENDRIX, M. S. & DAVIS, G. A. (eds) *Paleozoic and Mesozoic Tectonic Evolution of Central and Eastern Asia: From Continental Assembly to Intracontinental Deformation*, Memoir Geological Society of America, **194**, 71-99.

DUNKL, I., MIKES, T., FREI, D., GERDES, A., TOLOSANA-DELGADO, R. & VON EYNATTEN, H. 2014. UranOS: data reduction program for time-resolved U/Pb analyses. Available from http://www.sediment.uni-goettingen.de/staff/dunkl/software/uranos.html

EHLERS, T. A., & FARLEY, K. A. 2003. Apatite (U – Th)/He thermochronometry: Methods and applications to problems in tectonic and surface processes, *Earth and Planetary Sciences Letters*, 2061 – 14, doi: 10.1016/S0012-821X.

FARLEY, K. A. 2002. (U-Th)/He dating; techniques, calibrations, and applications, *Reviews in Mineralogy and Geochemistry*, **47**, 819-843, doi: 10.2138/rmg.2002.47.18.

FARLEY, K. A., WOLF, R. A. & SILVER L.T. 1996. The effects of long alpha-stopping distances on (U-Th)/He ages, *Geochimica et Cosmochimica Acta*, **60(21**), 4223-4229, doi: 10.1016/S0016-7037(96)00193-7.

FARRELL, K. M., 2001. Geomorphology, facies architecture, and high-resolution, non-marine sequence stratigraphy in avulsion deposits. Cumberland Marshes, Saskatchewan. *Sedimentary Geology*, **139(2)**, 93-150

FELD, CH., HABERLAND, CH., SCHURR, B., SIPPL, CH., WETZEL, H. U., ROESSNER, S., ICKRATH, M., ABDYBACHEV U. & ORUNBAEV S. 2015., Seismotectonic study of the Fergana Region (Southern Kyrgyzstan): distribution and kinematics of local seismicity. *Earth, Planets and Space*, **64:40**, doi: 10.1186/s40623-015-0195-1

FITZGERALD, P.G., SORKHABI, R.B., REDFIELD, T.F. & STUMP, E. 1995. Uplift and denudation of the central Alaska Range; a case study in the use of apatite fission track thermochronology to determine absolute uplift parameters. *Journal of Geophysical Research*, **20**,175-20,191, doi: 10.1029/95JB02150.

FU, B., NINOMIYA, Y. & GUO, J. 2010. Slip partitioning in the northeast Pamir–Tian Shan convergence zone. *Tectonophysics,* **483**, 344–364.

GALBRAITH, R.F. 1981. On statistical models for fission track counts. *Mathematical Geology*, **13**, 471-478, doi: 10.1007/BF01034498.

GALLAGHER, K., BROWN, R., & JOHNSON, C. 1998. Fission track analysis and its applications to geological problems. *Annual Review of Earth and Planetary Sciences*, **26(1)**, 519-572.

GALLAGHER, K., STEPHENSON, J., BROWN, R., HOLMES, C., & FITZGERALD, P. 2005. Low temperature thermochronology and modeling strategies for multiple samples 1: Vertical profiles. *Earth and Planetary Science Letters*, **237(1)**, 193-208.

GALLAGHER, K. 2012. Transdimensional inverse thermal history modeling for quantitative thermochronology. *Journal of Geophysical Research,* **117**, B02408.

GAUTHERON, C., TASSAN-GOT, L., BARBARAND, J. & PAGEL M. 2009. Effect of alpha-damage annealing on apatite (U-Th)/He thermochronology, *Chemical Geology*, **266(3–4),** 157-170, doi:10.1016/j.chemgeo.2009.06.001

GES´, M.D. & SELIVERSTOV, K.V. 1995. Geodynamics and magmatic-metallogenic zonation in the Paleo-Thetys margin (the Chatkal region, Tien Shan). *Geology of Ore Deposits*, **37 (2)**, 112-120

GLEADOW, A.J.W. & DUDDY, I.R. 1981. A natural long-term annealing experiment for apatite. *NuclearTracks*, **5**, 169-174.

GILDER, S.A., LELOUP, P.H., COURTILLOT, V., CHEN Y., COE, R.S., ZHAO, X., XIAO, W., HALIM, N., COGNÉ J.P. & ZHU, R.1999. Tectonic evolution of the Tancheng-Lujiang (Tan-Lu) fault via Middle Triassic to Early Cenozoic paleomagnetic data. *Journal of Geophysical Research*, **104 (B7)**, 15365–15390, doi: 10.1029/1999JB900123.

GLORIE, S., DE GRAVE, J., BUSLOV, M. M., ZHIMULEV, F. I., STOCKLI, D. F., BATALEV, V. Y., IZMER, A., VAN DEN HAUTE, P., VANHAECKE, F. & ELBURG, M.A. 2011. Tectonic history of the Kyrgyz South Tien Shan (Atbashi-Inylchek) suture zone: The role of inherited structures during deformation-propagation. *Tectonics*, **30**, TC6016, doi:10.1029/2011TC002949.

GOTFRID, P.Y. & PUCHKOV, A.I. 1980. Direction of exploration for oil and gas structures in northwest Fergana. *Neftegazovaya Geologiya I Geofizika*, **10**, pp. 4-6, (in Russian).

GRAHAM, S.A., CHAMBERLAIN, C.P., YUE, Y.J., RITTS, B.D., HANSON, A.D., HORTON, T.W., WALDBAUER, J.R., POAGE, M.A. & FENG, X. 2005. Stable Isotope Records of Cenozoic Climate and Topography, Tibetan Plateau and Tarim Basin. *American Journal of Science*, **305**, 101-118.

GREEN, P. F. 1981. A new look at statistics in fission track dating, *Nuclear Tracks*, **5**, 77 – 86.

GREEN, P.F., DUDDY, I.R., LASLETT, G.M., HEGARTY, K.A., GLEADOW, A.J.W. & LOVERING, J.F. 1989. Thermal annealing of fission tracks in apatite, 4, Quantitative modeling techniques and extension to geological timescales, *Chemical Geology (Isotope Geosci. Sec.)*, **79**, 155-182, doi: 10.1016/0168-9622(89)90018-3.

GREENE, T.J, CARROLL, A.R., HENDRIX, M.S., KEMING, C. & XIAO MING, Z. 2000. Sedimentology and paleogeography of the Middle Jurassic Qiketai formation, Turpan-Hami Basin, Northwest China. *In:* GIERLOWSKI-KORDESCH, E.H. & KELTS, K.R. (eds), *Lake Basins through space and time: AAPG Studies in Geology,* **46**, 141-152.

GREWINGK, C. 1853. Die Geognostischen Und Orographischen Verhaeltnisse Des Noerdlichen Persiens. In: *Verhandlungen Der R.K Mineralogischen Gesellschaft,* **1852- 1853**, 97-245, St. Petersburg.

GRIDNEV, N.I. 1971. *Cenozoic molasse of Fergana depression*. Tashkent. 250 pp. (in Russian)

GUENTHNER, W. R., REINERS, P. W., KETCHAM, R. A., NASDALA, L. & GIESTER G. 2013. Helium diffusion in natural zircon: radiation damage, anisotropy, and the interpretation of zircon (U-Th)/He thermochronology, *American Journal of Science*, **313(3),** 145-198, doi: 10.2475/03.2013.01.

HAMBURGER, M. W., SAREWITZ, D. R., PAVLIS, T. L. & POPANDOPULO, G. A. 1992. Structural and seismic evidence for intracontinental subduction in the Peter the First Range, central Asia, *Geological Society of America Bulletin*, **104**, 397 – 408

HAO, Y., GUAN, S., YE, L., HUANG, Y., ZHOU, Y. & GUAN, S. 2002. Neogene stratigraphy and paleogeography in the western Tarim basin. *Acta Geol. Sinica,* **76(3)**, 289–298.

HAUSBURG, M., RICHLING, S., VOIGT, T. & KLOCKE, M. 2012. Facies and provenance of syntectonic Neogene deposits of the eastern Alai Range (southwestern Tien Shan, Kyrgyzstan). In*: International Conference of the Geologische Vereinigung and SEDIMENT*, Abstract Volume, p 114.

HEGNER, E., KLEMD, R., KRÖNER, A., CORSINI, M., ALEXEIEV, D.V., IACCHERI, L.M., ZACK, T., DULSKI, P., XIA, X. & WINDLEY, B.F. 2010. Mineral ages and P-T conditions of Late Paleozoic high-pressure eclogite and provenance of mélange sediments in the South Tianshan orogen of Kyrgyzstan. *American Journal of Science*, **310**, 916-950.

HENDRIX, M.S., GRAHAM, S.A., CARROLL, A.R., SOBEL, E.R., MCKNIGHT, C.L., SCHULEIN, B.J. & WANG, Z. 1992. Sedimentary record and climatic implications of recurrent deformation in the Tian Shan: Evidence from Mesozoic strata of the north Tarim, south Junggar, and Turpan basins, Northwest China. *Geological Society of America Bulletin*, ***104*(1)**, 53-79, doi: 10.1130/0016-7606(1992)104<0053:SRACIO> 2.3.CO;2.

HENDRIX, M.S., DUMITRU, T.A. & GRAHAM S.A. 1994. Late Oligocene-Early Miocene unroofing in the Chinese Tian Shan: An early effect of the India-Asia collision. *Geology*, **22**, 487-490, doi: 10.1130/0091-7613(1994)022<0487:LOEMUI> 2.3.CO;2.

HENDRIX, M. S. 2000. Evolution of Mesozoic sandstone compositions, southern Junggar, northern Tarim, and western Turpan basins, northwestern China: A detrital record of the ancestral Tian Shan, *Journal of Sedimentary Research*, **70**, 520–532, doi:10.1306/2DC40924-0E47-11D7-8643000102C1865D.

HEERMANCE, R. V., CHEN, J., BURBANK, D.W. & WANG, C. 2007. Chronology and tectonic controls of Late Tertiary deposition in the southwestern Tian Shan foreland, NW China. *Basin Research*, **19**, 599–632, doi: 10.1111/j.1365-2117.2007.00339.x

HEERMANCE, R.V., CHEN, J., BURBANK, D.W. & MIAO, J., 2008. Temporal constraints and pulsed Late Cenozoic deformation during the structural disruption of the active Kashi foreland, northwest China. *Tectonics*, **27**, TC6012, doi: 10.1029/2007TC002226.

HAUSBURG, M., RICHLING, S., VOIGT T. & KLOCKE, M. 2012. Facies and provenance of syntectonic Neogene deposits of the eastern Alai Range (southwestern Tien Shan, Kyrgyzstan). In: *International Conference of the Geologische Vereinigung and SEDIMENT*, Abstract Volume, Hamburg, Germany, 114.

HENDRIX, M.S., GRAHAM, S.A., CARROLL, A.R., SOBEL, E.R., MCKNIGHT, C.L., SCHULEIN, B.J. & WANG, Z. 1992. Sedimentary record and climatic implications of recurrent deformation in the Tian Shan: Evidence from Mesozoic strata of the north Tarim, south Junggar, and Turpan basins, Northwest China, *Geological Society of America Bulletin*, 104(1), 53-79, doi: 10.1130/0016-7606(1992)104<0053:SRACIO> 2.3.CO;2.

HILLEY, G., BLISNIUK, P. M. & STRECKER, M. R. 2005. Mechanics and erosion of basement-cored uplift provinces, *Journal of Geophysical Research*, *110*, B12409, doi:10.1029/2005JB003704.

HOLDSWORTH, R. E., BUTLER, C. A. & ROBERTS, A. M. 1997. The recognition of reactivation during continental deformation, *Journal of the Geological Society*, **154(1)**, 73-78, doi: 10.1144/gsjgs.154.1.0073.

HORTON, B.K., SAYLOR, J.E., NIE, J., MORA, A., PARRA, M., REYES-HARKER, A., & STOCKLI, D.F. 2010. Linking sedimentation in the northern Andes to basement configuration, Mesozoic extension, and Cenozoic shortening: Evidence from detrital zircon U-Pb ages in the Eastern Cordillera of Colombia. *Geological Society of America Bulletin*, **122**, 1423–1442, doi:10.1130/B30118.1.

HURFORD, A.J. & GREEN, P.F. 1983. The zeta age calibration of fission track dating. *Chemical Geology*, 41, 285-317.

JACKSON, S.E., PEARSON, N.J., GRIFFIN W.L. & BELOUSOVA, E.A. 2004. The application of laser ablation-inductively coupled plasma-mass spectrometry to in situ U–Pb zircon geochronology. *Chemical Geology,* **211**, 47–69.

JOHNSSON, M.J., STALLARD, R.F. & LUNDBERG, N. 1991. Controls on the composition of fluvial sands from a tropical weathering environment: Sands of the Orinoco river drainage-basin, Venezuela and Colombia. *Geol. Soc. Am. Bull.*, **103**, 1622-1647.

JOLIVET, M., BRUNEL, M. SEWARD, D. XU, Z. YANG, J. ROGER, F. TAPPONNIER, P. MALAVIEILLE, J. ARNAUD, N. & WU, C. 2001. Mesozoic and Cenozoic tectonics of the northern edge of the Tibetan plateau: Fission-track constraints, *Tectonophysics*, **343**(1–2), 111–134.

JOLIVET, M., DOMINGUEZ, S., CHARREAU, J., CHEN, Y., LI, Y. & WANG Q. 2010. Mesozoic and Cenozoic tectonic history of the central Chinese Tian Shan: Reactivated tectonic structures and active deformation. *Tectonics*, **29**, TC6019, doi:10.1029/2010TC002712.

JOLIVET, M. 2015. Mesozoic tectonic and topographic evolution of Central Asia and Tibet: a preliminary synthesis. *In*: BRUNET, M.-F., MCCANN, T. & SOBEL, E. R. (eds) *Geological Evolution of Central Asian Basins and the Western Tien Shan Range*. Geological Society, London, Special Publications, 427, doi.org/10.1144/SP427.2

JONCKHEERE, R., ENKELMANN, E., MIN, M., TRAUTMANN, C. & RATSCHBACHER L. 2007. Confined fission tracks in ion-irradiated and step-etched prismatic sections of Durango apatite. *Chemical Geology*, **242(1)**, 202-217, doi: 10.1016/j.chemgeo.2007.03.015.

JORDAN, T.E., & ALLMENDINGER, R.W. 1986. The Sierras Pampeanas of Argentina, a modern analogue of Rocky Mountain foreland deformation, *American Journal of Earth Sciences*, **286**, 737-764, doi: 10.2475/ajs.286.10.737.

JORDAN, T.E., ALLMENDINGER, R.W., DAMANTI, J.F., & DRAKE, R.E. 1993. Chronology of motion in a complete thrust belt: The Precordillera, 30–31°S, Andes Mountains. *The Journal of Geology*, **101**, 135–156, doi:10.1086/648213.

KALMETIEVA Z.A., MIKOLAICHUK A.V., MOLDOBEKOV B.D., MELESHKO A.V., JANTAEV M.M. & ZUBOVICH A.V. 2009. *Atlas of earthquakes in Kyrgyzstan*. ECHO, UNISDR, and CAIAG, Bishkek, p. 233.

KETCHAM, R.A. 2005. HeFTy: Forward and inverse modeling thermochronometer systems. *In:* REINERS, P.W. & EHLERS, T.A. (eds) *Low-temperature thermochronology: Techniques*, *interpretations*, *and applications*, Reviews in Mineralogy and Geochemistry, **58**, 596-597, The Mineralogical Society of America, Chantilly, VA, USA.

KETCHAM, R.A., DONELICK, R.A. & CARLSON, W.D. 1999. Variability of apatite fission-track annealing kinetics: III. Extrapolation to geological time scales. *American Mineralogist*, ***84*(9)**, 1235-1255.

KETCHAM, R.A., CARTER, A.C., DONELICK, R.A., BARBARAND, J. & HURFORD, A.J. 2007. Improved modeling of fission-track annealing in apatite, *American Mineralogist*, **92**, 799-810, doi: 10.2138/am.2007.2281.

KHODJAEV, A.R. 1969. *Geology and oil-gas bearing of Northern Fergana*. Tashkent.187 pp. (in Russian)

KLOCKE, M., VOIGT, T., KLEY, J., PFEIFER, S., ROCKTÄSCHEL, T., KEIL, S. & GAUPP, R. 2015. Cenozoic evolution of the Pamir and Tien Shan Mountains reflected in syntectonic deposits of the Tajik Basin. *In*: BRUNET, M.-F., MCCANN, T. & SOBEL, E. R. (eds) *Geological Evolution of Central Asian Basins and the Western Tien Shan Range*. Geological Society, London, Special Publications, 427, http://doi.org/10.1144/SP427.7

KONOPELKO, D., BISKE, G., SELTMANN, R., EKLUND O. & BELYATSKY, B. 2007. Hercynian post-collisional A-type granites of the Kokshaal Range, Southern Tien Shan, Kyrgyzstan. *Lithos,* **97**, 140–160.

KONOPELKO, D., SELTMANN, R., APAYAROV, F., BELOUSOVA, E., IZOKH, A., & LEPEKHINA, E. 2013. U-Pb-Hf zircon study of two mylonitic granite complexes in the Talas-Fergana fault zone, Kyrgyzstan, and Ar-Ar age of deformations along the fault. *Journal of Asian Earth Sciences*, **73**, 334–346, doi:10.1016/j.jseaes.2013.04.046

KRAATZ, B.P. & GEISLER, J.H. 2010 Eocene- Oligocene Transition in Central Asia and Its Effects on Mammalian Evolution. *Geology*, **38**, 111-114.

KRÖNER, A., ALEXEIEV, D.V., ROJAS-AGRAMONTE, Y., HEGNER, E., WONG, J., XIA, X., BELOUSOVA, E., MIKOLAICHUK, A., SELTMANN, R., LIU, D.Y. & KISELEV, V.V. 2013. Mesoproterozoic (Grenville-age) terranes in the Kyrgyz North Tianshan: Zircon ages and Nd-Hf isotopic constraints on the origin and evolution of basement blocks in the southern Central Asian Orogen. *Gondwana Research*, **23**, 272-295, doi:10.1016/j.gr.2012.05.004

LESIK, O.M. & MIKOLAICHUK, A.V. 2001. Deep structure of the Turkestan paleo-ocean suture. *Russian Geology and Geophysics*, **42**, 10, 1386-1392.

LI, T., CHEN, J., THOMPSON, J., BURBANK, D.W. & XIAO, W. 2012. Equivalency of geologic and geodetic rates in contractional orogens: New insights from the Pamir Frontal Thrust. *Geophysical Research Letters*, **39**, L15305, doi:10.1029/2012GL051782

LIU, S., QIU, B., YIN, H., LI, J., ZHAI, S. & LI, W. 2005. Structural characteristics of Wupaer Thrust belts in the foreland of west Kunlun Mountain, *Acta Pet. Sin*., 26(6), 16–19.

LOURY, C., ROLLAND, Y., GUILLOT, S., MIKOLAICHUK, A. V., LANARI, P., BRUGUIER, O. & BOSCH, D. 2015. Crustal-scale structure of South Tien Shan: implications for subduction polarity and Cenozoic reactivation. *In*: BRUNET, M.-F., MCCANN, T. & SOBEL, E. R. (eds) *Geological Evolution of Central Asian Basins and the Western Tien Shan Range*. Geological Society, London, Special Publications, 427, doi.org/10.1144/SP427.4

LUDWIG, K. 2003. *User's manual for Isoplot 3.00: a geochronological toolkit for Microsoft Excel*, BerkeleyGeochronology Center Special Publication, 4, 70.

MACAULAY, E. A., SOBEL, E.R., MIKOLAICHUK, A., LANDGRAF, A., KOHN, B. & STUART, F. 2013. Thermochronologic insight into late Cenozoic deformation in the basement cored Terskey Range, Kyrgyz Tien Shan. *Tectonics*, **32(3)**, 487-500. doi: 10.1002/tect.20040.

MACAULAY, E. A., SOBEL, E.R., MIKOLAICHUK, A., KOHN, B. & STUART, F. 2014. Cenozoic deformation and exhumation history of the Central Kyrgyz Tien Shan. *Tectonics*, doi: 10.1002/2013TC003376.

MACAULAY, E.A., SOBEL, E.R., MIKOLAICHUK, A., WACK, M, GILDER, S.A., MULCH, A. FORTUNA, A.B., HYNEK, S. & APAYAROV, F. 2015. The sedimentary record of the Issyk Kul basin, Kyrgyzstan: climatic and tectonic inferences, *Basin Research*, doi: 10.1111/bre.12098

MAKAROV, V.I. 1977. *New Tectonic Structure of the Central Tien Shan*, 172 pp., Nauka, Moscow.

MAKSUMOVA, R. A., DJENCHURAEVA, A. V. & BEREZANSKII, A. V. 2001. Structure and evolution of the Tien Shan nappe-folded orogen. *Russian Geology and Geophysics*, **42** (10), 1367-1374.

MCCLAY, K. & BONORA, M. 2001. Analog models of restraining stepovers in strike-slip fault systems. AAPG Bulletin, **85**, 2, 233–260.

MENG, Q.-R. 1997. Tectonic evolution of southwest Tarim basin, postdoctoral research report, 129 pp., Inst. of Geophys., Chin. Acad. Of Sci., Beijing.

MIALL, A.D. 1996. *The Geology of Fluvial Deposits: Sedimentary Facies, Basin Analysis, and Petroleum Geology*. Berlin, Springer-Verlag, 582 p.

MIKOLAICHUK, A.V., F.KH. APAYAROV, T. YU. VOROB´EV AND D.A. CHERTKOV (2008), Quaternary removed geological map of the Inner Tien-Shan (Kyrgyzstan). 1:200,000. SNSF, Zurich, Switzerland.

MOLNAR, P & TAPPONNIER, P. 1975. Cenozoic Tectonics of Asia: Effects of a Continental Collision. *Science*, **189**, 4201,419-426.

LEI, J. 2011. Seismic tomographic imaging of the crust and upper mantle under the central and western Tien Shan orogenic belt. *Journal of Geophysical Research*, **116**, B09305, doi:10.1029/2010JB008000

NEELY, T. G. & ERSLEV, E. A. 2009. The interplay of fold mechanisms and basement weaknesses at the transition between Laramide basement-involved arches, north-central Wyoming, USA, *Journal of Structural Geology*, **31(9),** 1012-1027, doi:1025 10.1016/j.jsg.2009.03.008.

NIEMI, N. A., BUSCHER, J. T., SPOTILA, J. A., HOUSE, M. A. & KELLEY, S. A. 2013. Insights from low-temperature thermochronometry into transpressional deformation and crustal exhumation along the San Andreas fault in the western Transverse Ranges, California. *Tectonics*, **32**, 1602–1622, doi:10.1002/2013TC003377.

POPOV, S., RÖGL, F., ROZANOV, A.Y., STEININGER, F.F., SCHERBA, I.G. & KOVAC, M. 2004. Lithological- Paleogeographic Maps of Paratethys 10 Maps Late Eocene to Pliocene. *Courier Forschungsinstitut Senckenberg*, **250**, 1-46.

READING, H.G. & COLLINSON, J.D. 1996. Clastic Coasts. In: *Sedimentary Environments: Processes, Facies and Stratigraphy* (Ed. H.G. Reading), 3rd edn, pp. 154–231. Blackwell Science, Oxford.

REINERS, P. W. & FARLEY, K. A. 2001. Influence of crystal size on apatite (U-Th)/He thermochronology: an example from the Bighorn Mountains, Wyoming, *Earth and Planetary Science Letters*, **188(3),** 413-420, doi: 10.1016/S0012-821X(01)00341-7.

REINERS, P. W., SPELL, T. L., NICOLESCU, S. & ZANETTI, K. A. 2004. Zircon (U-Th)/He thermochronometry: He diffusion and comparisons with 40Ar/39Ar dating, *Geochimica et Cosmochimica Acta*, **68(8)**, 1857-1887, doi:10.1016/j.gca.2003.10.021.

ROBINSON, D.M., DECELLES, P.G., GARZIONE, C.N., PEARSON, O.N., HARRIOSN, T.M. & CATLOS, E.J. 2003. Kinematic model for the Main Central thrust in Nepal. *Geology*, **31 (4)**, 359-362. doi:10.1130/0091-7613(2003)031<0359:KMFTMC>2.0.CO

ROLLAND, Y., ALEXEIEV, D.V., KRÖNER, A., CORSINI, M., LOURY, CH. & MONIÉ P. 2013. Late Palaeozoic to Mesozoic kinematic history of Talas-Ferghana strike-slip Fault (Kyrgyz West Tianshan) as revealed by 40Ar/39Ar dating of syn-kinematic phengite. *Journal of Asian Earth Sciences*, **67-68**, 76-92.

RUHIN, L.B. & RUHINA, E.V. 1961. *Cretaceous sediments of Fergana basin (Stratigraphy and Lithology)*. Leningrad University. 163 pp. (in Russian).

SCHMALHOLZ, M., 2004. *The amalgamation of the Pamirs and their subsequent evolution in the far field of the India–Asia collision*, Tübinger Geowissenschaftliche Arbeiten, Reihe A 71. Dr.rer.nat. Thesis, Universitaet Tübingen, Tübingen, 103 pp.

SCHMIDT, J., HACKER, B.R., RATSCHBACHER, L., STÜBNER, K., STEARNS, M., KYLANDER-CLARK, A., COTTLE, J.M., ALEXANDER, A., WEBB, G., GEHRELS, G. & MINAEV, V. 2011. Cenozoic deep crust in the Pamir. *Earth and Planetary Science Letters,* **312**, 411–421.

SCHURR, B., RATSCHBACHER, L., SIPPL, C., GLOAGUEN, R., YUAN, X. & MECHIE ,J. 2014 Seismotectonics of the Pamir, *Tectonics*, **33**, 1501-1518, doi: 10.1002/2014TC00357.

SEARLE, M. P., WINDLEY, B.F., COWARD, M.P., REX, A.J., REX, D., TINGDONG, L., XUCHANG, X., JAN, M.Q., THAKUR, V.C. & KUMAR, S. 1987. The closing of Tethys and the tectonics of the Himalayas, *Geological Society of America Bulletin*, **98**, 678 – 701.

SELANDER, J., OSKIN, M., ORMUKOV, C. & ABDRAKHMATOV, K. 2012. Inherited strike-slip faults as an origin for basement-cored uplifts: Example of the Kungey and Zailiskey ranges, northern Tian Shan. *Tectonics*, **31**, TC4026, doi:10.1029/2011TC003002.

SELIVERSTOV, K.V. & GHES, M.D. 2001. Petrochemical features of magmatites and major kinematic parameters of middle Carboniferous–early Permian subduction of the Turkestan paleo-ocean (Tien Shan, Northern Ferghana). *Russian Geology and Geophysics,* **42 (10)**, 1393-1397.

SELTMANN, R., KONOPELKO, D., BISKE, G., DIVAEV, F. & SERGEEV, S. 2011. Hercynian postcollisional magmatism in the context of Paleozoic magmatic evolution of the Tien Shan orogenic belt. *Journal of Asian Earth Sciences*, **42**, 821–838.

ŞENGÖR, A. M. C., NATAL'IN, B. A. & BURTMAN, V. S. 1993. Evolution of the Altaid tectonic collage and Palaezoic crustal growth in Eurasia. *Nature*, **364**, 299-307.

SIDORENKO, A. V. 1972. *Geology of the USSR*, Volume XXIII. Moscow.719 pp. (in Russian)

SIMM, R. & BACON, M. 2014. *Seismic Amplitude: an interpreter handbook*. pp 271. Cambridge University Press, Cambridge.

SIPPL, C., SCHURR, B., YUAN, X., MECHIE, J., SCHNEIDER, F.M., GADOEV, M., ORUNBAEV, S., OIMAHMADOV, I., HABERLAND, C., ABDYBACHAEV, U., MINAEV, V., NEGMATULLAEV, S. & RADJABOV N. 2013. Geometry of the Pamir-Hindu Kush intermediate-depth earthquake zone from local seismic data. *Journal of Geophysical Research - Solid Earth*, **118**, 1-20, doi:10.1002/jgrb.50128.

SMIT, J.H.W., CLOETINGH, S.A.P.L., BUROV, E., TESAURO, M., SOKOUTIS, D. & KABAN, M. 2013. Interference of lithospheric folding in western Central Asia by simultaneous Indian and Arabian plate indentation. *Tectonophysics*, **602**, 176-193, doi.org/10.1016/j.tecto.2012.10.032

SOBEL, E.R. 1995. *Basin analysis and apatite fission track thermochronology of the Jurassic – Paleogene southwestern Tarim Basin, NW China*, Ph.D. thesis, Stanford Univ., Calif.

SOBEL, E. R. 1999. Basin Analysis of the Jurassic - Lower Cretaceous southwest Tarim basin, NW China. *Geological Society of America Bulletin*, **111 (5)**, 709-724.

SOBEL, E. R. & DUMITRU, T. A. 1997. Thrusting and exhumation around the margins of the western Tarim basin during the India-Asia collision. *Journal of Geophysical Research*, **102(B3)**, 5043-5063, doi: 10.1029/96JB03267.

SOBEL, E. R**.** & STRECKER, M. R. 2003. Uplift, exhumation, and precipitation: Tectonic and climatic control of Late Cenozoic landscape evolution in the northern Sierras Pampeanas, Argentina. *Basin Research*, **15**, 21 p. doi: 10.1046/j.1365-2117.2003.00214.x.

SOBEL, E.R. & SEWARD, D. 2010. Influence of etching conditions on apatite fission-track etch pit diameter. *Chemical Geology*, **271**, 59-69, doi:10.1016/j.chemgeo.2009.12.012.

SOBEL, E.R., CHEN, J. & HEERMANCE, R.V. 2006a. Late Oligocene - Early Miocene initiation of shortening in the Southwestern Chinese Tian Shan: Implications for Neogene shortening rate variations. *Earth and Planetary Science Letters*, **247**, 70-81, doi: 10.1016/j.epsl.2006.03.048.

SOBEL, E. R., OSKIN, M., BURBANK, D., & MIKOLAICHUK, A. 2006b. Exhumation of basement-cored uplifts: Example of the Kyrgyz Range quantified with apatite fission track thermochronology. *Tectonics*, **25**, 17, TC2008, doi:10.1029/2005TC001809.

SOBEL, E.R., CHEN, J., SCHOENBOHM, L.M., THIEDE, R., STOCKLI, D.F., SUDO, M. & STRECKER M.R. 2013. Oceanic-style subduction controls late Cenozoic deformation of the Northern Pamir orogen. *Earth and Planetary Science Letters*, **363**, 204-218, doi:10.1016/j.epsl.2012.12.009.

SOLOMOVICH, L.I. & TRIFONOV, B.A. 2002. Postcollisional granites in the South Tien Shan Variscan Collisional Belt, Kyrgyzstan. *Journal of Asian Earth Sciences,* **21**, 7–21.

SPOTILA, J.A., NIEMI, N., BRADY, R., HOUSE, M., BUSCHER, J. & OSKIN, M. 2007. Long-term continental deformation associated with transpressive plate motion: The San Andreas fault. *Geology*, **35**, 967-970, doi:10.1130/G23816A.1.

STRECKER, M.R., HILLEY, G.E., ARROWSMITH J.R. & COUTAND, I. 2003. Differential structural and geomorphic mountain-front evolution in an active continental collision zone: the northwest Pamir, southern Kyrgyzstan. *Geologial Society of America Bulletin,* **115**, 166–181.

SUN, J., LI, Y., ZHANG, Z. & FU, B. 2009. Magnetostratigraphic data on Neogene growth folding in the foreland basin of the southern Tianshan Mountains. *Geology*, **37**, 1051-1054, doi: 10.1130/G30278A.1.

SUN, X. & WANG, P. 2005. How Old Is the Asian Monsoon System? Palaeobotanical Records from China. *Palaeogeography, Palaeoclimatology, Palaeoecology*, **222**, 181-222.

TANG, T., YANG, H., LAN, X., YU, C., XUE, Y., ZHANG, Y., HU, L., ZHONG, S. & WEI, J. 1989. Marine Late Cretaceous and Early Tertiary Stratigraphy and Petroleum Geology in *Western Tarim Basin, China. Science Press*, Beijing.

TANG, T., XUE, Y. & YU, C. 1992. Characteristics and Sedimentary Environments of the Late Cretaceous to Early Tertiary Marine Strata in the Western Tarim, 138 pp., China, Sci. Press, Beijing.

TESHEBAEVA, K., SUDHAUS, H., ECHTLER, H., SCHURR B. & ROESSNER, S. 2014. Strain partitioning at the eastern Pamir-Alai revealed through SAR data analysis of the 2008 Nura earthquake, *Geophysical Journal International*, **198**, 760-774. doi: 10.1093/gji/ggu158.

THIEDE, R.C., SOBEL, E.R., CHEN, J., SCHOENBOHM, L.M., STOCKLI, D.F., SUDO, M. & STRECKER, M. R. 2013. Late Cenozoic extension and crustal doming in the India-Eurasia collision zone: New thermochronologic constraints from the NE Chinese Pamir, *Tectonics*, **32/3**, 763-779 , doi: 10.1002/tect.20050.

THOMAS, J., PERROUD, H., COBBOLD, P.R., BAZHENOV, M.L., BURTMAN, V.S., CHAUVIN, A., & SADYBAKASOV, E. 1993. A paleomagnetic study of Tertiary formations from the Kyrgyz Tien-Shan and its tectonic implications. *Journal of Geophysical Research*, **98**, 9571-9589.

THOMPSON, S., WELDON, R., RUBIN, C., ABDRAKHMATOV, K., MOLNAR, P., & BERGER G. 2002. Late Quaternary slip rates across the central Tien Shan, Kyrgyzstan, central Asia, *Journal of Geophysical Research*, **107**, ETG 7-1–ETG 7-32.

THOMPSON, J.A., BURBANK, D.W., LI, T., CHEN, J. & BOOKHAGEN, B. 2015. Late Miocene northward propagation of the northeast Pamir thrust system, northwest China. *Tectonics*, **34**, 510–534, doi:10.1002/2014TC003690.

TRIFONOV,V. G., MAKAROV,V. I. & SKOBELEV, S. F. 1992. The Talas-Ferghana active right-lateral fault. *Annales Tectonicae*, VI, suppl., 224–237.

TYMPEL, J.G., 2015. *Numerical modeling of the Cenozoic Pamir-Tien Shan orogeny*. Doctoral thesis, Univ. Potsdam.

UBA, C.E., HEUBECK, C., & HULKA, C., 2005, Facies analysis and basin architecture of the Neogene Subandean synorogenic wedge, southern Bolivia. *Sedimentary Geology*, **180**, 91–123, doi:10.1016/j.sedgeo .2005.06.013.

VERZILIN, N. N. 1968. On the problem of the Talas-Ferghana strike-slip fault, in OGNEV, V. N. (ed), Problems of regional geology: Leningrad, Leningrad Univ., p. 67–70 (in Russian).

VIALOV, O.S. 1948. *Palaeogenic Ostreids from Tajik Depression*. Tr. VNIGRI, n.s., Leningrad-Moskva.

VLASOV, N.G., Dyakov, Y.A., & Cherev, E.S. (eds), 1991, *Geological map of the Tajik SSR and adjacent territories*: 1:500000. Vsesojuznoi Geol. Inst. Leningrad, Saint Petersburg.

VOYTENKO V.N. & KHUDOLEY, A.K. 2012. Structural evolution of metamorphic rocks in the Talas Alatau, Tien Shan, Central Asia: Implication for early stages of the Talas-Ferghana Fault. *Comptes Rendus Geoscience*, **344**, 138–148, doi:10.1016/j.crte.2011.11.004.

VYALOV, O.S. 1937. Sur La Classification des Ostreides Et Leur Valeur Stratigraphique, Intern. Congr. Zool. Lisbonne, 1627-1638.

WACK, M. R., GILDER, S. A., MACAULAY, E. A., SOBEL, E. R., CHARREAU, J.& MIKOLAICHUK, A. 2014. Cenozoic magnetostratigraphy and rock magnetism of the southern Issyk-Kul basin, Kyrgyzstan. *Tectonophysics,* doi.org/10.1016/j.tecto.2014.03.030.

WANG, B., FAURE, M., CLUZEL, D., SHU, L., CHARVET, J., MEFFRE, S., & MA, Q. 2006a. Late Paleozoic tectonic evolution of the northern west Chinese Tianshan belt. *Geodinamica Acta*, **19(3-4)**, 237-247, doi: 10.3166/ga.19.237-247.

WANG, Y., LI, D., XIAO, X., CHI, Z., MIN, L., WANG, J. & WANG Y. 2006b. Late Cenozoic tectonic movement in the front of the west Kunlun mountains and uplift of the northwestern margin of the Qinghai-Tibetan plateau. *Geol. China*, **33(1)**, 41–47.

WANG, B., SHU, L., FAURE, M., JAHN, B.-M., CLUZEL, D.,CHARVET, J., CHUNG, S.-L., MEFFRE, S. 2011. Paleozoic tectonics of the southern Chinese Tianshan: Insights from structural, chronological and geochemical studies of the Heiyingshan ophiolitic mélange (NW China). *Tectonophysics,* **497**, 85–104.

WEI, H.-H., MENG, Q.-R., DING, L. & LI, Z.-Y. 2013. Tertiary evolution of the western Tarim basin, northwest China: A tectono-sedimentary response to northward indentation of the Pamir salient. *Tectonics*, **32**, 558–575, doi:10.1002/tect.20046.

WEI, Y. FAN, Z.F., ZHENG, J.ZH., YIN, J.Q., ZHANG, M.J., SHENG, X.F., GUO, J.J., & LI, Q.Y. 2012. Characteristics of strike-slip inversion structures of the Karatau fault and their petroleum geological significances in the South Turgay Basin, Kazakhstan. *Petroleum Science,* **9 (4)**, 444-454, doi: 10.1007/s12182-012-0228-3.

WINDLEY, B. F., ALLEN, M. B. ZHANG, C. ZHAO, Z. Y. & WANG G. R. 1990. Paleozoic accretion and Cenozoic redeformation of the Chinese Tien Shan range, central Asia, *Geology*, **18(2)**, 128-131, doi: 10.1130/0091-(1990)018<0128:PAACRO>2.3.CO;2.

WINDLEY, B.F., ALEXEIEV, D., XIAO, W., KRÖNER, A. & BADARCH, G. 2007. Tectonic Models for Accretion of the Central Asian Orogenic Belt. *Journal of the Geological Society,* **164**, 31–47.

WOLF, R. A., FARLEY, K. A. & KASS, D. M. 1998. Modeling of the temperature sensitivity of the apatite (U-Th)/He thermochronometer, *Chemical Geology*, **148(1)**, 105-114, doi: 10.1016/S0009-2541(98)00024-2.

WOLFE, M. R., & STOCKLI D. F. 2010. Zircon (U-Th)/He thermochronometry in the KTB drill hole, Germany, and its implications for bulk He diffusion kinetics in zircon, *Earth and Planetary Science Letters*, **295(1)**, 69-82, doi:10.1016/j.epsl.2010.03.025.

XBGMR (Xinjiang Bureau of Geology and Mineral Resources), 1993. *Regional geology of Xinjiang Uygur autonomous region*. Geological Memoirs. Geological Publishing House, Beijing, scale 1:1500000, 841 pp.

YANG, Y. & LIU, M. 2002. Cenozoic deformation of the Tarim plate and the implications for mountain building in the Tibetan Plateau and the Tian Shan. *Tectonics*, **21**. doi:10.1029/2001TC001300.

YANG, W., JOLIVET, M., DUPONT-NIVET G. & GUO, Z. 2014. Mesozoic – Cenozoic tectonic evolution of southwestern Tian Shan: Evidence from detrital zircon U/Pb and apatite fission track ages of the Ulugqat area, Northwest China. *Gondwana Research*, **26**, 986-1008, doi: 10.1016/j.gr.2013.07.020.

YANG, W., DUPONT-NIVET, G. JOLIVET, M, GUO, Z., BOUGEOIS, L., BOSBOOM, R., ZHANG, Z., ZHU, B. & HEILBRONN, G. 2015. Magnetostratigraphic record of the early evolution of the southwestern Tian Shan foreland basin (Ulugqat area), interactions with Pamir indentation and India–Asia collision. *Tectonophysics*, **644-645**, 122-137, doi.org/10.1016/j.tecto.2015.01.003

YIN, A., NIE, S., CRAIG, P., HARRISON, T. M., RYERSON, F. J., XIANGLIN, Q. & GENG, Y. 1998. Late Cenozoic tectonic evolution of the southern Chinese Tian Shan. *Tectonics*, **17(1)**, 1-27, doi: 10.1029/97TC03140.

YIN, A., RUMELHART, P.E., BUTLER, R., COWGILL, E., HARRISON, T. M., FOSTER, D. A., INGERSOLL, R.V., QING, Z., XIAN-QIANG, Z., XIAO-FENG, W., HANSON A. & RAZA A. 2002., Tectonic history of the Altyn Tagh fault system in northern Tibet inferred from Cenozoic sedimentation. *Geological Society of America Bulletin*, **114(10)**, 1257-1295, doi: 10.1130/0016-7606(2002)114<1257:THOTAT>2.0.CO;2.

XIAO, W., HAN, C., YUAN, C., SUN, M., LIN, S., CHEN, H., LI, Z., LI, J. & SUN, S. 2008. Middle Cambrian to Permian subduction-related accretionary orogenesis of Northern Xinjiang, NW China: implications for the tectonic evolution of central Asia. *Journal of Asian Earth Sciences*, **32(2**), 102-117.

ZHOU, Y., QIU, D. & WANG, Y. 1984. The Petroleum potential of Miocene Series in the southwest part of Tarim basin. *Oil Gas Geol*., **5(3)**, 261–270.

ZUBOVICH, A.V., X.Q. WANG, Y.G. SCHERBA, G.G. SCHELOCHKOV, R. REILINGER, C. REIGBER, O.I. MOSIENKO, P. MOLNAR, W. MICHAJLJOW, V.I. MAKAROV, J. LI, S.I. KUZIKOV, T.A. HERRING, M.W. HAMBURGER, B.H. HAGER, Y.M. DANG, V.D. BRAGIN, & R.T. BEISENBAEV 2010. GPS velocity field for the Tien Shan and surrounding regions. *Tectonics*, **29**, TC6014, doi:10.1029/2010TC002772.

ZUBOVICH, A.V., SCHÖNE, T., METZGER, S., MOSIENKO,O., MUKHAMEDIEV,SH., SHARSHEBAEV,A. & ZECH, C. 2016. Tectonic interaction between the Pamir and Tien Shan observed by GPS. *Tectonics*, **35**, doi: 10.1002/2015TC004055

Appendix 1

Additional data for Chapter 2

In this appendix the methodology and procedures involved in thermochronological analysis are outlined. Full Apatite fission track (AFT) data are presented in Tables A1.1.

AFT Methodology

Conventional mineral separation techniques were used as described in *Sobel & Strecker* (2003). Apatite grains were etched in 5.5 mol Nitric acid for 20 seconds at 21˚C. Samples were analyzed with a Leica DMRM microscope with drawing tube located above a digitizing tablet and a Kinetek computer-controlled stage driven by the FTStage program (*Dumitru*, 1993). Analysis was performed with reflected and transmitted light at 1250X magnification. Samples were irradiated at Oregon State University. Following irradiation, the mica external detectors were etched with 21˚C, 40% hydrofluoric acid for 45 minutes. The pooled age (central age) is reported for samples with P(χ^2) greater than (less than) 5% as they pass (fail) the χ^2 test (*Galbraith*, 1981; *Green*, 1981).

Kinetic properties where measured for every grain counted and/or containing measured horizontal confined fission track by making at least four D_{par} measurements (*Donelick* et al., 2005), that were subsequently averaged and corrected following *Sobel & Seward* (2010). Most AFT Ages are based on 20 dated grains, and all of them are based on >17 grains. Age errors are presented as one sigma, calculated using the zeta calibration method (*Hurford & Green*, 1983). Statistics were calculated using the MacTrackX software. As many horizontal confined fission tracks as possible where measured with the goal of acquire 100 lengths. Only tracks- in-tracks were measured. In 9 samples length of horizontal confined fission tracks were measured. To increase the number of horizontal confined AFT lengths that could be measured, additional mounts were irradiated with heavy ions (*Jonckheere et al.,* 2007).

Table A1.1. Apatite fission track full data

Sample	N Latitude (deg.)	E. Longitude (deg)	Elev. (m)	Age/Lith.	Xls[a]	Rho-S[b] x10^6	NS[c]	Rho-I[b] x10^5	NI[c]	P(χ^2)[d] %	RhoD[e] x10^6	ND[f]	Age (Ma)	±1σ	Dpar[g] mean	Dpar SD	# lengths[h]	Length (μm)	Length SD (μm)
Talas range																			
10TR02	42,163250	72,040472	2571	Pt/Ss	20	1,919	57	1,71	640	100	1,337	5231	22	3,1	2	0,15	104*	13,6	1,5
10TR03	42,138222	72,040528	2678	Pt/Ss	20	1,37	122	1,291	1294	57	1,321	5231	23	2,3	2,05	0,18	2	15,4	0,4
10TR04	42,108528	72,042611	3120	Pt/Ss	20	0,776	85	0,8	825	56	1,317	5231	25,4	2,9	1,98	0,18	5*	10,6	2,1
10TR05	42,121972	72,037083	2921	Pt/Ss	20	1,242	72	1,345	665	97	1,258	5231	25,1	3,1	1,95	0,22	71*	11,7	2,1
10TR17	42,458889	71,533806	1269	Pt/Ss	19	1,188	91	1,265	855	91	1,284	7234	25,2	2,80	1,92	0,26	13*	13,65	1,7
Ugam Range																			
10UM12	42,233083	71,406694	3,456	C/Granite	18	3,275	438	7,042	2037	85	1,301	5674	51,5	2,8	2	0,16	101	12,8	1,5
10UM14	42,240139	71,409833	2,082	C/Schist	7	3,127	87	3,598	756	50	1,286	5674	27,5	3,2	3	0,19	15	12,9	1,4
10UM15	42,241528	71,413306	2,945	C/Granite	17	1,304	115	2,095	716	82	1,27	5674	37,6	3,8	2	0,26	9	12,2	1,5
10CA26	41,886778	70,852194	3,161	C/Granite	8	1,406	103	2,546	569	83	1,228	5231	40,9	4,4	2	0,21	7	12,0	1,9
10CA27	41,881278	70,853806	2,953	C/Granite	21	1,963	260	3,815	1338	84	1,218	5231	43,6	3	2	0,17	101*	11,8	1,9
10CA29	41,874861	70,862750	2,535	C/Granite	19	2,433	197	3,286	1459	40	1,208	5231	30,1	2,3	2	0,15	106	11,5	1,8
Shandalash Range																			
10TR19	42,199194	71,585583	2978	C/Granite	19	3,469	185	4,293	1495	68	1,307	5231	29,8	2,4	2	0,19	19	11,6	2,3
10TR20	42,185528	71,574194	2815	C/Granite	20	0,599	70	0,686	611	97	1,297	5231	27,4	3,5	2,05	0,17	13*	11,8	2,0
10TR21	42,183722	71,569722	2778	Є/Tillite	20	3,266	266	3,368	2579	97	1,287	5231	24,5	2,6	2,17	0,19	49	12,2	2,4
10TR22	42,128722	71,557611	2458	Є/Tillite	19	1,27	135	1,389	1234	8	1,278	5231	26,4	2,9	2,82	0,47	28*	11,6	2,6
10TR23	42,119528	71,546611	2,713	Dev/Ss	17	1,75	53	0,824	1126	96	1,268	5231	11	1,6	2	0,21	4	13,0	2,4
Chatkal Range																			
10CK34	41,574028	70,699361	1,763	C/Granite	20	1,783	865	9,479	1627	5	1,298	7234	124	6,6	2,07	0,21	101*	12,8	1,5
10CK37	41,496722	71,023611	1,762	C/Granite	20	1,288	249	2,932	1094	61	1,277	7234	53,6	3,8	2,11	0,19	56	12,1	1,9
10CK41	41,437833	71,226806	1,369	Pz1/Gneiss	20	1,831	609	9,595	1162	35	1,248	5231	120	6,7	2,19	0,16	105*	11,7	1,9
10CK43	41,584250	71,526972	1,874	Dev/Ss	16	1,081	108	2,372	492	100	1,264	7234	51	5,5	2,22	0,26	14*	12,5	1,7
10CK44	41,565833	71,529167	1,695	Dev/Ss	20	1,326	241	3,751	852	65	1,238	5231	64,7	5	2,50	0,36	37*	12,2	2,1

continued. Table A1.1. AFT full data

Sample	N Latitude (deg.)	E. Longitude (deg)	Elev. (m)	Age/Lith.	Xls[a]	Rho-S[b] x10^6	NS[c]	Rho-I[b] x10^5	NI[c]	P(χ^2)[d] %	RhoD[e] x10^6	ND[f]	Age (Ma)	±1σ	Dpar[g] mean	Dpar SD	# lengths[h]	Length (μm)	Length SD (μm)
										Fergana range									
10SU67	41,530639	72,331833	0,922	Dev/Ss	7	0,667	13	0,667	130	100	1,041	7234	19,2	5,6	2,28	0,19	ND	ND	ND
10SU65	41,612972	72,364083	2,578	Dev/Ss	20	0,922	137	0,931	1356	84	1,118	7234	20,8	1,9	2,30	0,17	101*	13,2	1,4
10SU61	41,590000	72,328639	1,985	C/Granite	20	0,831	92	0,632	1209	7	1,131	7234	16,4	2	1,87	0,17	100*	11,6	1,9
10SU62	41,609194	72,356056	2,386	C/Granite	20	1,082	157	1,144	1365	91	1,125	7234	23,9	2,1	2,31	0,02	101*	13,2	1,7
10SU64	41,622861	72,367583	2,767	Dev/Granite	19	1,23	334	2,528	1625	50	1,136	4999	43	2,7	2,53	0,14	105*	12,4	1,9

[a] Xls is the number of individual crystals dated.
[b] Rho-S and Rho-I are spontaneous and induced track density; both measured in (tracks/cm^2).
[c] NS and NI are the number of spontaneous and induced tracks counted, respectively.
[d] P(χ2) (%) is the chi-squred probability (*Galbraith*, 1981; *Green*, 1981). All ages pass the P(χ2) test and are reported as pooled ages.
[e] Rho-D is the induced track density in external detector adjacent to CN5 dosimetry glass (tracks/cm^2).
[f] ND is the number of tracks counted in determining Rho-D.
[g] Mean of at least 4 Dpar measurements. The correction factor (*Sobel & Seaward*, 2010) is 0.89 with respect to Durango apatite standard (*Donelick et al*., 1999).
[h] Samples with asterisk (*) indicates track lengths measured from heavy ions irradiation slide.
[i] Zeta calibration used for apatite: AB: 369.5 ± 7.9 (A. Bande, unpublished, 2012)

Appendix 2

Additional data for Chapter 3

In this appendix Full AFT data are presented in Tables A2.1 and zircon U-Pb full measurements and analysis are presented in table A2.2

Table A2.2. Apatite fission track full data for Chapter 3

Sample	Latitude (° N)	Longitude (° E)	Elev. (masl)	Age/Lith.	Xls[a]	Rho-S[b] x10^6	NS[c]	Rho-I[b] x10^5	NI[c]	P(χ^2)[d] %	RhoD[e] x10^6	ND[f]	Age (Ma)	±1σ	Dpar[g] mean (µm)	Dpar SD (µm)	# lengths[h]	Length (µm)	Length SD (µm)
Takhtalik Range																			
10FR69	41,719139	72,956222	1844	P/Granite	21	0,979	143	1,22	1147	78	1,111	7234	25,5	2,4	1,57	0,17	49*	12,1	1,8
10FR71	41,710361	72,998528	2131	Pt/Ss	20	1,564	331	2,853	1814	8	1,38	5652	46,5	3,2	2,38	0,18	102*	12,8	1,6
10FR72	41,699806	73,028389	1939	Pt/Ss	20	0,423	62	0,457	573	95	1,104	7234	22	3	1,75	0,19	16*	12	2,1
10FR73	41,688778	73,014778	1789	C/Ss	20	1,761	106	0,902	2069	93	1,097	7234	10,4	1	1,67	0,16	72*	12,2	2,2
Kaldama Pass																			
11TS532	41,305817	73,654983	2758	C/Ss	20	3,764	77	1,004	2888	8	1,257	7234	6,3	0,9	1,73	0,17	21*	14	1,1
11TS533	41,294350	73,635833	2911	C/Ss	20	2,945	50	1,047	1407	7	1,236	7234	8,2	1,2	1,71	0,19	ND	ND	ND
11TS534	41,338250	73,647383	2036	P/Granite	20	2,578	175	4,65	970	60	1,25	7234	41,6	3,5	1,71	0,13	25	11,8	1,7
11TS535	41,345967	73,664150	2122	P/Granite	20	2,552	569	5,506	2637	0	1,243	7234	51	3,9	1,80	0,13	102	12,7	1,4
Fergana Range																			
12FE27	40,661467	73,871066	1947	D/Ss	11	1,947	28	0,977	558	36	1,152	4492	10,7	2,1	1,99	0,21	ND	ND	ND
12FE28	40,659566	73,792583	1424	K/Ss	20	1,424	235	2,57	1302	36	1,143	4492	38	2,9	2,32	0,22	80	11,3	1,9
12FE29	40,658600	73,787700	3605	C/Ss	4	3,605	13	1,961	239	44	1,134	4492	11,4	3,3	2,13	0,32	ND	ND	ND
12FE30	40,637483	73,731000	3605	P/Congl.	20	3,605	294	3,603	1316	0	1,124	4492	48,7	5,3	2,01	0,26	24	11,2	2,2
Alai Range																			
11T23	39,838192	74,843641	3117	Pt/Ss	20	2,462	63	0,726	2136	100	1,229	7234	6,7	0,9	1,79	0,12	5*	14,4	1,6
11T75	39,850390	74,498432	2800	Pt/Ss	20	3,699	66	1,144	2135	100	1,208	7234	6,9	0,9	1,69	0,15	2*	15,4	1,6
12KA21	40,003340	72,581800	3475	P/Granite	20	2,496	124	1,645	1881	100	1,115	4492	13,6	1,3	2,22	0,13	ND	ND	ND
12KA22	40,004733	72,571950	3860	P/Granite	19	2,468	163	2,6	1547	100	1,106	4492	21,5	1,8	2,40	0,16	63	12,4	2,0
12KA23	40,005560	72,576500	3660	P/Granite	20	2,681	181	2,698	1798	35	1,097	4492	20,4	1,7	2,34	0,20	ND	ND	ND
12KA24	39,998290	72,605740	3122	P/Granite	20	3,227	121	1,833	2130	99	1,088	4492	11,4	1,1	2,37	0,17	ND	ND	ND
12KA25	39,998920	72,608100	3297	P/Granite	21	2,453	129	1,602	1975	65	1,079	4492	13	1,2	2,31	0,24	58	13,3	2,0

Continued. Table A2.2. AFT full data for Chapter 3

Sample	Latitude (° N)	Longitude (° E)	Elev. (masl)	Age/Lith.	Xls[a]	Rho-S[b] x10^6	NS[c]	Rho-I[b] x10^5	NI[c]	P(χ^2)[d] %	RhoD[e] x10^6	ND[f]	Age (Ma)	±1σ	Dpar[g] mean (μm)	Dpar SD (μm)	# lengths[h]	Length (μm)	Length SD (μm)
									Alai Range										
12NU12	40,128583	73,525633	1838	P/Granite	20	1,298	66	0,674	1271	100	1,021	4039	9,8	1,3	1,86	0,17	ND	ND	ND
12NU13	40,165933	73,557300	2890	P/Granite	20	1,923	267	3,809	1348	86	1,011	4039	36,9	2,7	1,82	0,12	100	10,5	1,7
12NU14	40,165800	73,553100	2670	P/Granite	20	1,673	78	0,86	1517	49	1,001	4039	9,5	1,1	1,84	0,10	ND	ND	ND
12NU15	40,161467	73,548867	2500	P/Granite	20	4,573	216	2,742	4404	92	0,991	4039	9	0,7	1,92	0,12	ND	ND	ND
12NU16	40,151917	73,542850	2210	P/Granite	21	2,078	45	0,794	1177	99	0,981	4039	6,9	1,1	2,01	0,11	ND	ND	ND
12NU17	40,145217	73,539517	2056	P/Granite	20	4,052	85	1,79	1924	100	0,972	4039	7,9	0,9	2,10	0,16	6	12,9	2,2
									Nura - Alai Basin										
12NU02	39,616333	73,837167	2930	S/Ss	20	1,532	77	0,853	1383	92	1,04	4039	10,7	1,3	2,01	0,17	ND	ND	ND
12NU11	39,674667	73,777667	2939	S/Ss	20	1,432	91	0,886	1472	97	1,031	4039	11,8	1,3	2,09	0,23	ND	ND	ND

[a] Xls is the number of individual crystals dated.
[b] Rho-S and Rho-I are spontaneous and induced track density; both measured in (tracks/cm^2).
[c] NS and NI are the number of spontaneous and induced tracks counted, respectively.
[d] P(χ2) (%) is the chi-squred probability (*Galbraith*, 1981; *Green*, 1981). All ages pass the P(χ2) test and are reported as pooled ages.
[e] Rho-D is the induced track density in external detector adjacent to CN5 dosimetry glass (tracks/cm^2).
[f] ND is the number of tracks counted in determining Rho-D.
[g] Mean of at least 4 Dpar measurements. The correction factor (*Sobel & Seaward*, 2010) is 0.89 with respect to Durango apatite standard (*Donelick et al*., 1999).
[h] Samples with asterisk (*) indicates track lengths measured from heavy ions irradiation slide.
[i] Zeta calibration used for apatite: AB: 369.5 ± 7.9 (A. Bande, unpublished, 2012)

Table A2.2. Zircon LA-ICP-MS U/Pb full data

	$^{207}Pb/^{235}U$	2 s %	$^{206}Pb/^{238}U$	2 s %	Rho	$^{207}Pb/^{206}Pb$	2 s %	$^{207}Pb/^{235}U$ age (Ma)	± Ma	$^{206}Pb/^{238}U$ age (Ma)	± Ma	$^{207}Pb/^{206}Pb$ age (Ma)	± Ma	disc. 6/8 - 7/5	disc. 6/8 - 7/6	$^{232}Th/^{238}U$	U (ppm)	Th (ppm)	Pb (ppm)	Th/U
12KA23																				
zr-37	0,2491	6,9	0,03540	5,9	0,86	0,05107	3,6	225,9	15,6	224,3	13,2	242,6	8,7	1%	8%	0,21	156	58	6	0,37
zr-38	0,2740	6,8	0,03772	6,0	0,88	0,05270	3,2	245,9	16,7	238,7	14,3	314,5	10,1	3%	24%	0,54	378	370	12	0,98
zr-39	0,3186	7,5	0,04136	6,0	0,80	0,05591	4,5	280,9	21,1	261,3	15,7	447,5	20,1	7%	42%	0,35	120	74	5	0,62
zr-40	0,2642	7,0	0,03753	6,0	0,86	0,05108	3,5	238,1	16,7	237,5	14,3	243,0	8,5	0%	2%	0,34	165	97	6	0,59
zr-41	0,3078	6,6	0,04092	6,0	0,91	0,05459	2,8	272,5	18,0	258,6	15,5	394,0	11,0	5%	34%	0,38	267	175	11	0,66
zr-42	0,2748	7,0	0,03472	6,3	0,90	0,05744	3,2	246,5	17,3	220,0	13,9	507,0	16,2	11%	57%	0,22	148	57	5	0,39
zr-43	0,3503	7,3	0,04416	6,0	0,82	0,05756	4,1	305,0	22,3	278,6	16,7	512,0	21,0	9%	46%	0,33	140	81	5	0,58
zr-44	0,2951	7,7	0,04071	6,0	0,78	0,05262	4,8	262,6	20,2	257,2	15,4	311,0	14,9	2%	17%	0,32	71	38	3	0,54
zr-45	0,3120	7,3	0,04362	6,2	0,85	0,05190	3,8	275,8	20,1	275,3	17,1	280,0	10,6	0%	2%	0,32	185	105	7	0,57
zr-46	0,3424	7,1	0,04508	6,0	0,85	0,05513	3,7	299,0	21,2	284,2	17,1	416,5	15,4	5%	32%	0,23	62	24	3	0,39
zr-51	0,4477	7,2	0,05391	6,2	0,86	0,06027	3,7	375,7	27,0	338,5	21,0	612,0	22,6	10%	45%	0,40	172	120	8	0,70
zr-52	0,3421	7,3	0,04335	6,2	0,85	0,05728	3,9	298,8	21,8	273,5	17,0	501,0	19,5	8%	45%	0,23	199	80	8	0,40
zr-53	0,3504	7,3	0,04190	6,2	0,85	0,06069	3,8	305,0	22,3	264,6	16,4	627,0	23,8	13%	58%	0,20	159	57	6	0,36
zr-54	0,3618	7,0	0,04438	6,2	0,89	0,05916	3,3	313,5	21,9	279,9	17,4	572,0	18,9	11%	51%	0,20	152	54	6	0,36
zr-55	0,3238	7,6	0,04509	6,2	0,82	0,05212	4,3	284,8	21,6	284,3	17,6	289,5	12,4	0%	2%	0,23	86	32	3	0,37
zr-56	0,4311	7,5	0,05245	6,2	0,83	0,05964	4,3	363,9	27,3	329,6	20,4	589,5	25,3	9%	44%	0,68	150	178	6	1,19
zr-57	0,3130	6,9	0,04253	6,1	0,88	0,05340	3,1	276,5	19,1	268,5	16,4	344,5	10,7	3%	22%	0,31	159	88	6	0,55
zr-58	0,3439	6,9	0,04328	6,2	0,90	0,05766	2,9	300,1	20,7	273,1	16,9	515,5	14,9	9%	47%	0,78	181	243	8	1,34
zr-59	0,4174	7,5	0,04280	6,2	0,83	0,07076	4,3	354,2	26,6	270,2	16,8	950,0	40,9	24%	72%	0,53	254	236	10	0,93

continued Table A2.2. Zircon LA-ICP-MS U/Pb full data

	$^{207}Pb/^{235}U$	2 s %	$^{206}Pb/^{238}U$	2 s %	Rho	$^{207}Pb/^{206}Pb$	2 s %	$^{207}Pb/^{235}U$ age (Ma)	± Ma	$^{206}Pb/^{238}U$ age (Ma)	± Ma	$^{207}Pb/^{206}Pb$ age (Ma)	± Ma	disc. 6/8 - 7/5	disc. 6/8 - 7/6	$^{232}Th/^{238}U$	U (ppm)	Th (ppm)	Pb (ppm)	Th/U
12NU13																				
zr-37	0,3378	3,9	0,04353	2,1	0,54	0,05631	3,3	295,5	11,5	274,7	5,8	463,5	15,3	7%	41%	0,67	551	600	23	1,09
zr-38	0,3188	5,2	0,03938	2,3	0,44	0,05875	4,7	281,0	14,6	249,0	5,7	556,5	26,2	11%	55%	0,42	222	153	8	0,69
zr-39	0,3039	4,1	0,03763	2,2	0,54	0,05860	3,4	269,4	11,0	238,1	5,2	551,0	18,7	12%	57%	0,23	393	147	14	0,37
zr-40	0,4313	3,8	0,04505	2,2	0,58	0,06948	3,1	364,1	13,8	284,1	6,2	912,0	28,3	22%	69%	0,35	410	231	17	0,56
zr-41	0,4934	4,6	0,04340	2,3	0,50	0,08249	4,0	407,2	18,7	273,9	6,3	1256,0	50,2	33%	78%	0,52	882	762	33	0,86
zr-42	0,3217	3,8	0,04150	2,1	0,55	0,05626	3,1	283,2	10,8	262,1	5,5	461,5	14,3	7%	43%	0,21	393	134	15	0,34
zr-43	0,4013	3,6	0,04210	2,1	0,58	0,06917	2,9	342,6	12,3	265,9	5,6	902,5	26,2	22%	71%	0,44	903	652	34	0,72
zr-44	0,3140	3,7	0,04200	2,2	0,59	0,05425	3,0	277,3	10,3	265,2	5,8	380,0	11,4	4%	30%	0,20	464	155	18	0,33
zr-45	0,3893	3,7	0,03429	2,1	0,57	0,08240	3,0	333,9	12,4	217,3	4,6	1254,0	37,6	35%	83%	0,21	573	202	17	0,35
zr-46	0,2825	4,2	0,03910	2,1	0,50	0,05243	3,7	252,6	10,6	247,3	5,2	303,0	11,2	2%	18%	0,15	299	74	11	0,25
zr-50	0,3329	4,4	0,04200	2,3	0,52	0,05752	3,8	291,8	12,8	265,3	6,1	510,5	19,4	9%	48%	0,14	207	47	8	0,23
zr-51	0,3409	5,2	0,03416	2,5	0,48	0,07243	4,5	297,9	15,5	216,5	5,4	997,0	44,9	27%	78%	0,43	264	181	9	0,69
zr-52	0,3183	5,3	0,04004	2,4	0,45	0,05768	4,7	280,6	14,9	253,1	6,1	516,0	24,3	10%	51%	0,25	284	114	11	0,40
zr-53	0,2848	3,9	0,04007	2,4	0,62	0,05157	3,1	254,5	9,9	253,3	6,1	265,0	8,2	0%	4%	0,13	545	119	21	0,22
zr-54	0,2986	4,8	0,04089	2,6	0,54	0,05299	4,0	265,3	12,7	258,4	6,7	327,0	13,1	3%	21%	0,16	296	78	12	0,26
zr-55	0,3607	4,3	0,04018	2,5	0,58	0,06516	3,5	312,8	13,4	253,9	6,3	778,0	27,2	19%	67%	0,28	540	248	20	0,46
zr-56	0,2798	4,3	0,02333	2,4	0,56	0,08703	3,6	250,5	10,8	148,7	3,6	1360,0	49,0	41%	89%	0,25	647	262	8	0,40
zr-57	0,3078	5,2	0,03871	2,6	0,50	0,05770	4,5	272,5	14,2	244,8	6,4	517,0	23,3	10%	53%	0,16	314	84	11	0,27
zr-58	0,2905	3,9	0,04042	2,2	0,56	0,05215	3,2	259,0	10,1	255,5	5,6	290,5	9,3	1%	12%	0,15	470	118	18	0,25
zr-59	0,3204	8,3	0,04167	3,1	0,37	0,05579	7,6	282,2	23,4	263,2	8,2	443,0	33,7	7%	41%	0,21	194	69	7	0,36